Photochemical Transformations in Ice: Implications for the Fate of Chemical Species

Thesis by

Yael Dubowski

In Partial Fulfillment of the Requirements

for the degree of

Doctor of Philosophy

California Institute of Technology
Pasadena, CA
2001

(Defended May 29, 2001)

Acknowledgments

There are many people I would like to acknowledge for their assistance and friendship during my time here at Caltech.

First, I would like to thank my advisor Professor Mike Hoffmann for his help and encouragement all along the way. Even when nothing worked and I was about to give up, (and actually started to work in parallel on OCS oxidation reactions...) Mike convinced me to keep on trying, and for that I am tremendously grateful. Despite all the challenges involved in trying to measure quantum yields in ice, the last five years gave me the opportunity to become familiar with this complex and exciting medium.

This project would not have been the same without the help of A.J. Colussi who tried with all his heart to make a chemist out of me. His insightful comments and suggestions have been invaluable in conducting this research. I thank Professor Janet Hering for her attention and genuine effort to improve this dissertation. I would also like to thank Professor Paul Weinberg for his insights, expertise, and willingness to help. Finally, I would like to acknowledge Professor Geoff Blake for his constructive comments and support.

During this work many analytical instruments were used, and without the help and guidance of the members of the Environmental Analysis Center (Peter, Nathan, Yaniv and Bob) much of the work would not have been possible, Thanks. I would also like to acknowledge David Cocker and the other students of the roof lab as well as Prof. Kamb and his group (Hermann and Robin) at GPS for their help and for letting me use their facilities.

Furthermore, I would like to thank all the members of the Hoffmann and Hering groups: Steve, Catherine, Hui-Ming, Tim (the e-mail man), Hugo, Bill, Fok, Weng-Ki, Anna, Pat, Jeff, John, Jennie, Dan, Tina, Mariu, Penny, Tatiana, and finally Chris, who inherited this project and helped with some of the analysis presented here. All of you made the last five years a wonderful experience! Speaking of wonderful experiences, what would Keck be like without the humor and kindness (and candy) of Linda, Fran and Irene? A big thanks for all your help and support.

Literally speaking, this project would not have "worked" without the artistry of Rick at the Caltech glass shop and the expertise of Mike and Rich in the Keck machine shop. And of course funding from the Environment Now Foundation.

The decision to come to the US for such a long period was not a simple one, and I would like to thank Ronit and the professors at the Earth Science Institute at the Hebrew University (especially Jonathan, Yigal, Boaz and Yeshu) who encouraged me to do so.

To the whole Israeli "Kibbutz" here at Caltech, especially Ronit, Re'em and Ma'ayan, I cannot imagine being here without your friendship and encouragement.

Last, but not least, I would like to thank my family; my parents (Miriam and Avigdor Beiles) and sisters (Diti and Gali) who were always with me regardless of the physical distance. There are not enough words to describe my love and gratitude to my husband Yaniv for his love and continuous support that made it all possible, and of course to my children, Omer and Yuval, that brought so much joy into my life.

Since so many people have helped me in so many ways to reach this point of my life, I might have forgotten to mention some them and for that I apologize; Thank you all.

Abstract

Post-depositional photochemical alterations in snowpacks and sea ice may affect the chemical records in polar caps and the chemistry of the polar atmospheric boundary layer. Although it is known that UV-induced photochemistry actually occurs in ice matrices, quantitative information on such processes is still lacking. With new methods for determining the light absorption by chromophores embedded in packed ice, this study investigates the rates and products of the photodegradation of 4-nitrophenol and nitrate in ice.

A quantum yield (ϕ_{ice}) of $(2.3 \pm 0.4) \times 10^{-4}$ was obtained for the photochemical degradation of 4-nitrophenol over the wavelength range of 300 to 370 nm in ice pellets (pH 5.6). Five reaction products were positively identified: hydroquinone, benzoquinone, 4-nitrosophenol, nitrate, and nitrite. Indirect evidence suggests the formation of organic polymers. These results are similar to those found for 4-nitrophenol photolysis in aqueous solutions, indicating that comparable mechanisms operate in both phases.

Upon irradiation ($\lambda = 313 \pm 15$ nm) of NO_3^- doped ice layers, the formation of $NO_2(g)$ and NO_2^- was observed. The yield for both products increased with temperature over the range 248 – 268 K; with values of $\phi_{NO_2^-} \sim (4.8 \pm 1.5) \times 10^{-3}$ and ϕ'_{NO_2} $(1.2 \pm 0.9) \times 10^{-3}$ at 263 K, 10 mM KNO_3. The formation of NO_2^- during the photolysis of NO_3^- in ice pellets has apparent activation energy, E_a, of 5.8 kcal mole^{-1}. This E_a is similar to the water cage-effect for supercooled water. ϕ_{NO_2} showed a much stronger temperature dependence ($E_a \sim 10$ kcal mole^{-1}); This can be interpreted as the

probability of the product NO_2 escaping into the gas-phase, before it is photolyzed into NO.

These results suggest that, under our experimental conditions, the photochemical transformations occur within the quasi-liquid layer, which behaves as a supercooled solution.

The experimental data for ϕ'_{NO_2}, coupled with snow absorptivity data, lead to a predicted NO_2 fluxes in reasonable agreement with recent measurements in Antarctic snow under solar illumination. NO_3^- photolysis within snowpacks may also be a significant source for $^{\cdot}OH$ radicals, which may further react and cause chemical changes in important species, such as H_2O_2 and H_2CO and CH_3CHO.

Table of Contents

List of figures

List of tables:

Chapter 1

Introduction

Fundamental interest in ice chemistry has increased dramatically since heterogeneous reactions on Polar Stratospheric Clouds were found to play a crucial role in polar ozone depletion (e.g., McElroy et al., 1986; Solomon et al., 1986; Molina, 1991). Since then, numerous studies have been carried out to evaluate the rates and stoichiometries of different photochemical and heterogeneous reactions on ice surfaces (e.g., Abbatt and Molina, 1992; Purcell et al., 1995, 1996; Lee et al., 1999).

Over the last decade there has also been a growing interest in the chemical composition of snow packs and ice cores in polar regions as they may contain important paleoatmospheric and paleoclimate information (Bales and Wolff, 1995; Chappellaz et al., 1997; Legrand, 1997). Understanding the air-surface exchange and the postdepositional reactions that may take place within the snow is important for interpreting these ice core chemical records (Neftel 1991). Moreover, recent experiments and modeling studies have shown that snowpacks can evolve gas-phase compounds, which may exert a significant influence on the chemistry of the lower polar troposphere (Michalowski et al., 2000). Several groups have hypothesized that UV radiation is involved in this gas-evolution chemistry (Hoffmann, 1996; Honrath et al., 1999, Sumner and Shepson, 1999, Couch et al., 2000), and that the photolysis of nitrate and natural organic matter within the snow pack drive the formation of NO_x, HCHO and CH_3CHO. The understanding of the mechanisms involved in these photochemical processes is still lacking, mainly due to the scarcity of controlled lab experiments in this relatively young research field.

In order to develop a better understanding of photochemical processes involving ice particles, the present study has several objectives:

1. Develop techniques that would enable the measurements of light absorption by chromophores embedded in packed ice.
2. Investigate quantitatively (under controlled conditions) the photochemistry of nitrate and 4-nitrophenol in ice, including the determination of rate constants, quantum yields and product analysis for each process.
3. Compare the results obtained from ice systems with the photochemical mechanisms known for aqueous solutions. This comparison may provide insight as to the nature of the microenvironment in which various photochemical processes are taking place in these ice experiments.
4. Apply the basic understanding of photochemical reactions in ice to snowpacks at mid- and high-latitudes and to atmospheric ice particles.

These objectives are addressed in the subsequent chapters of this thesis. A short background is given in Chapter 2. The use of ice pellets to study the photochemical degradation of 4-nitrophenol in ice pellets is presented in Chapter 3. Motivated by recent field observations of NO_x emissions from snowpack, Chapter 4 addresses the production of NO_2 and NO_2^- during the photolysis of spray-frozen NO_3^- solutions. The formation rates of NO_2 and NO_2^- in these experiments showed a strong temperature dependence. To further investigate the bases for this temperature dependence, the formation rate of NO_2^- during NO_3^- photolysis in ice pellets was measured as a function of temperature and

initial NO_3^- concentration. The results of these experiments are presented in Chapter 5. The overall conclusions of these studies are presented in Chapter 6.

References

1. Abbatt J. P. D. and Molina M. J. (1992) The Heterogeneous Reaction HOCl + HCl $\longrightarrow$ Cl_2 +H_2O on Ice and Nitric Acid Trihydrate: Reaction Probabilities and Stratospheric Implications. *Geophys. Res. Lett.* 19, 461-464.
2. Bales R. C. and Wolff E. W. (1995) Processes of Chemical Exchange Between the Atmosphere and Polar Snow: Key to Interpreting Natural Climate Signals in Ice Cores. *EOS, Transactions, Amer. Geophys. Union* 76, 477, 482-483.
3. Chappellaz J., Brook E., Blunier T., and Malaize B. (1997) CH_4 and Delta O-18 of O_2 Records from Antarctic and Greenland Ice: A Clue for Stratigraphic Disturbance in the Bottom Part of the Greenland Ice Core Project and the Greenland Ice Sheet Project 2 Ice Cores. *J. Geophys. Res. - Ocean* 102, 26547-26557.
4. Couch T. L., Sumner A. L., Dassau T. M., Shepson P. B., and Honrath R. E. (2000) An Investigation of the Interaction of Carbonyl Compounds with the Snowpack. *Geophys. Res. Lett.* 27, 2241-2244.
5. Hoffmann M. R. (1996) Possible Chemical Transformations in Snow and Ice Induced by Solar (UV Photons) and Cosmic Irradiation (Muons). In *Chemical Exchange Between the Atmosphere and Polar Snow* (ed. W. Wolff and R. C. Bales), pp. 353-377. Springer.
6. Honrath R. E., Peterson M. C., Guo S., Dibb J. E., Shepson P. B., and Campbell B. (1999) Evidence of NO_x Production within or upon Ice Particles in the Greenland Snowpack. *Geophys. Res. Lett.* 26, 695-698.

7. Lee S. H., Leard D. C., Zhang L. R., Molina L. T., and Molina M. J. (1999) The HCl + $ClONO_2$ Reaction Rate on Various Water Ice Surfaces. *Chem. Phys. Lett.* 315, 7-11.

8. Legrand M. (1997) Ice-Core Records of Atmospheric Sulphur. *Philos. T. Roy. Soc. B* 352, 241-250.

9. McElroy M. B., Salawitch R. J., Wofsy S. C., and Logan J. A. (1986) Reductions of Antarctic Ozone Due to Synergistic Interactions of Chlorine and Bromine. *Nature* 321, 759-762.

10. Michalowski B. A., Francisco J. S., Li S. M., Barrie L. A., Bottenheim J. W., and Shepson P. B. (2000) A Computer Model Study of Multiphase Chemistry in the Arctic Boundary Layer during Polar Sunrise. *J. Geophys. Res.-Atmos.* 105, 15131-15145.

11. Molina M. J. (1991) Heterogeneous Chemistry On Polar Stratospheric Clouds. *Atmos. Environ. A.* 25, 2535-2537.

12. Neftel A. (1991) Use of Snow and Firn Analysis to Reconstruct Past Atmospheric Composition. In *NATO ASI Series*, Vol. G 28 (ed. T. D. D. e. al.), pp. 385-411. Springer-Veriag Berlin Heidelberg.

13. Pursell C. J., Conyers J., Alapat P., and Parveen R. (1995) Photochemistry of Chlorne Dioxide in Ice. *J. Phys. Chem.* 99, 10433-10437.

14. Pursell C. J., Conyers J., and Denison C. (1996) Photochemistry of Chlorne Dioxide in Polycrystalline Ice (T=140-185 K): Production of Chloryl Chloride, Cl-(OClO). *J. Phys. Chem.* 100, 15450-15453.

15. Solomon S., Garcia R. R., Rowland F. S., and Wuebbles D. J. (1986) On the Depletion of Antarctic Ozone. *Nature* 321, 755-758.

16. Sumner A. L. and Shepson P. B. (1999) Snowpack Production of Formaldehyde and its Effect on the Arctic Troposphere. *Nature* 398, 230-233.

Chapter 2

Background

2.1 Physical properties of ice and snow

Water forms more discrete crystalline solid phases than any other known substance (Hobbs, 1974). If liquid water is frozen under normal atmospheric conditions or water vapor is deposited at temperature between 193 K to 273 K, then it forms crystalline ice with hexagonal symmetry (*ice Ih*). The various high-pressure phases of ice have been numbered up to ice XIV. Cubic ice (*ice Ic*) is a close variant of *ice Ih* and is formed when water vapor is deposited at temperatures between 143 K and 193 K. Deposition of water vapor onto a substrate at temperatures below 140 K results in the formation of amorphous ice deposits.

2.1.2 Diffusion through Ice

Due to molecular vibrations and the existence of lattice defects, water molecules may be displaced and diffuse through the ice. Neftel et al. (1985) pointed out that impurities might diffuse within the ice structure, smoothing their chemical profile in the ice record. Electrons, protons, hydroxide and hydroxyl radicals are known to have relatively high diffusion rates in ice (Goto et al., 1986; Woafo et al., 1995). However, for impurities such as HNO_3 and HCl, lower diffusion coefficients in ice were measured; in these cases D_{ice} was on the order of 10^{-11} to10^{-12} cm^2 s^{-1} (Domine and Thibert, 1995; Sommerfeld et al., 1998). Since the apparent diffusion coefficient seems to be very sensitive to the effect of small-angle boundaries, which act as diffusion short circuits, there is still much debate over these measured diffusion rates in ice.

2.1.3 Incorporation of Impurities into Ice Growing from Liquid Solutions

During the freezing of aqueous solutions, most solutes are excluded from the ice phase. As a result, the solutes are concentrated into the remaining liquid solution pockets. Due to different degrees of incorporation of ions into the ice, an electric potential may be generated between the ice and the solution; this effect is known as the *Workman-Reynolds effect* (Workman and Reynolds, 1950).

Takenaka et al. (1998) pointed out that protons could be excluded from or included in the advancing ice phase, depending on the nature of the electrolyte present. Thus, the electrolyte can induce local pH changes at the surface of the ice crystals and in between adjacent crystals.

Different studies have observed that freezing of dilute solutions of oxidizable species (e.g., NO_2^-, SO_3^-, and I^-) can accelerate their apparent rates of auto-oxidation (Finnegan, 1991, Takenaka et al., 1996; Betterton and Anserson, 2001). Several factors can contribute to such accelerations: (1) a freeze concentration effect; (2) a possible catalytic effect of the ice crystals; (3) greater proton mobility in ice than in liquid water; (4) a favorable substrate-catalyst orientation caused by freezing; and (5) a greater dielectric constant for water than for ice. Takenaka et al.(1996) showed that, at least for the rate of oxidation of the species mentioned above, the freezing concentration effect is the major factor.

2.1.4 The Quasi-Liquid Layer (QLL) on Ice Surfaces

Faraday first proposed the existence of a quasi-liquid layer on ice surfaces below the bulk melting temperature (Faraday, 1850), which is known today as surface melting, or premelting, of ice.

The premelting of ice is believed to play an important role in phenomena such as reduction of the frictional coefficient, electrification of thunder clouds, glacier flow, frost heaves, and atmospheric chemistry (see review by Dash et al., 1995). The nature of this process has been the subject of many theoretical investigations (e.g., Fletcher, 1968; Wettlaufer, 1999; Bolton and Pettersson, 2000) and experimental studies (e.g., Conklin and Bales, 1993; D□ppenschmidt et al., 1998; D□ppenschmidt and Butt, 2000; Wei et al., 2001). While most of these experiments have confirmed the existence of quasi-liquid layer on ice surface, the temperature range over which this layer exists, its thickness, and a theoretical explanation for its formation are still subject to debate.

Premelting is well known to occur on surfaces of many classes of solids (e.g., metals, semiconductors, solid rare gases and molecular solids) and is driven by the tendency to reduce the interfacial free energy (Dash et al., 1995). The melting of the interface between a solid and its vapor indicates that the free energy of the wetted boundary is lower than it would be without the liquid. The competition between the lower free energy of the wetted boundary and the energy cost of melting a solid layer determine the actual thickness of the liquid-like layer (d) at the value for which the free energy of the system is at a minimum.

The total surface energy of the ice – vapor interface, γ, is equal to the sum of three contributions: the interfacial energy of the bulk ice – liquid layer ($\gamma_{\ell s}$), the interfacial energy of the liquid layer – vapor ($\gamma_{\ell v}$), and an additional term ($\Delta\gamma$) which depends on the thickness of the liquid layer. Based on the boundary conditions ($d = 0$ and $d = \infty$), it can be calculate that $\Delta\gamma \equiv \gamma_{\ell v} + \gamma_{\ell s} - \gamma_{sv}$ (γ_{sv} is the interfacial energy of bulk ice – vapor) and that for intermediate cases the surface energy is predicted by a suitable function, f, such

that $\gamma(d) = \gamma_s + \Delta\gamma f(d)$ (Dash et al., 1995). The choice of $f(d)$ depends on the surface forces acting among the interfaces. For van der Waals forces alone, $f(d) = d^2/(d^2 + \sigma^2)$ (where σ is a typical interatomic distance).

At equilibrium, the thickness of the liquid-like layer, d, (in the range of $d >> \sigma$) can be expressed as

$$d = \left(-2\sigma^2 \frac{\Delta\gamma}{\rho_\ell q_m} \times \frac{T_0}{T_0 - T} \right)^{1/3} \quad (1)$$

where ρ_ℓ is the density of bulk liquid, q_m is the latent heat of melting per molecule, T_0 represents the normal melting temperature of the bulk solid, and T is the actual ambient temperature.

In the case of short range forces (exponentially decaying forces), $f(d) = 1 - \exp(-d/\lambda)$, where λ is the decay length. Under such conditions, the thickness of the QLL varies logarithmically with temperature (Dash, 1989; Takagi, 1990):

$$d = \lambda \times \ln\left(-\frac{\Delta\gamma}{\rho_\ell q_m \lambda} \times \frac{T_0}{T_0 - T} \right) \quad (2)$$

Although experimental data support this model, the absolute values of d and the value of parameters in its dependence on temperature vary widely (Wettlaufer and Dash, 2000).

Both adsorption experiments (e.g., Miranda et al., 1998; Salmeron and Bluhm, 1999) and computer simulations (e.g., Löwen, 1994) have shown that the thin liquid layer is more ordered in the proximity of the solid surface (*proximity effect*). This ordering falls off exponentially with distance from the solid wall with a characteristic length of a few molecular diameters. Wei et al. (2001) showed that the disordering of the surface of a hexagonal ice (using sub-frequency vibrational spectroscopy to measure orientational

order of dangling >OH bonds) is detectable at 200 K and increases dramatically with temperature. Furthermore, they have shown that even at temperatures close to the bulk melting point, the quasi-liquid layer on ice is structurally different from normal liquid water. On the other hand, experiments on interfacial melting against graphite and polystyrene (Maruyama et al., 1992; Gay et al., 1992; Fu, 1993) showed that the diffusion coefficient of the quasi-liquid layer is approximately equal to that of supercooled water.

Unlike other surface disorders, surface premelting is related to the melting point of the bulk phase, in that the thickness of the melt is a function of the temperature difference from the normal melting point of the bulk solid ($T_0 - T$) rather then T alone. The thickness of the QLL increases with increasing temperature and reaches infinity when $T = T_0$. In addition to the temperature effect, surface disorders (such as roughness, polycrystallinity, and impurities) will tend to enhance the degree of surface premelting.

Impurities adsorbed at interfaces reduce the associated free energy in a manner analogous to bulk energies *(freezing point depression)*. Because the impurities are non-volatile and insoluble in ice, the interfacial coefficient in $\Delta\gamma$ (see above) will be reduced, but due to low vapor pressure, γ_{sv} may be reduced to a lesser extent. Hence, surface melting may be enhanced relative to the pure ice phase. At constant pressure, impurities shift the melting temperature by an amount which depends on the solute concentration (and not on its chemical nature). For a solution consisting of n_i moles of solute in n moles of solvent, Raoult's law expresses this shift (*Freezing Point Depression*) as

$$T_c = T_0\left(1 - \frac{RT_0 n_i}{q_m n}\right) \tag{3}$$

where T_c is the freezing temperature of a solution containing an amount of n_i/n of solutes, T_0 is the freezing temperature of the pure solid, R is the gas constant and q_m is the heat of fusion of the solvent.

Conklin and Bales (1993) estimated the thickness of the QLL based on the amount of SO_2 (g) adsorbed by ice, assuming that oxidation of SO_2 occurs only in the liquidlike layer. Their results indicate that the layer thickness increased with temperature and ionic strength, and under most conditions was higher than predicted by simple freezing-point depression. Atomic Force Microscopy (contact mode) measurements of d by D□ppenschmidt and Butt (2000) showed that it could best be described by $d \propto -\log \Delta T$ (T between 0 and -35° C). The addition of salts (10 mM KCl) increased the thickness of the quasi-liquid layer and the observed temperature dependence was following the power law $d \propto T^{-1}$, in agreement with the predictions by Wettlaufer (1999).

2.1.5 Optical Properties of Snow

Light interacts with snow grains by two mechanisms, scattering and absorption. The importance of each mechanism changes with wavelength. In the near infrared spectral region, the absorption and scattering strengths of snow are comparable. On the other hand, in the visible and UV regions, the absorption of light by snow is weak and scattering dominates (Warren, 1982). The depth to which light penetrates into snow is a combination of these two factors. At short wavelengths, multiple scattering enhances the effective pathlength for photons propagating in snow, increasing their probability of absorption and leading to a complex relationship between the penetration depth, absorption, and scattering.

Near the surface of the snow (i.e., the upper few centimeters), the relationship between light intensity and depth is complicated. Light, penetrating the snow, can be scattered back into the atmosphere before it reaches a depth at which all memory of its incident direction is lost. This effect leads to the solar zenith angle dependence of the reflectivity (albedo) of snow. Light that penetrates deeper into the snow becomes isotropic due to multiple scattering and its attenuation within the snowpack varies exponentially with depth, following the *Bouger-Lambert Law* (Barkstrom, 1972):

$$I(d) = I(d')e^{-k(\lambda)(d-d')} \tag{4}$$

where $k(\lambda)$ is the asymptotic flux extinction coefficient, I(d) and I(d') are light intensities at depths d and d', respectively.

The asymptotic flux extinction coefficient should not depend on solar zenith angle or cloud cover because the light has already become totally diffused before reaching the asymptotic region (Warren, 1982).

Early field studies on light penetration into snow have shown that light scattering within snow depends on snow density, grain size, and the concentration of impurities. However, all of these studies were done in the visible and IR spectral regions, and only a few used monochromatic light (Warren, 1982). The first close examination of snowpack extinction properties in the UV range was recently done by Beaglehole et al. (1998) in Antartica. However, only spectrally integrated light was measured in their study.

Petrovich and Govoni (1991) showed that the extinction coefficient of bubble-free single ice crystal is minimal at ~450 nm and increases toward higher and lower wavelengths. The extinction coefficients in the UV range are comparable to those at visible wavelengths from 580 to 720 nm, suggesting that existing data on the visible light

interaction with snow and sea ice can be used as a first-order estimate of the optical properties of UV in snow and ice.

King and Simpson (in press) recently measured light penetration in surface snow using monochromatic light over 300 – 548 nm wavelength rage. For a uniform snowpack (average snow diameter ~ 200 μm), they reported *e*-folding depths (i.e., the depth over which the monochromatic light intensity decreases by a factor of e) in the range of 5 to 6 cm^{-1}, and equivalent extinction coefficients, in water-equivalent units, of k = 66 - 86 m^{-1}. These data imply that photochemical processes in snowpack occur primarily in its upper 10 cm. Comparison of these results with measurements from previous studies (Warren, 1982; Beaglehole et al., 1998) shows that UV radiation is highly attenuated in the specific site (at Alert, Canada) studied by King and Simpson. These authors hypothesized that this is due to larger amount of soil and/or aerosol matter within the snowpack.

2. 2 Photochemistry in ice

Photochemical transformations in ice were first studied in regard to interstellar ice systems. Allamandola and coworkers (Allamandola et al., 1988) showed that under astrophysical conditions ultraviolet ($\lambda < 170$ nm) photolysis of ices containing H_2O, CH_3OH, NH_3, and CO at a temperature of 10 K produces H_2CO, CH_4, HCO, CO and CO_2. Similar results were also observed by Berstein et al. (1995) and Schutte and Gerakines (1995). Berstein et al. (1994) investigated the photolysis ($\lambda < 170$ nm) of hexamethylenetetramine (HMT, $C_6H_{12}N_4$) in ice at temperatures from 12 K to 200 K. The products of the direct photolysis were found to be HOCN, H_2NCN, HNCO, CH_3CN and $N(CH_3)_3$. The photolysis ($\lambda < 170$ nm) of polycyclic aromatic hydrocarbons (PAH) in H_2O ice was studied by Berstein and others (1999). Their results showed that irradiation

of PAH's results in the partial reduction of the PAH's, which produced partially hydrogenated aromatic hydrocarbons, and the partial oxidation of the PAH's, yielding ketones, alcohols, and bridging ethers when bay regions exist in the parent PAH.

Klan et al. (2000a) observed that photolysis of chlorobenzene in ice ($\lambda > 254$) has very different photoproducts than those observed in aqueous solution. Their results suggested that aggregation of the starting molecules plays a significant role in the reaction in ice. In a separate study on the photochemistry of valerophenone in various solid solutions (Klan et al., 2000b), they demonstrated that molecules that possess a favorable configuration for hydrogen abstraction react with the same photochemical efficiency, regardless of the nature of the solvent. However, in all their experiments, ice samples were produce by bulk freezing of relatively large volumes of solution. This procedure is expected to cause a significant concentrating effect on the solutes (Takenaka et al., 1996).

Following the recognition of the importance of heterogeneous ice-particle chemistry to stratospheric ozone depletion, several experiments were carried out on photochemistry of OClO in ice under stratospheric conditions (Pursell et al., 1995,1996; Graham et al., 1996; Anderson et al., 1998). The photoreactivity of OClO is known to have strong medium dependence. In amorphous ice at 80K, ClOO is the only product (Pursell et al., 1995), whereas at 140 –180 K in polycrystalline ice, chloryl chloride (Cl-ClO_2) is observed as the dominant photoproduct (Pursell et al., 1996). Anderson and coworkers (1998) showed that, under more concentrated conditions in which OClO clusters are present, the production of Cl-ClO_2 could also occur in amorphous ice (100 K).

Over the last several years, there is a growing body of evidence from field studies (e.g., Impey et al., 1997; Honrath et al., 1999; Sumner and Shepson 1999; Ridley et al., 2000) that snowpacks are photochemically active and that they are likely a net source, during certain times of the year, of many gas phase species and effect the chemistry of the atmospheric boundary layer.

Field observations during Polar Sunrise Experiments in the arctic in 1997 and 1998 showed effluxes of Br_2 (Impey et al., 1999), HCHO (Sumner and Shepson, 1999; Hutterli et al., 1999) from the snowpack. CH_3CHO and $(CH_3)_2CO$ were also found to be elevated in snowpack air and released from the snowpack at a rate similar to that of HCHO (Couch et al., 2000). Photochemical production of NO_x in snowpacks has been found to occur at mid- and high-latitudes in the northern hemisphere (Honrath et al., 1999, 2000; Ridley et al., 2000) as well as in the Antarctic (Jones et al., 2000; Davis, personal communication). The early conclusion is that these NO_x emissions are related to the photolysis of nitrate (which present in the snow). This conclusion was supported by a more controlled lab experiment (Honrath et al., 2000), which used both natural and artificial (i.e., nitrate doped) snow. Ridley et al. (2000) observed a diurnal variation in NO_x and NO_y with amplitudes as large as 30-40 pptv. As Ridley pointed out, such diurnal variation requires large enough NO_x emission to increases its mixing ratio in the boundary layer by 2-8 pptv h^{-1} in the morning hours, and a compatible removal process during the afternoon. The latter maybe due to formation (and removal) of HNO_3 via reaction with OH, which requires [OH] ~ 10^6 molec cm^{-3} (as was measured by Davis and others, at the South Pole; personal communication). The formation of halogen nitrates with subsequent deposition and hydrolysis are also possible.

Recent computer-genereated models indicated that the chemistry, taking place in the snowpack needs to be considered in order to explain the observed surface ozone depletion chemistry in the arctic (Michalowski et al., 2000).

However, in all of the previous photochemical studies, there was no attempt to determine the quantum yields for these processes, mainly due to the difficulty of estimating the specific photon absorption rates for each chromophore.

2.3 Nitrate in Polar Ice

Nitrate is a major ion across most of the polar ice sheet, accounting for about 34 % (in μeq ratios) of the total anions at the South Pole (Legrand and Delmas, 1984), and 43% and 50% of the inorganic anions in recent and pre-industrial ice from Summit Greenland (Whitlow et al., 1992). As a major ion in polar ice, which is also rather easy to analyze, there is large amount of information on nitrate concentrations in snow and ice cores available in the literature. The interpretation of this data in terms of past environmental changes, however, remains unclear. A major difficulty arises from incomplete understanding of the sources of nitrate in polar snow and its fate after deposition.

Deposition of inorganic nitrate (aerosol NO_3^- and gaseous HNO_3) is believed to be the major sink for atmospheric reactive nitrogen oxides, NO_x, (e.g., Logan, 1983; Platt, 1986). Since NO_2 and NO have a strong impact on the mixing ratios of the main tropospheric oxidants (O_3, OH, and HO_2), ice core records of NO_3^- (if preserved) could provide important information regarding the N - cycle in the atmosphere as well as paleoatmospheric and paleoclimatic information. However, since the sources and sinks of

NO_x and HNO_3 are highly variable in time and space, their global distribution and trends in time are still poorly understood.

A positive linear correlation is generally found between the nitrate deposition flux and the snow accumulation rate, with a relatively small y-intercept (Legrand and Delmas, 1986; Legrand and Kichner, 1990; Yang et al., 1995). These results suggest a large atmospheric supply of NO_3^- that is incorporated into snow predominantly by wet deposition (assuming that the intercept represents dry deposition and that it is not significantly altered by post-depositional effects). Hence, if the atmospheric supply of NO_3^- is large enough, nitrate concentration in the snow may represent its atmospheric concentration as long as the deposition environment does not change much.

2.3.2 Sources for Nitrate at High Latitudes

Nitrogen oxides are emitted from the Earth's surface (via anthropogenic emissions, biomass burning, soil exhalation) as well as produced within the atmosphere by various processes including: N_2 fixation by lightning, NH_3 oxidation, N_2O oxidation and oxidation of atomic nitrogen generated by N_2 photolysis or by galactic and solar energetic particles deposition (Fig. 2.1).

Legrand and Kirchner (1990) showed that there is no evidence of a correlation between the NO_3^- content of south polar snow and solar activity (11-year solar cycle, low solar activity time period, and solar proton events). Thus, NO_x production above the middle stratosphere appears to be an insignificant source of NO_3^- to the Antarctic troposphere. On the other hand, nitrate profiles sampled along the route of the International Trans-Antarctic expedition indicated that nitrate distribution may be affected by electron fluxes (Dahe et al., 1992). For the southern hemisphere, Legrand and

Kirchner (1990) suggested a major contribution to the NO_3^- content of high latitude precipitation by lightning at mid-low latitudes (30 to 50 %) and by NO_x produced in the lower stratosphere (~ 33 %), with the remaining portion related to surface sources of NO_x. Stratospheric NO_y can reach the troposphere via air exchange and via deposition of polar stratospheric clouds (PSCs). Due to warmer winter temperatures (less PSC sedimentation), this source is less significant over the Arctic. Nitrate profiles from Southern Greenland ice suggest a larger contribution to the NO_3^- budget of the high latitudes at the northern hemisphere from surface sources (with PAN as a major carrier to high latitudes), especially over the past few decades due to increasing anthropogenic NO_x emissions (Neftel et al., 1985; Mayewski et al., 1986).

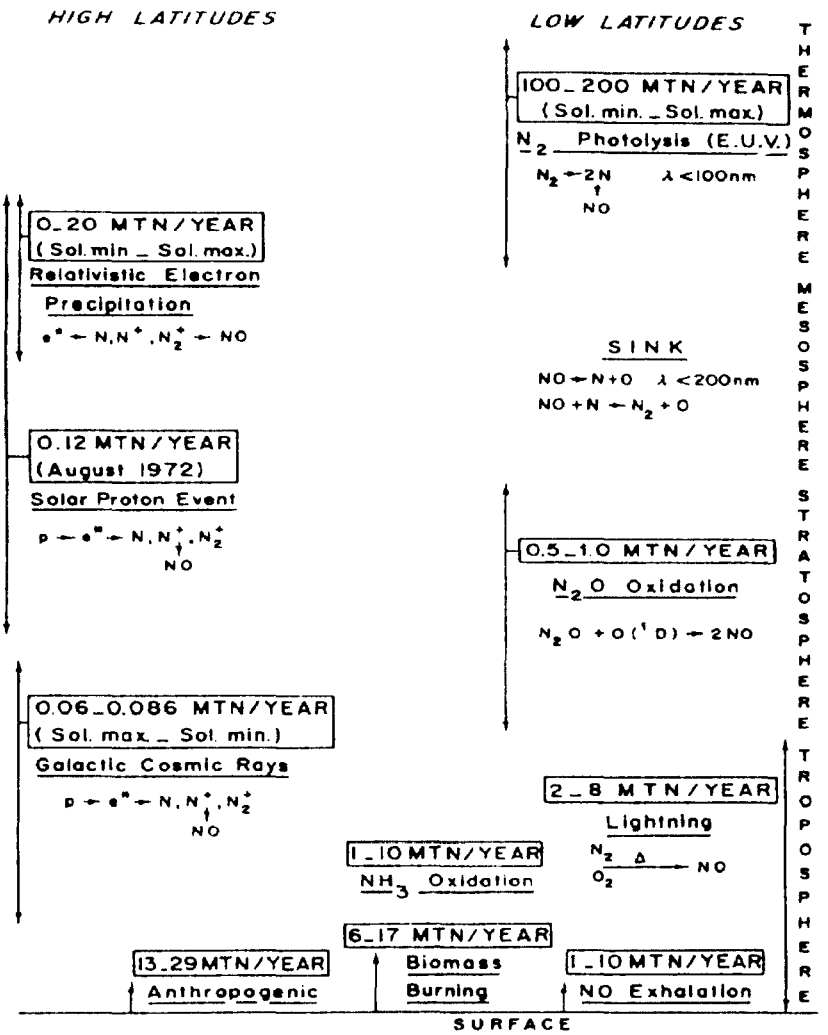

Figure 2.1. Altitudes and latitudes of the atmosphere where various NO_x production mechanisms take place (Legrand and Kirchner, 1990).

2.3.3 Postdepositional Processing of Nitrate

There is strong evidence for postdepositional losses of NO_3^- from the snow pack, which include rapid loss of nitrate from surface snow within days of deposition, followed by a slower loss which may take several years in low accumulation sites (Neubauer and

Heumann, 1988a,b; Mayewski and Legrand, 1990; Silvente and Legrand, 1995; Wolff, 1995, Yang et al., 1995). The mean levels of nitrate in polar ice cores are around 10-100 $ng \cdot g^{-1}$, while nitrate in surface snow may reach levels above 300 $ng \cdot g^{-1}$. The processes involved in this nitrate loss are still unclear. Candidate processes include photochemical destruction of nitrate, wind-scouring of the surface layer, volatilization of nitric acid, and scavenging of nitrate by other wind-blown particles or gases, probably aided by wind-pumping of the snowpack (e.g., Pomeroy and Jones, 1996).

High levels of nitrate in Antarctica ice from glacial periods (Legrand et al., 1999) and at the High Qinghai-Tibetan Plateau (Hou et al., 1999) coincide with elevated concentrations of mineral dust. These observations may reflect efficient scavenging of HNO_3 by mineral dust (Legrand et al., 1988) and / or that postdepositional nitrate loss is limited in the presence of high levels of mineral dust (Legrand et al., 1999). In Greenland, on the other hand, nitrate levels in ice cores are lower during the last glacial maximum. The reason for this decrease is still unclear but it seems to represent a genuine reduction in source emissions, transport or deposition efficiency (Wolff, 1995).

2.3.4 Seasonal Cycle of Nitrate Deposition

Despite the postdepositional loss of nitrate and the potential for diffusional smoothing, many high-resolution studies of ice cores show a clear seasonal cycle (e.g., Mulvaney et al., 1998). In Antarctica, the nitrate records show a seasonal maximum in spring to mid-summer, which is believed to be of stratospheric origin, and two secondary peaks at late summer (stratospheric air mass exchange) and in late winter (PSC sedimentation) (Legrand et al., 1999). The seasonal pattern of nitrate deposition in

Greenland has been altered during the past several decades. A persistent summer maximum is observed in Greenland ice over the last 800 years. Yang and coworkers (1995) suggested that this might be due to NO_x released from PAN by thermal decomposition in the presence of higher OH concentration in summer. In modern Greenland snow, additional nitrate deposition peaks occur in late winter (Wolff, 1995). These winter peaks are probably the result of higher pollution input into the Arctic at this time when the polar front lies further south (Heidam, 1986; Barrie, 1986).

2.4 Nitrate Photolysis in The Aqueous Phase

The aqueous photochemistry of nitrate has been the focus of numerous studies, with emphasis on elucidation of nitrate's electronic transition (e.g., Meyerstein and Treinin, 1961; Strickler and Kasha, 1964, Maria et al., 1973) and the mechanism and products of its photolysis (e.g., Zepp et al., 1987; Warneck and Wurzinger, 1988; Alif and Boula, 1991; Mark et al., 1996; Jankowski et al., 1999; Mack and Bolton, 1999). The ultraviolet absorption spectum of aqueous nitrate solutions (Fig. 2.2) feature a weak band with a maximum at 305 nm (7.5 M^{-1} cm^{-1}) and a stronger band with a maximum at 201 nm (9500 M^{-1} cm^{-1}). The intense band is regarded as a π–π^* transition and the weak band as the highly forbidden n-π^* transition (Fig. 2.3), although it is also suggested that the latter may be complex, containing both singlet and triplet n-π^* and σ–π^*excitation (Strickler and Kasha, 1964; Maria et al., 1973).

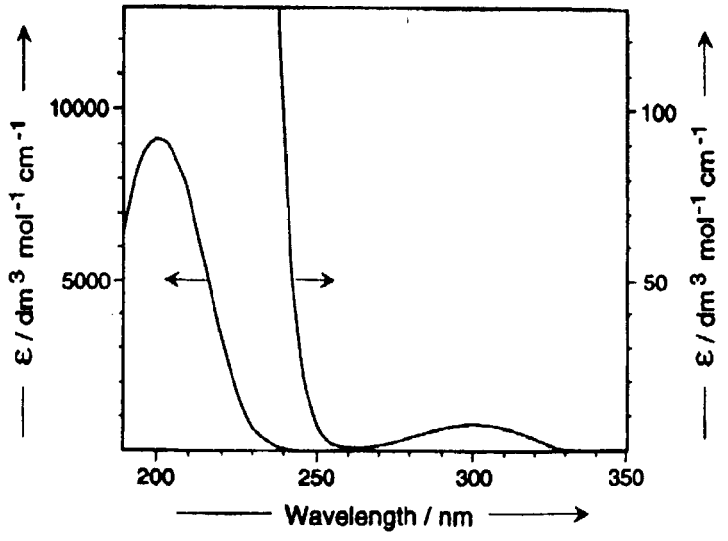

Figure 2.2. UV absorption spectrum of aqueous nitrate (Mark et al., 1996).

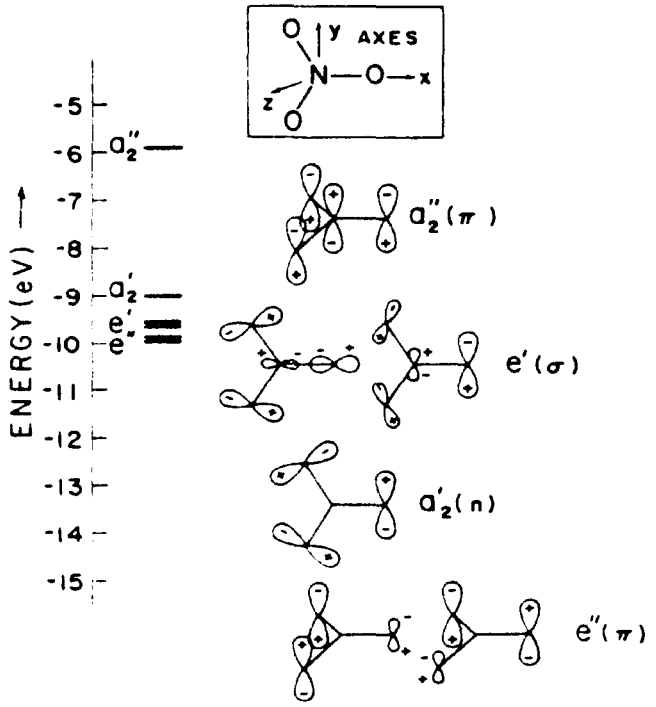

Figure 2.3 Molecular orbital energy diagram for NO_3^-. The forms of the MOs are represented in pictorial form on the right (Maria et al., 1973).

The overall stoichiometry for NO_3^- photolysis is (see also fig. 2.4):

$$NO_3^- + h\nu \rightarrow NO_2^- + \tfrac{1}{2} O_2 \qquad (5)$$

In the absence of $^{\cdot}OH$ scavengers, this stoichiometry is thought to be maintained over the entire pH range during irradiation with $\lambda > 200$ nm (Shuali et al., 1969; Wagner et al., 1980). Isotope enrichment studies indicate that NO_3^- is the origin of both O atoms in the generated O_2 (Bayliss and Bucat, 1975). The $\lambda > 300$ nm photolysis of nitrate is believed to proceed via two primary pathways:

$$NO_3^- + H^+ + h\nu \rightarrow NO_2 + OH \qquad \phi \sim 9 \times 10^{-3} \qquad (6)$$

$$NO_3^- + h\nu \rightarrow NO_2^- + O(^3P) \qquad \phi \sim 1 \times 10^{-3} \qquad (7)$$

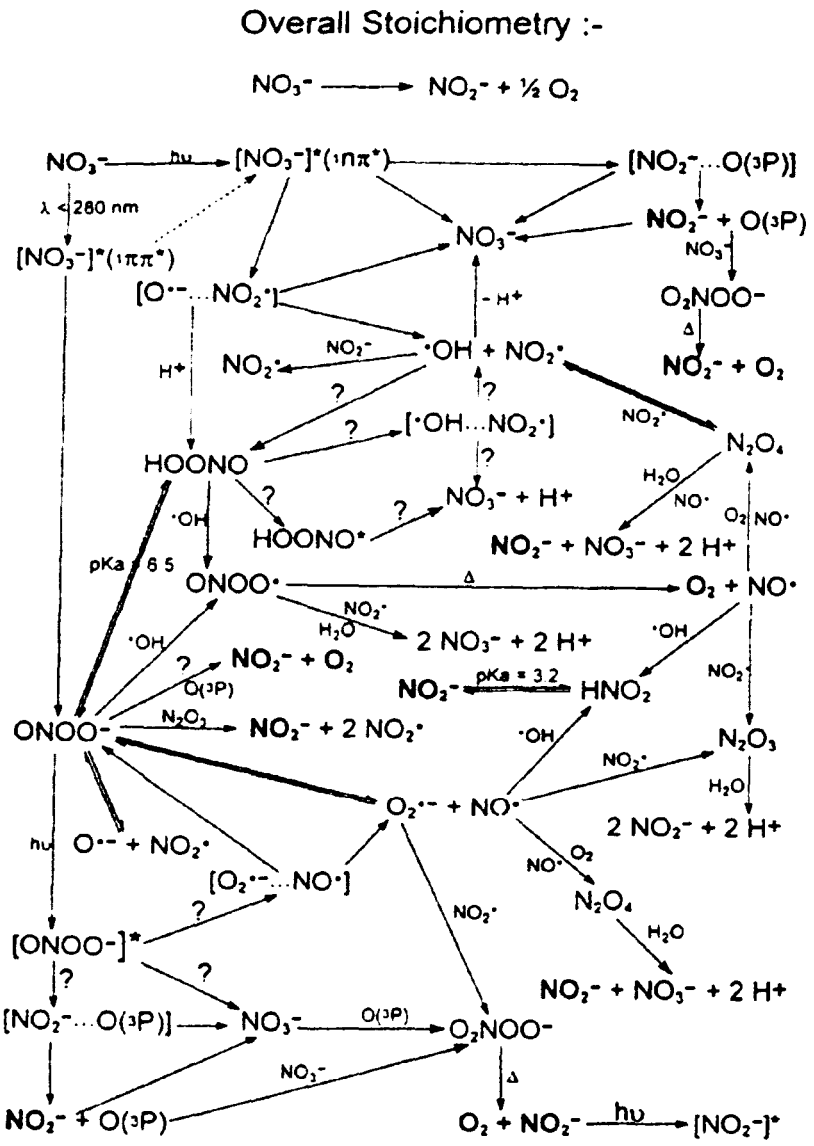

Figure 2.4 Primary photoprocess and subsequent reactions during nitrate photolysis (from Mack and Bolton, 1999).

A third primary pathway is the formation of peroxynitrite anion, $ONOO^-$, via the isomerization of $[NO_3^-]^*$ during irradiation at $\lambda < 280$ nm (Mack and Bolton, 1999):

$$[NO_3^-]^* \rightarrow ONOO^- \leftrightarrow HOONO \qquad pK_a = 6.5 \qquad (8)$$

There is an additional pathway leading to $ONOO^-$, since the radicals formed in reaction 1 can recombine within the solvent cage to form peroxynitrous acid (HOONO). At pH < 7, HONOO isomerizes rapidly to nitrate (Wagner et al., 1980). Under basic conditions however, this reaction slows dramatically due to higher stability of $ONOO^-$ at higher pH.

The O-atoms generated in reaction 3 may react with O_2 ($[O_2]_{water}$ ~ 0.3 mM) via reaction 9 or with nitrate via reaction 10. Nitrite (ε_{max}= 22.5 M^{-1} cm^{-1} at 360 nm) will undergo secondary photolysis, reaction 11, and oxidation by OH radicals, reaction 12:

$$O_2 + O(^3P) \rightarrow O_3 \qquad k_3 = 4 \times 10^9\ M^{-1}\ s^{-1} \qquad (9)$$

$$NO_3^- + O(^3P) \rightarrow NO_2^- + O_2 \qquad k_4 = 2 \times 10^8\ M^{-1}\ s^{-1} \qquad (10)$$

$$NO_2^- + H^+ + h\nu \rightarrow NO + OH \qquad \phi \sim 0.06 \qquad (11)$$

$$NO_2^- + OH \rightarrow NO_2 + OH^- \qquad k_6 = 2 \times 10^{10}\ M^{-1}\ s^{-1} \qquad (12)$$

Warneck and Wurzinger (1988) reported the formation of OH and $O(^3P)$ in relatively low quantum yields: 0.9 % and 0.01 %, respectively. ϕ_{+OH} increases at shorter and longer wavelengths within the $n \rightarrow \pi^*$ band, and increases by a factor of 2.2 between 273 K and 308 K (Jankowski et al., 1999).

The quantum yield for nitrite production, $\phi_{NO_2^-}$, has been shown to increase with increasing pH (Daniels et al.,1968; Shuali et al., 1969; Mark et al., 1996). However, additional nitrite is generated during the decay of $ONOO^-$ when the solutions are acidified as part of traditional colorimetric nitrite assays (Plumb et al., 1992). Thus, many of the reported values for ϕ_{NO_2} from studies of nitrate photolysis before 1990 appear to be

flawed. In addition, the increasing stability of $ONOO^-$ at pH > 7 can produce additional nitrite via reactions 13 to 16 (Kissner et al., 1997):

$$ONOO^- + {}^{\cdot}OH \rightarrow ONOO^{\cdot} + OH^- \qquad k_8 = 5\times10^9\ M^{-1}\ s^{-1} \qquad (13)$$

$$ONOO^{\cdot} \rightarrow NO^{\cdot} + O_2 \qquad (14)$$

$$NO^{\cdot} + NO_2^{\cdot} \rightarrow N_2O_3 \qquad k_{10} = 1.1\times10^9\ M^{-1}\ s^{-1} \qquad (15)$$

$$N_2O_3 + H_2O \rightarrow 2NO_2^- + 2H^+ \qquad k_{11} = 5.3\times10^2\ s^{-1} \qquad (16)$$

2.5 Organic Matter in Polar Ice

The concentrations and reactivity of organic compounds in Polar Regions (especially in Antarctica) have received less attention than inorganic compounds. However, it is well known now that during winter time, the Arctic (and to a lesser extent the Antarctic) atmosphere contains variety of anthropogenic species, including numerous organic and inorganic species (Rahn, 1985: Wolff, 1992). Legrand et al. (1992) studied ammonium perturbations in Greenland snow. These summertime events were accompanied by an increase of organic acid levels ($HCOO^-$, CH_3COO^-, $C_2O_4^=$, and $C_2H_3SO_3$), and were suggested to originate from high latitude forest fires. Atmospheric measurements in Summit, Greenland (Dibb et al., 1994) showed very high concentrations of formic and acetic acid (more than an order of magnitude higher than p-$SO_4^=$), yet their concentrations in the snow were orders of magnitude less than both NO_3^- and $SO_4^=$. Resent investigations of several water soluble organic carbon and carbonyls (e.g., HCHO, CH_3CHO, $CH_3C(O)CH_3$) in fresh snow and snowpack at Alert, Canada (Leithead et al., 2000; Couch et al., 2000), indicated that these compounds undergo physicochemical processing in the snowpack. These processes, which also occur during the dark, appear to

drive the loss of the above organics from the snowpack. The level of these organic compounds in surface snow increased during light periods, which indicated that they were, at least partially, the result of photochemical production from organic matter trapped in snow (Leithead et al., 2000; Houdier et al., 2000).

Since atmospheric aerosols contain a substantial fraction of humic-like material, it is possible that this natural organic matter (NOM) will be deposited on polar ice sheets as well (Kawamura, 1996). Light absorption by NOM in surface water will result indirect production of singlet oxygen (Schwarzenbach et al., 1993), which can lead to the formation of hydroperxyl radical and eventually to organic peroxides (Hoffmann, 1996).

References

1. Abbatt J. P. D. and Molina M. J. (1992) The Heterogeneous reaction HOCl + HCl $\longrightarrow$ Cl_2 +H_2O on Ice and Nitric Acid Trihydrate: Reaction Probabilities and Stratospheric Implications. *Geophys. Res. Lett.* 19, 461-464.
2. Alif A. and Boule P. (1991) Photochemistry and Environment Part XIV. Phototransformation of Nitrophenols Induced by Excitation of Nitrite and Nitrate Ions. *J. Photochem. Photobio. A: Chem.* 59, 357-367.
3. Allamandola L. J., Sandford S. A., and Valero G. J. (1988) Photochemical and Thermal Evolution of interstellar/Precometary Ice Analogs. *Icarus* 76, 225-252.
4. Anderson L. D., Roberts J. T., and Grassian V. H. (1998) The 367 nm Photochemistry of Chlorine Dioxide in and on Amorphous Ice. *Laser Tech. Surf. Sci. III* 3272, 286-295.
5. Bales R. C. and Wolff E. W. (1995) Processes of Chemical Exchange Between the Atmosphere and Polar Snow: Key to Interpreting Natural Climate Signals in Ice Cores. *EOS, Transactions, American Geophysical Union* 76, 477, 482-483.
6. Barkstrom B. R. (1972) Some Effects of Multiple Scattering on the Distribuion of Solar Radiation in Snow and Ice. *J. of Glaciology* 11, 357-368.
7. Barrie L. A. (1986) Arctic Air Chemistry: an Overview. In *Studies in Polar Research: Arctic Air Pollution* (ed. B. Stonehouse). Cambridge University Press.
8. Bayliss N. S. and Bucat R. B. (1975) The Photolysis of Aqueous Nitrate Solutions. *Aust. J. Chem.* 28, 1865-1878.
9. Beaglehole D., Ramanathan B., and Rumberg J. (1998) The UV to IR Transmittance of Antarctic Snow. *J. Geophys. Res.-Atmos.* 103, 8849-8857.

10. Bernstein M. P., Sandford S. A., Allamandole J. L., Seb Gillette J., Clemett S. J., and Zare R. N. (1999) UV Irradiation of Polycyclic Aromatic Hydrocarbons in Ices: Production of Alcohols, Quinones, and Ethers. *Science* 283, 1135-1138.

11. Bernstein M. P., Sandford S. A., et al. (1994) Infrared-Spectrum of Matrix-Isolated Hexamethylenetetramine in Ar and Water at Cryogenic Temperatures. *J. Phys. Chem.* 98, 12206-12210.

12. Chappellaz J. et al. (1997) CH_4 and Delta O-18 of O_2 Records from Antarctic and Greenland Ice: A Clue for Stratigraphic Disturbance in the Bottom Part of the Greenland Ice Core Project and the Greenland Ice Sheet Project 2 Ice Cores. *J. Geophys. Res. - Ocean* 102, 26547-26557.

13. Conklin M. H. and Bales R. C. (1993) SO_2 Uptake On Ice Spheres - Liquid Nature of the Ice-Air Interface. *J. of Geophys. Res.-Atmos.* 98, 16851-16855.

14. Couch T. L., Sumner A. L., Dassau T. M., Shepson P. B., and Honrath R. E. (2000) An Investigation of the Interaction of Carbonyl Compounds with the Snowpack. *Geophys. Res. Lett.* 27(15), 2241-2244.

15. Dahe Q., Zeller E. J., and Drechhoff G. A. M. (1992) The Disribution of Nitrate Content in the Surface Snow of the Antarctic Ice Sheet Along the Route of the 1990 International Trans-Antarctica Expedition. *J. of Geophys. Res.* 97, 6277-6284.

16. Daniels M., Meyers R.V., and Belardo E. V. (1968) Photochemistry of the Aqueous Nitrate System. I. Excitation in the 300 nm Band. *J. Phys. Chem.* 72, 389-398.

17. Dash, J.G. (1989) Thermomolecular Pressure in Surface Melting - Motivation For Frost Heave, *Science*, *246*, 1591-1593.

18. Dash J. G., Fu H. Y., and Wettlaufer J. S. (1995) The Premelting of Ice and Its Environmental Consequences. *Rep. Prog. Physic.* 58, 115-167.

19. Dibb J. E., Talbot R. W., and Bergin M. H. (1994) Soluble Acidic Species in Air and Snow At Summit, Greenland. *Geophys. Res. Lett.* 21, 1627-1630.

20. Doppenschmidt A. and Butt H. J. (2000) Measuring the Thickness of the Liquid-Like Layer on Ice Surfaces with Atomic Force Microscopy. *Langmuir* 16, 6709-6714.

21. Doppenschmidt A., Kappl M., and Butt H. J. (1998) Surface Properties of Ice Studied by Atomic Force Microscopy. *J. of Phys. Chem. B* 102, 7813-7819.

22. Faraday M. (1850) *Athenaeum* 1181, 640.

23. Finnegan W. G., Pitter R. L., and Young L. G. (1991) Preliminary-Study of Coupled Oxidation Reduction Reactions of Included Ions in Growing Ice Crystals. *Atmos. Environ. A -General Topics* 25, 2531-2534.

24. Fu H. Y. and Dash J. G. (1993) Characterization of Frost Susceptibility of Soils by Mercury Porosimetry. *J. Coll. Inter. Sci.* 159, 343-348.

25. Gay J. M., Suzanne J., Dash J. G., and Fu H. Y. (1992) Premelting of Ice in Exfoliated Graphite - a Neutron- Diffraction Study. *J. Crystal Growth* 125(1-2), 33-41.

26. Goto K., Hondoh T., and Higashi A. (1986) Determination of Diffusion Coefficients of Self-Interstitials in Ice With a New Method of Observing Climb of Dislocations by X-ray Topography. *Jpn. J. App. Phys.* 25, 351-357.

27. Graham J. D., Roberts J. T., Anderson L. D., and Grassian V. H. (1996) The 367 nm Photochemistry of OClO Thin Films and OClO Adsorbed on Ice. *J. Phys. Chem.* 100, 19551-19558.

28. Heidan N. Z. (1986) The Greenland Aerosols: Elemental Composition, Seasonal Variations and Likely Sources. In *Studies in Polar Research: Arctic Air Pollution* (ed. B. Stonehouse). Cambridge University Press.

29. Hobbs P. V. (1974) *Ice Physics*, Clarendon, Oxford.

30. Hoffmann M. R. (1996) Possible Chemical Transformations in Snow and Ice Induced by Solar (UV Photons) and Cosmic Irradiation (Muons). In *Chemical Exchange Between the Atmosphere and Polar Snow* (ed. W. Wolff and R. C. Bales), pp. 353-377. Springer.

31. Honrath R. E., Guo S., Peterson M. C., Dziobak M. P., Dibb J. E., and Arsenault M. A. (2000) Photochemical Production of Gas-Phase NOx from Ice-Crystal NO_3^-. *J. Geophys. Res. – Atmos.*, *105*, 24183-24190. (b) Honrath R. E., Peterson M. C., Dziobak M. P., Green S., Dihbb J. E., and Arsenault M. A. (2000) Release of NO_x from Sunlight-Irradiated Midlatitude Snow. *Geophys. Res. Lett. 27*, 2237-2240.

32. Honrath R. E., Peterson M. C., Guo S., Dibb J. E., Shepson P. B., and Campbell B. (1999) Evidence of NOx Production within or upon Ice Particles in the Greenland Snowpack. *Geophys. Res. Lett.* 26, 695-698.

33. Hou S. G., Qin D. H., and Ren J. W. (1999) Different Post-Depositional Processes of NO_3^- in Snow Layers in East Antarctica and on the Nnorthern Qinghai-Tibetan Plateau. In *Annal. Glacio.* 29, 73-76.

34. Houdier S., Perrier S., Domine F., Cobanes A., Legagneux L., Grannas A. M., Guimbaud C., Shepson P. B., Boudries H., and Bottenheim J. (2000) Snow-Phase Acetaldehyde (CH_3CHO) and Acetone $(CH_3)_2CO$ in the Arctic Snowpack. *AGU* Meeting, San Francisco.

35. Hutterli M. A., Rothlisberger R., and Bales R. C. (1999) Atmosphere-to-Snow-to-Firn Transfer Studies of HCHO at Summit, Greenland. *Geophys. Res. Lett.* 26, 1691-1694.

36. Impey G. A., Mihele C. M., Anlauf K. G., Barrie L. A., Hastie D. R., and Shepson P. B. (1999) Measurements of Photolyzable Halogen Compounds and Bromine Radicals during the Polar Sunrise Experiment 1997. *J. Atmos. Chem.* 34, 21-37.

37. Impey G. A., Shepson P. B., Hastie D. R., Barrie L. A., and Anlauf K. G. (1997) Measurements of Photolyzable Chlorine and Bromine during the Polar Sunrise Experiment 1995. *J. Geophys. Res.-Atmos.* 102, 16005-16010.

38. Jankowski J. J., Kieber D. J., and Mopper K. (1999) Nitrate and Nitrite Ultraviolet Actinometers. *Photochem. Photobio.*70, 319-328.

39. Jones A. E., Weller R., Wolff E. W., and Jacobi H.-W. (2000) Speciation and Rate of Photochemical NO and NO_2 Production in Antarctic Snow. *Geophys. Res. Lett.* 27, 345-348.

40. Kawamura, K., I. Suzuki, Y. Fujii, and O. Watanabe, Ice Core Record of Fatty Acids over the Past 450 Years in Greenland, *Geophys. Res. Lett. 23*, 2665-2668, 1996.

41. Kissner R., Nauser T., Bugnon P., Lye P. G., and Koppenol W. H. (1997) Formation and Properties of Peroxynitrite as Studied by Laser Flash Photolysis, High-Pressure Stopped-Flow Technique, and Pulse Radiolysis. *Chem. Res. Toxic.* 10, 1285-1292.

42. Klan P., Ansorgova A., Del Favero D., and Holoubek I. (2000a) Photochemistry of chlorobenzene in ice. *Tetrahedron Lett.* 41, 7785-7789.

43. Klan P., Janosek J., and Kriz Z. (2000b) Photochemistry of Valerophenone in Solid Solutions. *J. Photochem. and Photobio A-Chemistry* 134, 37-44.

44. Lee S. H., Leard D. C., Zhang L. R., Molina L. T., and Molina M. J. (1999) The HCl +$ClONO_2$ Reaction Rate on Various Water Ice Surfaces. *Chem. Phys. Lett.* 315, 7-11.

45. Legrand M. (1997) Ice-Core Records of Atmospheric Sulphur. *Philos. T. Roy. Soc. B* 352, 241-250.

46. Legrand M. R. and Delmas R. J. (1984) The Ionic Balance of Antactic Snow: a 10-Year Detailed Record. *Atmos. Environ.* 18, 1867-1874.

47. Legrand M. R. and Delmas R. J. (1986) Relative Contributions of Tropospheric and Stratospheric Sources for Nitrate in Antarctic Snow. *Tellus* 38B, 236-249.

48. Legrand M. R. and Kirchner S. (1990) Origins and Variations of Nitrate in South Polar Precipitation. *J. Geophys. Res.-Atmos.* 95, 3493-3507.

49. Legrand M. R., Lorius C., Barkov N. I., and Petrov V. N. (1988) Vostok (Antarctica) Ice Core - Atmospheric Chemistry Changes Over the Last Climatic Cycle (160,000 Years). *Atmos. Environ.* 22, 317-331.

50. Legrand M., Wolff E., and Wagenbach D. (1999) Antarctic Aerosol and Snowfall Chemistry: Implications for Deep Antarctic Ice-Core Chemistry. In *Annal. Glaciology,* 29, 66-72.

51. Leithead A., Li S. M., Toom-Sauntry D., Anderson K., and Gaudenzi A. (2000) Water Soluble Organic Carbon and Carbonyls in Fresh Snow and Snowpack During the Alert 2000 Experiment. *AGU* Meeting, San Francisco.

52. Logan J. A. (1983) Nitrogen Oxides in the Troposphere: Global and Regional Budgets. *J. of Geophys. Res.* 88, 10785-10807.

53. Lowen, H. (1994) Melting, Freezing and Colloidal Suspensions, *Physics Rep. 237,* 249-324.

54. Mack J. and Bolton J. R. (1999) Photochemistry of Nitrite and Nitrate in Aqueous Solutions: A Review. *J. Photochem. Photobio.* 128, 1-13.

55. Maria H. J., McDonald J. R., and McGlynn S. P. (1973) Electronic Absorption Spectrum of Nitrate Ion and Boron Trihalides. *J. Am. Chem. Soc.* 95, 1050-1056.

56. Mark G., Korth H. G., Schuchmann H. P., and von Sonntag C. (1996) The Photochemistry of Aqueous Nitrate Ion Revisited. *J. Photochem. and Photobio. A: chemistry* 101, 89-103.

57. Maruyama M., Bienfait M., Dash J. G., and Coddens G. (1992) Interfacial Melting of Ice in Graphite and Talc Powders. *J. of Crystal Growth* 118, 33-40.

58. Mayewski P. A. and Legrand M. R. (1990) Recent Increase in Nitrate Concentration of Antarctic Snow. *Nature* 346, 258-260.

59. Mayewski P. A., Lyons W. B., Spencer M. J., Twickler M., Dansgaard W., Koci B., Davidson C. I., and Honrath R. E. (1986) Sulfate and Nitrate Concentrations From a South Greenland Ice Core. *Science* 232, 975-977.

60. McElroy M. B., Salawitch R. J., Wofsy S. C., and Logan J. A. (1986) Reductions of Antarctic Ozone Due to Synergistic Interactions of Chlorine and Bromine. *Nature* 321, 759-762.

61. Meyerstein D. and Treinin A. (1961) Absorption spectra of NO_3^- in Solution. *Trans. Faraday Soc.* 57, 2104-2112.

62. Michalowski B. A., Francisco J. S., Li S. M., Barrie L. A., Bottenheim J. W., and Shepson P. B. (2000) A Computer Model Study of Multiphase Chemistry in the Arctic Boundary Layer During Polar Sunrise. *J. Geophys. Res. - Atmos.* 105, 15131-15145.

63. Miranda P. B., Xu L., Shen Y. R., and Salmeron M. (1998) Icelike water monolayer adsorbed on mica at room temperature. *Phys. Rev. Lett.* 81, 5876-5879.

64. Molina M. J. (1991) Heterogeneous Chemistry On Polar Stratospheric Clouds. *Atmos. Environ. Part a-General Topics* 25, 2535-2537.

65. Mulvaney R., Wagenbach D., and Wolff E. W. (1998) Postdepositional change in snowpack nitrate from observation of year-round near-surface snow in coastal Antarctica. *J. Geophys. Res.* 103, 11021-11031.

66. Neftel A. (1991) Use of Snow and Firn Analysis to Reconstruct Past Atmospheric Composition. In *NATO ASI Series*, Vol. G 28 (ed. T. D. D. e. al.), pp. 385-411. Springer-Veriag Berlin Heidelberg.

67. Neftel A., Beer J., Oeschger H., Zurcher F., and Finkel R. C. (1985) Sulfate and Nitrate Concentrations in Snow From South Greenland 1895-1978. *Nature* 314, 611-613.

68. Neftel A., Beer J., Oeschger H., Zurcher F., and Finkel R. C. (1985) Sulfate and Nitrate Concentrations in Snow From South Greenland 1895-1978. *Nature* 314, 611-613.

69. Neubauer J. and Heumann K. G. (1988a) Determination of Nitrate at the ng/g Level in Antarctic Snow Samples with Ion Chromatography and Isotope Dilution Mass Spectrometry. *Fres. Z. Anal. Chem.* 331, 170-173.

70. Neubauer J. and Heumann K. G. (1988b) Nitrate Trace Determinations in Snow and Firn Core Samples of Ice Shelves at the Weddell Sea, Antarctica. *Atmos. Environ.* 22, 537-545.

71. Perovich D. K. and Govani J. W. (1991) Absorption-Coefficients of Ice from 250 to 400 nm. *Geophys. Res. Lett.* 18, 1233-1235.

72. Platt U. (1986) The Origin of Nitrous and Nitric Acid in the Atmosphere. In *Chemistry of Multiphase Atmospheric Systems* (ed. W. Jaeschke). Springer-Verlag.

73. Plumb R. C., Edwards J. O., and Herman M. A. (1992) Problem of Concurrent Measurements of Peroxonitrite and Nitrite Contents. *Analyst* 117, 1639-1641.

74. Pomeroy J. W. and Jones H. G. (1996) Wind-Blown Snow: Sublimation, Transport and Changes to Polar Snow. In *Chemical Exchange Between the Atmosphere and Polar Snow, NATO ASI Ser., Ser. I*, Vol. 43 (ed. E. W. Wolff and R. C. Bales), pp. 453-489. Springer-Verlag.

75. Pursell C. J., Conyers J., Alapat P., and Parveen R. (1995) Photochemistry of Chlorne Dioxide in Ice. *J. Phys. Chem.* 99, 10433-10437.

76. Pursell C. J., Conyers J., and Denison C. (1996) Photochemistry of Chlorne Dioxide in Polycrystalline Ice (T=140-185 K): Production of Chloryl Chloride, Cl-(OClO). *J. Phys. Chem.* 100, 15450-15453.

77. Rahn K. A. (1985) Progress in Arctic Air Chemistry, 1980-1984. *Atmos. Environ.* 19, 1987-1994.

78. Ridley B., Walega J., Montzka D., Grahek F., Atlas E., Flocke F., Stroud V., Deary J., Gallant A., Boudries H., Bottenheim J., Anlauf K., Worthy D., Sumner A. l., Splawn B., and Shepson P. (2000) Is the Arctic Surface Layer a Source and Sink of NO_x in Winter/Spring? *J. of Atmos. Chem.* 36, 1-22.

79. Salmeron M. and Bluhm H. (1999) Structure and properties of ice and water film interfaces in equilibrium with vapor. *Surface Rev. Lett.* 6, 1275-1281.

80. Schutte W. A. and Gerakines P. A. (1995) Recent Results from the Leiden Observatory Laboratory: (a) Band Strength in Mixed Ices; (b) UV Photolysis of Solid Methanol. *Planet. Space. Sci.* 43, 1253-1256.

81. Schwarzenbach R. P., Gschwend P. M., and Imboden D. M. (1993) *Environmental Organic Chemistry*. John Wiley & Sons, INC.

82. Shuali U., Ottolenghi M., Rabani J., and Yelin Z. (1969) On the Photochemistry of Aqueous Nitrate Solutions Exited in the 195-nm Band. *J. Phys. Chem.* 73, 3445-3451.

83. Silvente E. and Legrand A. (1995) A preliminary Study of the Air-Snow Relationship for Nitric Acid in Greenland. In *Ice Cores Studies of Global Biogeochemical cycles, NATO ASI ser. Ser I*, Vol. 30 (ed. R. J. Delmas), pp. 225-240. Springer-Verlag.

84. Solomon S., Garcia R. R., Rowland F. S., and Wuebbles D. J. (1986) On the Depletion of Antarctic Ozone. *Nature* 321, 755-758.

85. Sommerfeld R. A., Knight C. A., and Laird S. K. (1998) Diffusion of HNO_3 in Ice. *Geophys. Res. Lett.* 25, 935-938.

86. Strickler S. J. and Kasha M. (1964) *Molecular Orbitals in Chemistry, Physics and Biology*. Academic Press.

87. Sumner A. L. and Shepson P. B. (1999) Snowpack Production of Formaldehyde and its Effect on the Arctic Troposphere. *Nature* 398, 230-233.

88. Takagi S. (1990) Approximate Thermodynamics of the Liquid-Like Layer on an Ice Sphere Based on an Interpretation of the Wetting Parameter. *J. Coll. Inter. Sci.* 137, 446-455.

89. Takenaka N., Diamon T., Ueda A., Sato K., Kitano M., Bandow H., and Maeda Y. (1998) Fast Oxidation Reaction of Nitrite by Dissolved Oxygen in the Freezing Process in the Tropospheric Aqueous Phase. *J. Atmos. Chem.* 29, 135-150.

90. Takenaka N., Ueda A., Daimon T., Bandow H., Dohmaru T., and Maeda Y. (1996) Acceleration Mechanism of Chemical Reaction by Freezing: The Reactionof Nitrous Acid with Dissolved Oxygen. *J. Phys. Chem.* 100, 13874-13884.

91. Thibert E. and Domine F. (1998) Thermodynamics and Kinetics of the Solid Solution of HNO_3 in Ice. *J. Phys. Chem. B* 102, 4432-4439.

92. Wagner I. and Strehlow H. (1982) *Z. Phys. Chemie. Neue Folge* 132, 151.

93. Wagner I., Strehlow H., and Busse G. (1980) *Z. Phys. Chemie. Neue Folge* 123, 1.

94. Warneck P. and Wurzinger C. (1988) Product Quantum Yield for the 305-nm Photodcomposition of NO_3^- in Aqueous Solution. *J. Phys. Chem.* 92, 6278-6283.

95. Warren S. G. (1982) Optical-Properties of Snow. *Rev. Geophys.* 20, 67-89.

96. Wei X., Miranda P. B., and Shen Y. R. (2001) Surface vibrational spectroscopic study of surface melting of ice. *Phys. Rev. Lett.* 86, 1554-1557.

97. Wettlaufer J. S. (1999) Impurity effects in the premelting of ice. *Phys. Rev. Lett.* 82, 2516-2519.

98. Wettlaufer, J.S., and Dash J.G. (2000) Melting below zero, *Sci. Am. 282*, 50-53.

99. Whitlow S., Mayewski P. A., and Dibb J. E. (1992) A Comparison of Major Chemical-Species Seasonal Concentration and Accumulation at the South Pole and Summit, Greenland. *Atmos. Environ. A - General Topics* 26, 2045-2054.

100. Woafo P., Takontchoup R., and Bokosah A. S. (1995) Soliton Mechanism of Proton Migration in Hydrogen-Bonded Solids. *J. Phys. Chem. of Solids* 56, 1277-1283.

101. Wolff E. W. (1992) The Influence of Global and Local Atmospheric Pollution on the Chemistry of Antarctic Snow and Ice. *Marine Pollution Bulletin* 25, 274-280.

102. Wolff E. W. (1995) Nitrate in Polar Ice. In *Ice Cores Studies of Global Biogeochemical cycles, NATO ASI ser. Ser I*, Vol. I30 (ed. R. J. Delmas), pp. 195-224. Springer-Verlag.

103. Workman E. J. and Reynolds S. E. (1950) Electrical Phenomena Occuring during the Freezing of Dilute Aqueous Solutions and Their Possible Relationship to Thunderstorm Electricity. *Phys. Rev.* 78, 1950.

104. Yang Q., Mayewski P. A., Whitlow S., Twickler M., Morrison M., Talbot R., Dibb J., and Linder E. (1995) Global Perspective of Nitrate Flux in Ice Cores. *J. Geophys. Res.* 100, 5113-5121.

105. Zepp R. G., Hoigne J., and Bader H. (1987) Nitrate-Induced Photooxidation of Trace Organic Chemicals in Water. *Env. Sci. and Tech.* 21, 443-450.

Chapter 3

Photochemical degradation of 4-nitrophenol in ice pellets

(Geophysical Research Letters, **2000**, 27: (20) 3321-3324)

3.1 Abstract

A quantum yield of $\phi_{ice} = 2.3 \times 10^{-4}$ ($\pm$ 4 $\times$ 10^{-5}) was determined for the photochemical degradation of 4-nitrophenol over the wavelength range of 300 to 370 nm in ice pellets (pH 5.6). Five reaction products were identified: hydroquinone, benzoquinone, 4-nitrosophenol, nitrate, nitrite, and the likely formation of organic polymers. The similarities of these results to the observations of 4-nitrophenol photolysis in aqueous solutions indicate that similar mechanisms are operative in both phases. The photochemical decomposition of 4-nitrophenol under conditions similar to those in polar snow and ice suggests that other direct and indirect photochemical process can occur in the polar ice/snow during spring and summer.

3.2 Introduction

Over the last decade there has been a growing interest in the chemical composition of snow packs and ice cores in polar regions (Bales and Wolff, 1995; Chappellaz et al., 1997; Legrand, 1997). In addition, there is increasing evidence for postdepositional chemical alterations in the accumulated ice and snow, including photochemical processes (Honrath et al., 1999,2000; Sumner and Shepson, 1999), that may explain some of the inconsistencies in observed time-series of different chemical species (Sigg and Neftel, 1991; Delmas, 1993; Anklin et al., 1995).

There have been several previous reports of photochemical transformations in ice relative to interstellar or stratospheric ice systems (e.g., Allamandola et al. 1988; Berstein et al.,1995, 1999; Schutte and Gerakines, 1995, and Pursell et al. 1996). These studies have shown that breakage and formation of chemical bonds due to UV radiation can take place in ice. However, all of these studies were done at very low

temperatures (10 K - 200 K) using thin ice films and were addressing the photochemical processes only qualitatively.

4-nitrophenol was selected for the present study as a convenient aromatic chromophore with a strong absorption over the UV range that is relevant for the earth's surface, and that may represent the photochemical behavior of other simple polar aromatic compound in ice. In addition, phenols and nitrophenols are phytotoxic and have been detected in relatively high concentrations (up to 100μg/L) in rain, fog, and snow (e.g., Kawamura and Kaplan, 1986; Alber et al., 1989; Richartz et al., 1990, Herterich and Herrmann, 1990, Levsen et al., 1993). 4-nitrophenol is introduced into the environment by the following processes: combustion from motor vehicles (Tremp et al., 1993), photochemical reactions in the atmosphere during smog photochemical events (e.g., Leone and Seinfeld, 1985), and degradation of pesticides, such as parathion and parathion-methyl (Kishk et al., 1976; Woodrow et al., 1977). Field measurements suggest that 4-nitrophenol is mainly particle-bound and has a longer lifetime in the atmosphere than 2-nitrophenol (Luttke et al., 1997). This suggests that 4-nitrophenol can find its way to the rural areas at the upper latitudes. In this study, the photochemical decomposition of 4-nitrophenol in uniform ice pellets under conditions that are representative of the earth's surface (258 K, 10^5 Pa, and under UV irradiation over the wavelength range of 300 to 370 nm) is clearly demonstrated.

3.3 Experimental Methods

In order to create uniform ice samples that are suitable for light absorption measurements and chemical analysis, a new method was used. Solutions of 250 μM 4-nitrophenol in milli-Q water were frozen and then pulverized at 77 K. Pulverization was achieved using a porcelain mortar and pestle, which were cooled with liquid

nitrogen before and during pulverization. 13 mm × 4 mm polycrystalline ice pellets were made from the ice powder under an applied pressure of 7.1 MPa using a French press. After annealing overnight at 248 K under ambient pressure (10^5 Pa), the pellets were irradiated with light over the wavelength range of 300-370 nm. A high pressure 1000 W Hg-Xe arc lamp was used as a light source in combination with a 320 nm band filter and a 300 nm cutoff filter. The incident light intensity was determined to be 8.5×10^{16} photons·s^{-1}·cm^{-2} using Aberchrome-540 as a chemical actinometer (Heller, 1978). During the experiments, the ice pellets were placed (one at a time) in an isolated slot in a copper block, which was maintained at a constant temperature of 258 K. After irradiation, the pellets were thawed and analyzed using liquid chromatography (HP 1090), ion chromatography (Dionex BIO-LC) and total organic carbon analysis (Shimadzu TOC-5000A). As a result of light scattering and the uncertainties associated with the path length of light propagation through the ice, the light absorbance of the 4-nitrophenol in the pellets was determined using a UV-VIS spectrophotometer (Shimadzu UV-2101 PC) with an attached integrating sphere (Shimadzu ISR-260). This was accomplished with a duplicate set of pellets. The average intensity of scattered light was measured by a photomultiplier located at the bottom of the integrating sphere, which quantifies the light transmission through the pellet, with air used as a reference. The reflections from the pellets were measured off of the ice pellets contained in a slit at the wall of the integrating sphere (with a depth equal to the pellet thickness), with pressed $BaSO_4$ powder used as a reference.

3.4 Results

The percentage of light transmitance (T) through the ice and the reflectance (R) off of the ice pellets as measured with an integrating sphere technique (see

methods) are shown in Fig 3.1. The percent of incident light absorbed by a 250 μM 4-nitrophenol solution distributed in ice pellets was determined based on a light flux balance, as described in equation 1, where pure H_2O ice pellets were used as a reference blank.

$$\left.\frac{I_a}{I_0}\right|_\lambda = \left\{(100-T-R)_{\lambda,4NP\ ice} - (100-T-R)_{\lambda,H_2O\ ice}\right\} \quad , \qquad (1)$$

where I_a/I_0 is the percent of incident light absorbed by 250 μM 4-NP in an ice pellet, I_a = absorbed light flux, I_0 = incident light flux, $(100\text{-}T\text{-}R)_{\lambda,4\text{-}NP\ ice}$ = light absorption by an ice pellet containing 250 μM 4-NP (in % of I_0), $(100\text{-}T\text{-}R)_{\lambda,H2O\ ice}$ = light absorption by pure H_2O pellet (in % of I_0), T = light transmission through the ice pellet (in % of I_0), and R = light reflection from the ice pellet (in % of I_0).

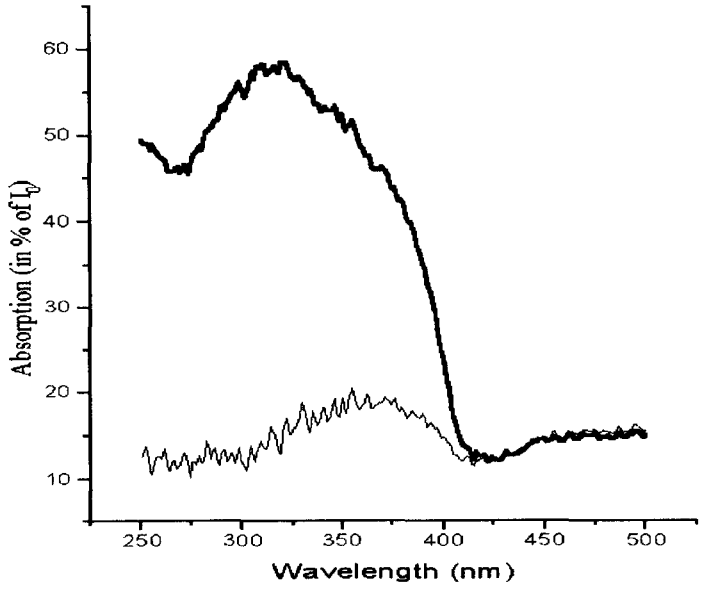

Figure 3.1 The absorption spectrum (in percent of the incident light) of 250 μM 4-nitrophenol in an ice pellet (thick line) and of pure water ice pellet (thin line). Both pellets are 4 mm thick. The light absorption by the 4-nitrophenol is given by the difference spectrum.

The calculations described in eq. 1 were performed over the wavelength range of 200 to 500 nm in intervals of $\Delta\lambda$ = 0.2 nm. Over the range of wavelengths for active photochemistry (300 nm to 370 nm) we find that 38.9 % ± 3.6 % of the incident light is absorbed by a frozen 250 μM 4-nitrophenol solution in a 4 mm-thick ice pellet.

During irradiation of the ice pellets (300nm ≤ λ ≤ 370nm), the measured 4-nitrophenol concentration decreased with time according to apparent pseudo-first order kinetics (Fig. 3.2) with an observed rate constant of 7.2×10^{-3} min^{-1} ($\pm 4 \times 10^{-4}$).

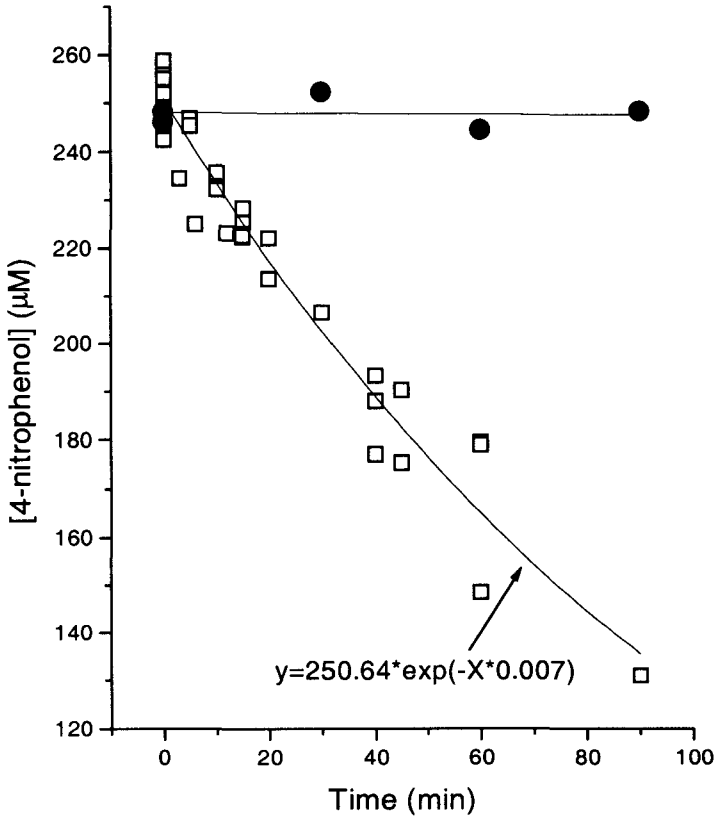

Figure 3.2. 4-nitrophenol concentration vs. time for the irradiation of ice pellets by light over the wavelength range of 300 to 370nm light (open squares) and at wavelengths ≥ 420 nm (solid circles). $[4\text{-nitrophenol}]_0$ = 250 μM, T = 258 K.

Three aromatic compounds, hydroquinone, benzoquinone and, 4-nitrosophenol (Fig. 3.3) and two inorganic anions, nitrate and nitrite (data are not shown), were detected as reaction products of the solid ice-phase photolysis of 4-nitrophenol.

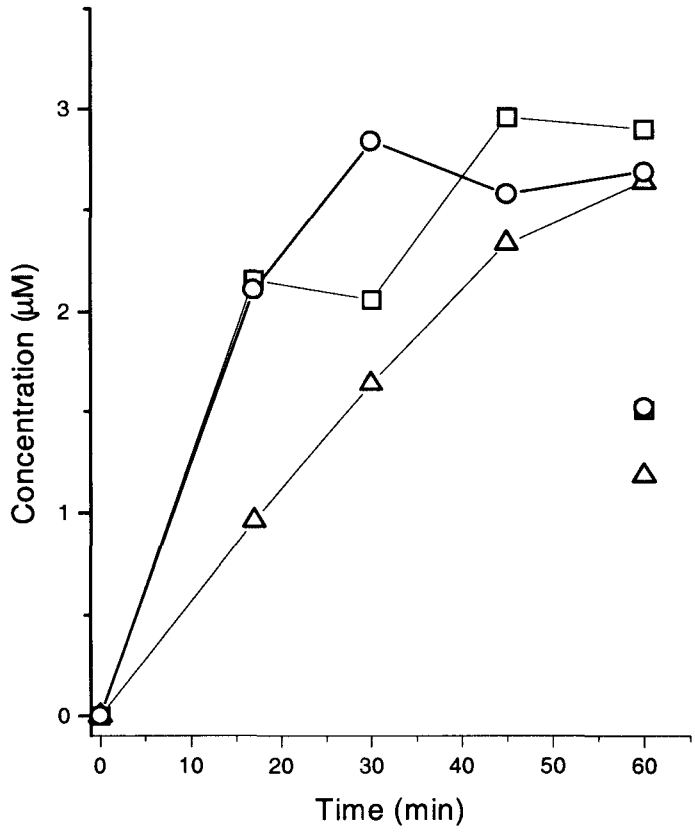

Figure 3.3 Concentration of hydroquinone (squares), benzoquinone (circles), and 4-nitrosophenol (triangles) vs. irradiation time, $[4\text{-nitrophenol}]_0 = 250\ \mu M$, T = 258 K.

Even though the sum of the detected aromatic reaction products did not account for the total amount of 4-nitrophenol that disappeared, TOC analysis showed that the latter did not change significantly over a time period of 90 min (Fig. 3.4).

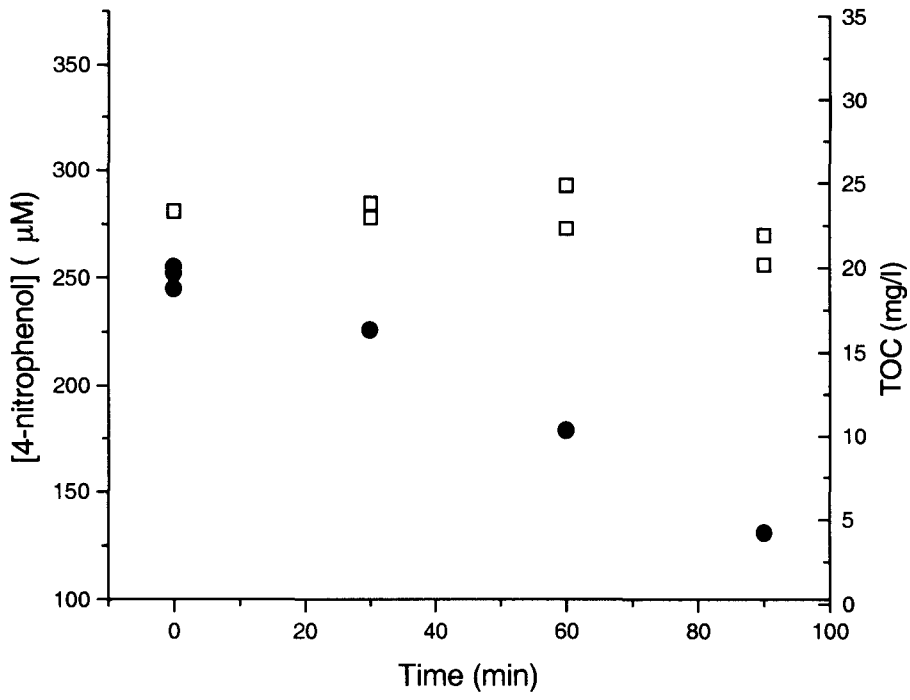

Figure 3.4 4-nitrophenol (solid circles) and total organic carbon (open squares) concentrations vs. time of irradiation of the ice pellets for 300 nm $\leq \lambda \leq$ 370 nm at T = 258 K.

Above 420 nm. where the light absorption by 4-nitrophenol is very small (Fig. 3.1), no apparent change in the 4-nitrophenol concentration was observed (Fig. 3.2) and none of the aromatic degradation products were detected. Nitrate and nitrite were detected in the ice pellets of the control experiment but no increase in their concentration with time was observed.

3.5. Discussion

During the freezing process, most solutes are excluded from the growing ice crystals resulting in higher concentrations on crystal surfaces and between the adjacent ice crystals (Takenaka et al. 1996). Because of the low aqueous-phase solubility of 4-nitrophenol, these inclusions are too dilute with respect to the solute to

remain exclusively in the liquid phase. Extrapolation of the 4-nitrophenol solubility data of Benes and Dohnal (1999) to temperatures below 273 K shows that the mole fraction of 4-nitrophenol cannot exceed 10^{-3}.

These concentrations are too small for freezing point depression down to 258 K. Thus, for our experiments, 4-nitrophenol is trapped in the solid ice phase.

Based on the observed photolysis rate, the incident light intensity and the fraction of the measured light absorbed by the 4-nitrophenol, a quantum yield of $(2.3 \pm 0.4) \times 10^{-4}$ was determined for the UV photolysis of 4-nitrophenol according to eq. 2 as follows:

$$\phi\,(4-\mathrm{NP}\,,300\text{ - }370\text{ nm}) = \frac{\left(\mathrm{d}[4-\mathrm{NP}]/\mathrm{dt}\right)_0}{I_{\mathrm{absorbed}}\,(300\text{ - }370\text{ nm})/\mathrm{dt}}\quad , \tag{2}$$

where ϕ(4-NP,300–700nm) is the apparent quantum yield for 4-NP photolysis over the wavelength range of 300 to 370 nm , $(d[4\text{-NP}]/dt)_0$ is the initial loss of 4-NP when irradiated at this wavelength range (mole·s^{-1}), and $I_{absorbed}$(300–370nm)/dt is the photon flux (over 300 to 370nm) absorbed by the 4-NP (einstein·s^{-1}).

Both the quantum yield and the products observed in the ice photolysis experiments are similar to those observed in homogeneous aqueous-phase measurements for the photolysis of 4-nitrophenol (Masayuki and Crosby,1974; Alif et al., 1987, Lemaire et al., 1985). This similarity in observed photochemical product arrays suggests a similar mechanism for photochemical decomposition for both phases (eqs. 3 and 4, after Alif et al., 1987):

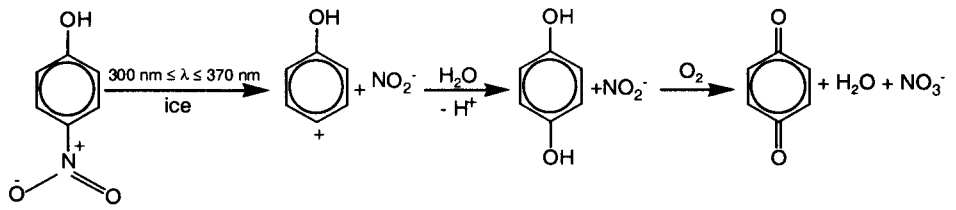

(3)

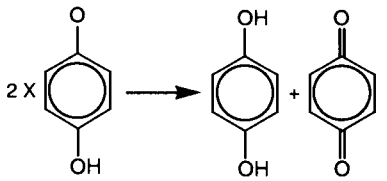

(4)

In spite of the much stronger cage effects expected in ice, the exclusion of 4-nitrophenol from the ice crystal and its concentration between the ice crystals, the photochemical reaction occurs at rates that are similar to the corresponding reaction rates in the aqueous phase at 25° C. The main difference between the two phases is that in aqueous solutions, the aromatic products account for a larger fraction of the degraded 4-nitrophenol. As can be seen from the data in Fig. 3.3, the detected organic reaction products reach concentrations in the micromolar range suggesting that their photochemical lifetimes are relatively short. As previously mentioned, during the course of photolysis the decrease in the total organic carbon levels (TOC) is much lower then the degradation of the 4-nitrophenol. Over an irradiation exposure of 90 minutes, the TOC decreased by only 2.25 mgC/L whereas the 4-nitrophenol concentration decreased by 120 μM (i.e., 8.64 mgC/L). Thus, it is likely that organic polymers were formed during the photodegradation of 4-nitrophenol. Formation of

polymeric material was previously observed by Masayuki and Crosby (1974) during irradiation of 4-nitrophenol in aqueous solution. Oxidative polymerization of polyphenols is also a well-known mechanism for the formation of humic acids in soils (Shindo, 1990; Naidja et al., 1998; Kung and McBride, 1988). The small decrease in the TOC may suggest that CO_2 was produced. This requires breakage of the aromatic ring, as was observed previously during 4-nitrophenol photocatalysis in TiO_2 slurries by Dieckmann and Gray (1995).

3.6 Conclusions

In this study, the photochemistry of 4-nitrophenol over the wavelength range of 300 to 370 nm in ice pellets was investigated. A quantum yield of $\phi_{ice} = 2.3 \times 10^{-4}$ ($\pm 4 \times 10^{-5}$) was determined for the photochemical degradation of 4-NP in ice pellets. This value of ϕ_{ice} is of the same magnitude as the aqueous-phase quantum yield which we measured under similar irradiation conditions ($\phi_{aq} \approx 7.7 \times 10^{-5}$). The observed products of 4-nitrophenol photolysis in ice were nitrate, nitrite, hydroquinone, benzoquinone, 4-nitrosophenol, and the likely formation of organic polymers. These results and their similarity to the observations from 4-nitrophenol photolysis in aqueous solutions indicate that similar mechanisms are operative in both phases. The photochemical decomposition of 4-NP under conditions similar to those in polar snow and ice (i.e., temperature, pressure, and UV wavelength range), suggests that other direct and indirect photochemical process can occur in the polar ice/snow during spring and summer. For example, naturally occurring organic matter (NOM) that has a substantial aromatic character and serves as an excellent absorber of UV and visible radiation, is most likely to be present in significant amounts in polar snow. Absorption of light by NOM can lead to the indirect production of hydroperoxyl

radicals and eventually organic peroxides (Hoffmann, 1996). These free radicals may further react with other impurities present in the polar snow (e.g., organic matter) causing chemical changes in important species such as H_2O_2 and H_2CO and CO_2. These alterations may effect the interpretations of the time-records of these species in polar ice cores regarding the oxidation capacity of past atmospheres (Staffelbach et al., 1991) and related climate changes (Fuhrer et al., 1993).

The present results are consistent with recent studies by Honrath et al. (1999, 2000), Jones et al. (2000), and Sumner and Shepson (1999), who reported on the photochemical production of NO_x and HCHO in surface accumulated snow. These observations were interpreted in terms of nitrate photolysis in snow, followed by the production of hydroxyl radical which, in turn, is expected to lead to the production of H_2O_2, HCHO, and other organic compound destruction in polar snow during spring and summer.

Since polar ice cores are used extensively to probe the atmospheric paleo-chemistry and to predict the evolution of climate, more systematic investigations of postdepositional chemical changes due to direct and indirect photolysis are needed.

Reference

1. Alber, M., H.B. Bohm, J. Brodesser, J. Feltes, K. Leysen, H. Scholer, Determination of Nitrophenols in Rain and Snow. *Fresenius Zeitschrift Fur Analytische Chemie*, 334, 540-545, 1989.
2. Alif, A., P.Boule, and J. Lemair, Comportement photochemique du Nitro-4 Phenol en Solution Aqueuse. *Chemosphere*, 16, 2213-2223, 1987.
3. Allamandola, L.J., S.A. Sandford, and G.J. Valero, Photochemical and Thermal Evolution of Interstellar/Precometary Ice Analogs. *Icarus*, 76, 225-252, 1988.
4. Anklin, M., J.M. Barnola, , J. Schwander, B. Stauffer, D. Raynaud, Processes Effecting the CO_2 Concentrations Measured in Greenland ice. *Tellus B*, 47, 461-470, 1995.
5. Bales, R. C., and E. W. Wolf, Processes of Chemical Exchange Between the Atmosphere and Polar Snow: Key to Interpreting Natural Climate Signals in Ice Cores. *EOS Trans* AGU, 76, 477-482, 1995.
6. Benes M., Dohnal, V. (1999) Limiting Activity Coefficients of Some Aromatic and Aliphatic Nitro Compounds in Water. *J. Chem. Eng. Data* , 44, 1097-1102.
7. Bernstein, M.P., S.A. Sandford, L.J. Allamandola, S. Chang, and M.A. Scharberg, Organic Compounds Produced by Photolysis of Realistic Interstellar and Commentary Ice Analogs Containing Methanol. *The Astrophysical J.*, 454, 327-344, 1995.
8. Bernstein, M.P., S.A.Sandford, L.J. Allamandola, , J.S. Gillette, S.J. Clemett, and R.N. Zare, UV Irradiation of Polycyclic Aromatic Hydrocarbons in Ices: Production of Alcohols, Quinones and Ethers. *Science*, 283, 1135-1138, 1999.
9. Chappellaz J, E. Brook, T. Blunier, B. Malaize, CH_4 and Delta O-18 of O_2 Records from Antarctic and Greenland Ice: A Clue for Stratigraphic Disturbance

in the Bottom Part of the Greenland Ice Core Project and the Greenland Ice Sheet Project 2 ice cores. *J. Geophys. Res.-Ocean*, 102, 26547- 26557, 1997.

10. Delmas, R.J., A Natural Artifact in Greenland Ice-Core CO_2 Measurements. *Tellus B*, 45, 391- 396, 1993.
11. Dieckmann, M. S., and K.A Gray, Comparison of Degradation of 4-nitrophenol via Direct and Sensitized photocatalysis in TiO_2 Slurries. *Wat. Res.* 30, 1169-1183, 1995.
12. Doppenschmidt A. and Butt H.-J. (2000) Measuring the Thickness of the Liquid-like Layer on Ice Surfaces with Atomic Force Microscopy. *Langmuir,* 16 6709-6714.
13. Fuhrer, K., A. Neftel, M. Anklin, and V. Maggi, Continuous Measurements of Hydrogen Peroxide, Formaldehyde, Calcium and Ammonium Concentrations Along the New Grip Ice Core from Summit, Central Greenland. *Atmos. Env. A,* 27, 1873-1880, 1993.
14. Heller, H.G., The Development of Photochromic Compounds for use in Optical Information Stores, *Chem. Ind.* 18, 193-196, 1978.
15. Herterich, R. and R. Herrmann, Comparing the Distribution of Nitrated Phenols in the Atmosphere of Two German Hill Sites. *Environ. Tech.* 11, 961-972, 1990.
16. Hoffmann, M.R., Possible Chemical Transformations in Snow and Ice Induced by Solar (UV photons) and Cosmic Irradiation (muons) in: *Chemical Exchange between the Atmosphere and Polar Snow,* edited by W. Wolff, and R.C. Bales, pp. 353-377, Springer, Berlin, 1996.
17. Honrath, R.E., *et al.*, Photochemical Production of Gas-Phase NO_x from Ice-Crystal NO_3^-. *J. Geophys. Res. Atmos.* 105, 24183-24190, 2000.

18. Honrath, R.E., M.C. Peterson, S. Guo, J.E. Dibb, P.B. Shepson, and B. Campbell, Evidence of NO_x Production Within or Upon Ice Particles in Greenland Snowpack, *Geophys. Res. Lett.* 26, 695-698, 1999.

19. Jones, A.E., R. Weller, E.W. Wolff, H.W. Jacobi, Speciation and Rate of Photochemical NO and NO_2 Production in Antarctic Snow. *Geophys. Res. Lett.* 27, 345-348, 2000.

20. Kawamura, K. and I. Kaplan, Biogenic and Anthropogenic Organic-Compounds in Rain and Snow Samples Collected in Southern California., *Atmos. Env.* 20, 115-124, 1986.

21. Kishk, F.M., T. El-Essawi, S. Abdel-Ghafar, M.B. Abou-Donia, Hydrolysis of Methylparathion in Soils. *J. Agric. Fd. Chem.*, 24, 305-307, 1976.

22. Kung, K.H., and M.B. McBride, Electron-Transfer Processes between Hydroquinone and Hausmannite (MN_3O_4). *Clay Miner.* 36, 297-302, 1988.

23. Legrand M., Ice-core Records of Atmospheric Sulphur. *Philos. T. Roy. Soc. B*, 352, 241-250, 1997.

24. Lemaire J., J.A. Guth et al., Ring Test of a Method for Assessing the Phototransformation of Chemicals in Water. *Chemosphere*, 14, 53-77, 1985

25. Leone, J.A., R.C. Flagan, D. Grosjean, J.H. Sienfeld, An Outdoor Smog Chamber and Modeling Study of Toluene - NO_x Photooxidation. *Inter. J. Chem. Kinetics*, 17, 177-216, 1985.

26. Levsen, K., S. Behnert, B. Priess, M. Svoboda, H.D. Winkeler, J. Zietlow, Organic-Compounds in Precipitation. *Chemosphere*, 21, 1037-1061, 1990.

27. Luttke, J., V. Scheer, K. Levsen, G. Wunsch, J.N Cape, K.J. Hargreaves, R.L. StoretonWest, K. Acker, W. Wieprecht, B. Jones, Occurrence and Formation of Nitrated Phenols in and out of Cloud. *Atmos. Env.* 31, 2637-2648, 1997

28. Mark, G., H. G. Korth, H.P. Schuchmann, and C. Von Sonntag, The Photochemistry of Aqueous Nitrate Ion Revisited. *J. Photochem. Photobio. A: Chemistry*, 101, 89-103, 1996.

29. Naidja A., P.M. Huang, and J.M. Bollag, Comparison of Reaction Products from the Transformation of Catechol Catalyzed by Birnessite or Tyrosinase. *Soil Sci. Soc. Am. J.* 62, 188-195, 1998.

30. Nojima, K., et al., Studies on Photochemistry of Aromatic Hydrocarbons-II. *Chemosphere*, 4, 77-82, 1975.

31. Pursell, C.J., J. Conyers, and C. Denison, Photochemistry of Chlorine Dioxide in Polycrystaline Ice (T=140-185 K): Production of Chloryl Chloride, Cl-(OClO). *J. Phys. Chem.*, 100, 15450-15453, 1996.

32. Schutte, W.A., and P.A. Gerakines, Recent Results from the Leiden Observatory Laboratory: (a) Band Strengths in Mixed Ices; (b) UV Photolysis of Solid Methanol. *Planet. Space Sci*, 43, 1253-1256, 1995.

33. Sigg, A., and A. Neftel, Evidence for a 50% Increase in H_2O_2 Over the Past 200 Years from a Greenland Ice Core. *Nature*, 351, 557-559, 1991.

34. Staffelbach, T., A. Neftel, B. Stauffer, and D. Jacob, A Record of the Atmosphere Methane Sink from Formaldehyde in Polar Ice Cores. *Nature*, 349, 603-605, 1991.

35. Sumner, A.L. and P.B. Shepson, Snowpack Production of Formaldehyde and Its Effect on the Arctic Troposphere. *Nature*, 398: p. 230-233, 1999.

36. Takenaka, N., A. Ueda, T. Daimon, H. Bandow, T. Dohmaru, and Y. Maeda, Acceleration Mechanism of Chemical Reaction by Freezing: The Reaction of Nitrous Acid with Dissolved Oxygen. *J. Phys. Chem.*, 100, 13874-13884, 1996.

37. Tremp, J., P. Mattrell, S. Fingler, W. Giger, Phenols and Nitrophenols as Tropospheric Pollutants - Emissions from Automobiles Exhausts and Phase-transfer in the Atmosphere. *Water Air Soil Poll.* 68, 113-123, 1993.

38. Woodrow, J.E., J.N. Seiber, D.G. Crosby, K.W. Moilanen, C.J. Soderquist, C. Mourer, Airborne and Surface Residues of Parathion and Its Conversion Products in a Treated Plum Orchard Environment. *Arch. Envir. Contam. Toxicol*, 6, 175-191, 1977.

Appendix 3.1 Scheme of the integrating Sphere.

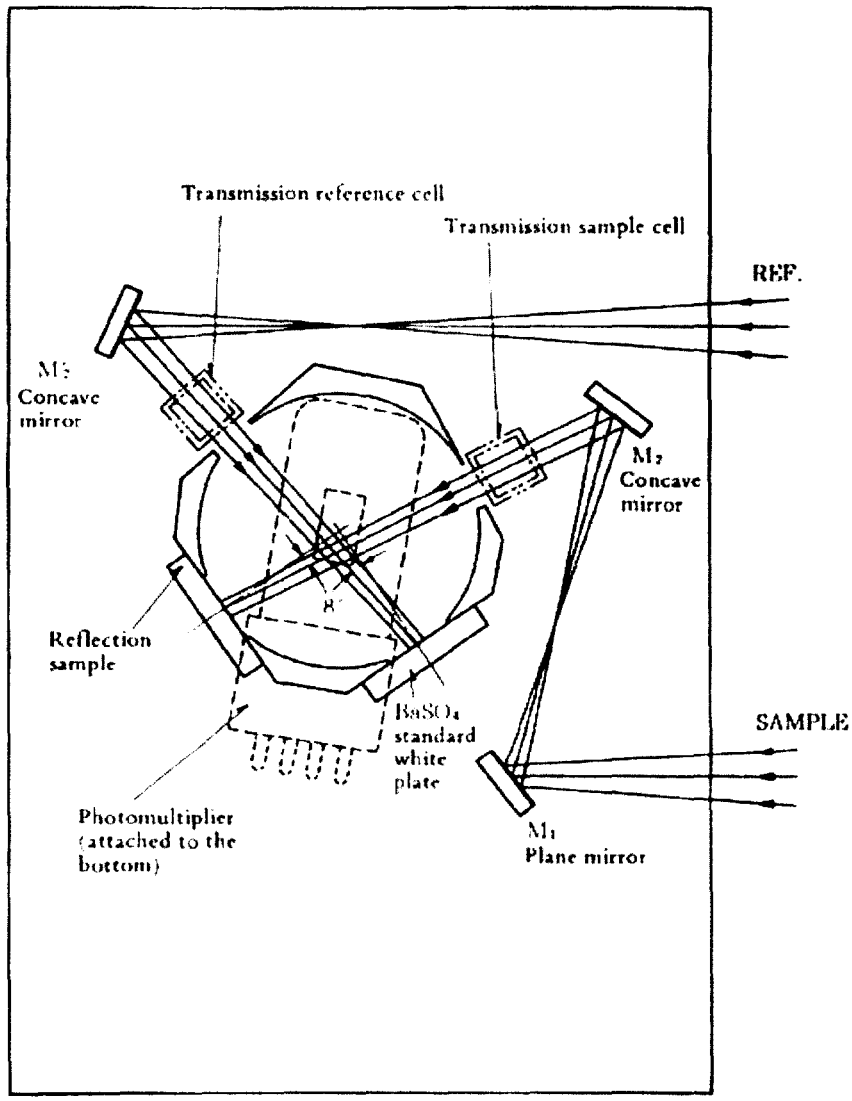

Figure 3.5 Scheme of the integrating sphere (Shimadzu ISR-260).

Light absorption was then calculated as follows:

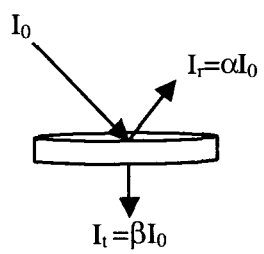

$$I_{absorbed}=(1-\alpha-\beta)I_0$$

Appendix 3.2 Light absorption by 4NP in ice pellets and in aqueous solution.

Light absorption by 4-nitrophenol at various concentrations in aqueous solution and in ice pellets, indicates similar extinction coefficient in both phases: 2185 M^{-1} 0.4 cm^{-1} (i.e., 5463 M^{-1} cm^{-1}) in aqueous solution vs. 2407 M^{-1} 0.4 cm^{-1} in the ice pellets (Figure 3.6).

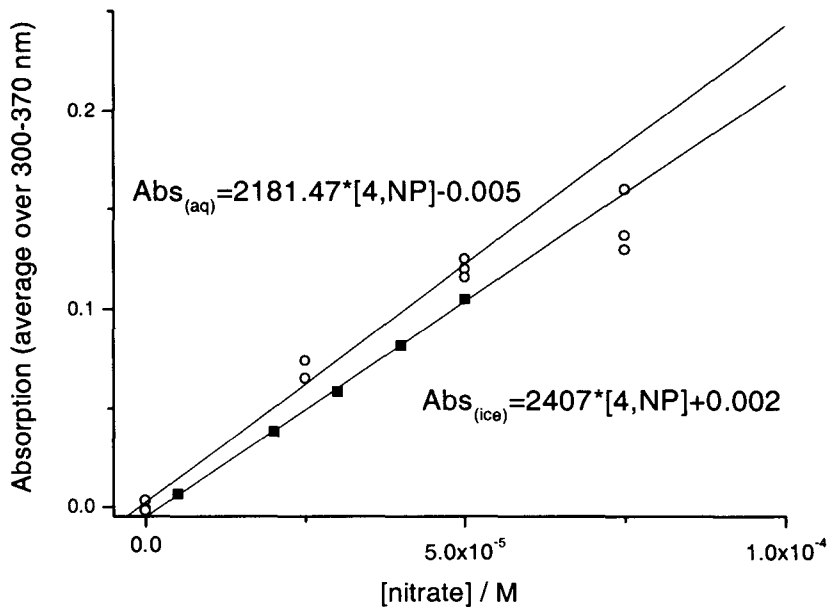

Figure 3.6 Absorption of 4-nitrophenol in aqueous solution (after correction to ℓ = 0.4 cm; solid squares) and in ice pellets (ℓ = 0.4 cm; open circles), as a function of its initial concentration. The absorption in ice pellets was measured using an integrating sphere. Linear fits of the data (excluding the measurement in ice pellets containing 75 μM 4 NP) indicate extinction coefficients of 2185 M^{-1} $(0.4\ cm)^{-1}$ and 2294 M^{-1} $(0.4\ cm)^{-1}$ in aqueous solution and ice pellets, respectively.

As seen in Figure 3.6, at initial concentrations of [4-nitrophenol] > 50 μM the measured absorption does not seem to follow the *Beer-Lambert* law. It is possible that due to exclusion of 4-nitrophenol from the ice matrix during freezing (see above), the solute is concentrated on crystals surfaces and between adjacent crystals where it reaches super-saturation and precipitates. If crystalline 4-nitrophenol absorbs less light than in the frozen solution, we would expect a decrease in the overall light absorption.

Extrapolation of the 4-nitrophenol solubility data of Benes and Dohnal (1999) (Figure 3.7) to temperatures below 273 K, shows that at 258 K the solubility of 4-nitrophenol, in super-cooled water, is about 30 mM.

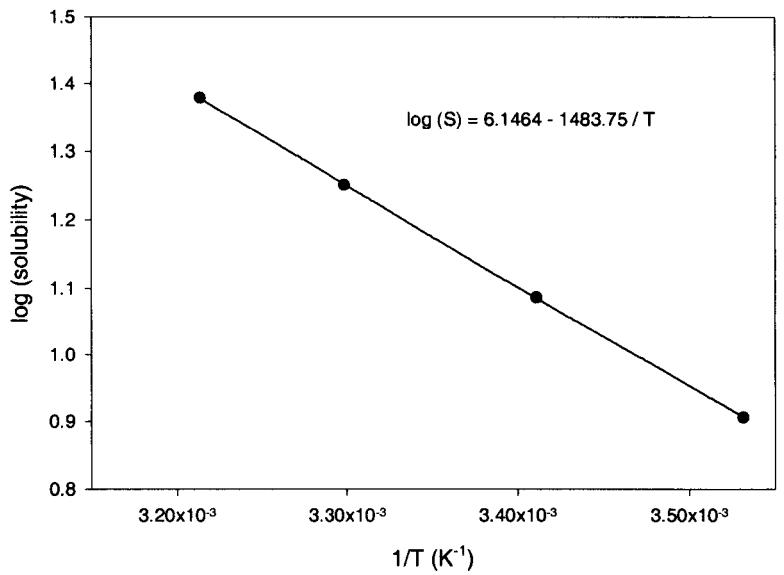

Figure 3.7 Solubility of 4-nitrophenol in water as a function of temperature (after Benes and Dohnal, 1999).

Atomic force microscopy measurements of the thickness (h) of the quasi-liquid layer on pure ice surface (Doppenschmidt et al., 1998) show that at 258 K it is about

14 nm thick. Assuming similar layer on the surface of the ice crystals in our experiments ([4-nitrophenol]$_0$ = 250 μM) and a complete rejection of the 4-nitrophenol from the ice matrix, we calculate (eq. 5) that for ice crystal diameters bigger then 14 μm, 4-nitrophenol is expected to precipitate according to

$$[4NP]_{QLL} = [4NP]_0 \times \frac{R_{ice}^{\ 3}}{(R_{ice}+h)^3 - R_{ice}^{\ 3}} \quad , \qquad (5)$$

where [4NP]$_{QLL}$ and [4NP]$_0$ are the concentrations of 4-nitrophenol within the quasi-liquid layer and in the initial solution, respectively, R_{ice} is the radius of the ice crystals, and h is the thickness of quasi-liquid layer.

Appendix 3.3 4-NP distribution and degradation rate in solid ice cylinders

During the initial stage of this project, solid ice cylinders were used for photolysis which were prepared by slowly freezing 2 ml of a 4-nitrophenol solution in small beakers. Freezing was achieved by placing beakers filled with the target solution on a cold surface (263 K) for a period of several hours. The observed rate constants for the degradation of 4-nitrophenol in these experiments (Fig. 3.8) were found to be very similar to those observed in experiments in which crushed ice pellets were used (Fig 3.2). However, the centers of these ice cylinders were filled with voids and light absorption measurements were imprecise because of light scattering (Fig. 3.9 a). Moreover, chemical analysis of the 4-nitrophenol distribution within the ice cylinders (Fig. 3.9 b,c) showed a very uneven distribution of the chromophore with extremely high concentrations accumulating within the voids, which were the last to freeze. This observations suggest that 4-nitrophenol is excluded from the ice matrix during freezing. Similar concentration effects were observed by Takaneka at al.(1996) during the freezing of nitrite solutions.

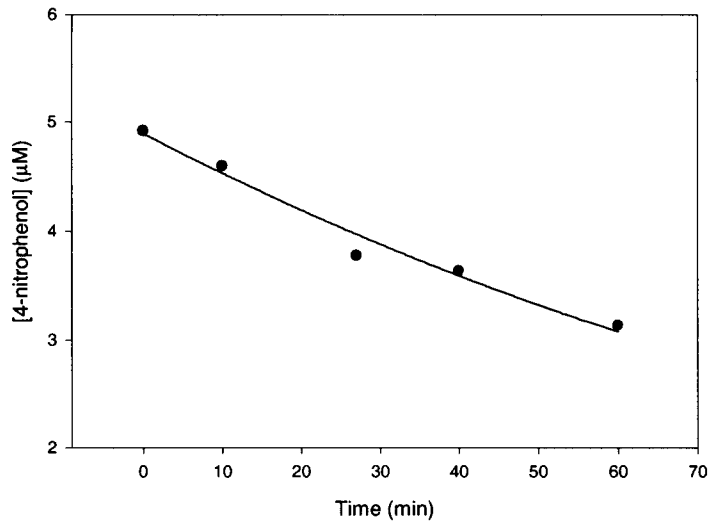

Figure 3.8 4-nitrophenol concentration within the bulk ice chunk as a function of irradiation (300 nm < λ < 370 nm) time. Exponential regression through the data indicate a rate constant of 7.73×10^{-3} (min^{-1}).

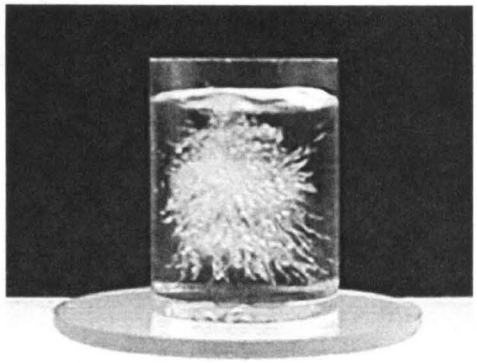

(a)

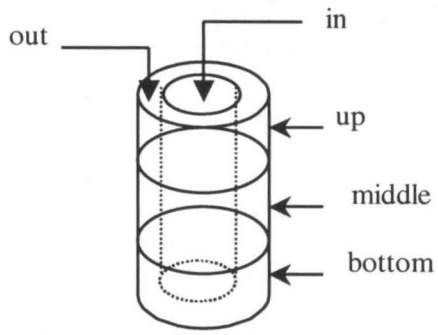

(b)

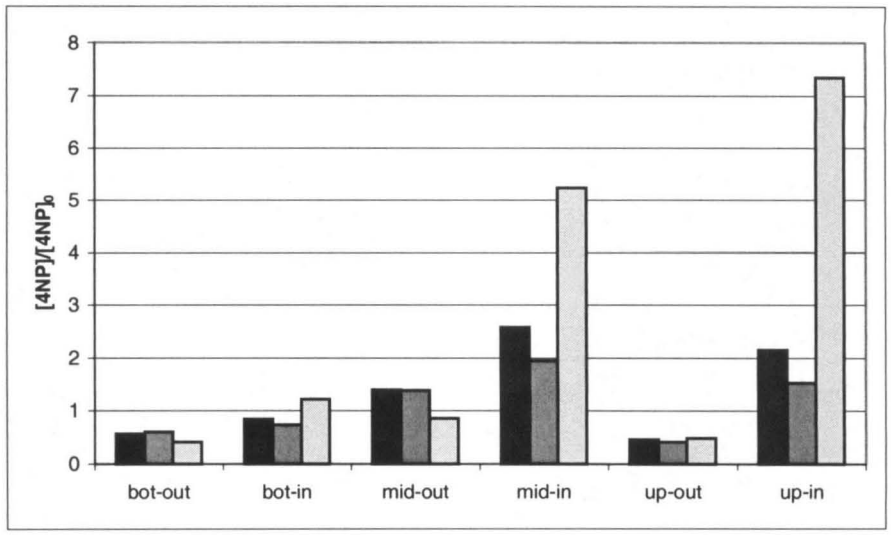

(C)

Figure 3.9 A picture of the produced ice cylinders (see text). Degassing the original solution decreased the amount of voids but did not eliminate them completely (a). The distribution of 4-NP within the ice sample was analyzed in six different parts (B) and was found to be very inhomogeneous (C). Most of the 4-NP is concentrated (up to 7-folds its original concentration) in the voids area at the central part of the ice sample.

Chapter 4

Nitrogen dioxide release in the 302 nm band photolysis of spray-frozen aqueous nitrate solutions. Atmospheric implications.

(Published in part: *Journal of Physical Chemistry A*, **2001**, 105: 4928-4932)

4.1 Abstract

We quantify the NO_2 fluxes released into the gas-phase during the continuous $\lambda \sim 300$ nm photolysis of NO_3^- in sub-millimeter ice layers produced by freezing aqueous KNO_3 sprays on cold surfaces. Fluxes, F_{NO_2}, increase weakly with $[NO_3^-]$ between 5 mM to 50 mM, and increase markedly with temperature in the range 248 K to 268 K. We found that F_{NO_2}, the photostationary *concentration* of NO_2^- (another primary photoproduct), and the *quantum yield* of 2-nitrobenzaldehyde in situ photoisomerization are nearly independent of ice layer thickness h within the range of 80 μm - 400 μm. We infer that radiation is uniformly absorbed over the depth of the ice layers, where NO_3^- is photodecomposed into NO_2 (+ OH) and NO_2^- (+ O), but that only the NO_2 produced on the uppermost region is able to escape into the gas-phase. The remainder is trapped and further photolyzed into NO. We obtain $\phi_{NO_2^-} \sim 4.8 \times 10^{-3}$ at 263 K (i.e., about the quantum yield of nitrite formation in neutral NO_3^- aqueous solutions) and an apparent quantum yield of NO_2 release $\phi'_{NO_2} \sim 1.2 \times 10^{-3}$ that is about a factor of 3 smaller than solution ϕ_{OH} data extrapolated to 263 K. These results suggest that NO_3^- photolysis in ice takes place in a liquid-like environment, and that actual ϕ'_{NO_2} values may depend on the morphology of ice deposits. Present ϕ'_{NO_2} data, in conjunction with snow absorptivity data, lead to F_{NO_2} values in reasonable agreement with recent measurements in Antarctic snow under solar illumination.

4.2 Introduction

Deposition of inorganic nitrate on ice surfaces is a major sink for atmospheric reactive nitrogen oxides (Logan, 1985; Platt, 1986). The fact that nitrate concentrations in Antarctic ice, in contrast with other major anions, are remarkably constant across the continent suggest remote, global sources (Mulvaney et al., 1998). Therefore, nitrate levels within ice cores would provide, if preserved (Wolff, 1995), valuable paleoatmospheric and paleoclimatic information. However, the relationship between the NO_3^- concentration in the snow and that of NO_y in the overlying atmosphere is not straightforward, nor it is certain that ice cores preserve a simple record of the deposition of inorganic nitrogen at a given site (Wolff, 1995). Moreover, there is strong evidence for postdepositional losses of NO_3^- from the snow pack both on fast (days) and slow (years) time scales (Neubauer and Heumann, 1988a,b; Mayewski and Legrand, 1990; Silvente and Legrand, 1995; Wolff, 1995). The mean levels of nitrate in Antarctic ice cores are around 20-80 $ng \cdot g^{-1}$, while nitrate in surface snow may reach levels above 300 $ng \cdot g^{-1}$. The processes involved in this nitrate loss are still unclear. Candidate processes include photochemical destruction of nitrate, wind-scouring of the surface layer, volatilization of nitric acid, and scavenging of nitrate by other wind-blown particles or gases, probably aided by windpumping of the snowpack (e.g., Pomeroy and Jones, 1996). Recent experiments reveal the photochemical production of NO and NO_2 in and above surface snow at polar and mid-latitude regions (Honrath et al., 1999, 2000a,b; Jones et al., 2000).

The photochemical lability of the nitrate incorporated into cirrus clouds is also relevant to various atmospheric processes regulated by the partitioning between NO_x and

NO_y species. Laboratory studies confirm that ice surfaces can efficiently remove HNO_3 from the gas phase. However, although nitrate photolysis in aqueous solutions has been extensively investigated in the UV-A and UV-B regions (Zepp et al., 1987; Warneck and Wurzinger, 1988; Alif and Boula, 1991; Mark et. al,1996; Mack and Bolton, 1999; Jankowski et al., 1999), the photochemical behavior of nitrate in ice and snow under ambient conditions prevalent at high latitudes remains an open issue. In this chapter, we report quantitative data on nitrite formation and NO_2 emissions during the 302 nm UV band photolysis of nitrate in spray-frozen aqueous solutions as a function of temperature, nitrate concentration (in the mM range) and ice layer thickness. We find that primary quantum yields for NO_2 and NO_2^- production in ice are comparable to solution phase values. However, the photodecomposition of the NO_2 rejected by the solid under dim sunlight competes favorably with NO_2 diffusion in ice over submillimeter lengths, limiting its release into the gas-phase. Present results are then used to estimate NO_2 fluxes from illuminated snowpacks. The accord obtained vis-a-vis recent field measurements in Antarctica (Jones et al., 2000) at 70°S is within the experimental uncertainties.

4.3 Experimental Section

The experimental setup is shown in Figs. 4.1a, b. Nitrate-doped ice deposits were prepared by spraying pre-cooled KNO_3 (Fisher Scientific) solutions of variable concentration at pH < 6, onto a gold-coated cylindrical cold finger, CF (Fig 4.1b; total area A = 182.2 cm^2), maintained at 248 K by coolant circulation. The ice-covered cold finger was then sealed inside a quartz sheath, QS, and the array placed inside a reflective

aluminum chamber (Fig. 4.1a). Ice deposits were brought to the desired temperature (268 K, 263 K or 248 K), and then irradiated by three Hg Pen-Ray® UV lamps (UVP, modal 90-0001-04), symmetrically located around QS, emitting at λ = (313 ± 20) nm. The stability of the lamp output during the (necessarily) long experiments was monitored with a photocell (UDT Sensors, model PIN UV 100L) attached to the top of the aluminum chamber. The chamber was flushed with dry air to prevent moisture condensation on the outer QS surface.

The photon flux incident onto QS, $I_i = (9.8 \pm 1.2) \times 10^{14}$ photons cm^{-2} s^{-1}, was determined from actinometric measurements using a potassium ferrioxalate solution (Calvert and Pitts, 1966) filling QS at 298 K. The photon flux actually absorbed by nitrate-doped ice I_{a,NO_3^-} was evaluated (see below) from the rates of 2-nitrobenzaldehyde (2-NBA) photoisomerization into 2-nitrosobenzoic acid within ice layers. The latter were similarly obtained by spray-freezing a 33 μM aqueous 2-NBA solution, which has an absorbance comparable to nitrate solutions in the relevant spectral range, onto CF. We assume that the intramolecular photoisomerization of 2-NBA in ice, as in all the phases in which it has been studied, has a quantum yield of $\phi_{iso} = 0.5$, independent of temperature (Pitt et al., 1965; George and Scaiano, 1980; Filby and Gunther, 1981). The concentrations of 2-NBA and 2-nitrosobenzoic acid were determined, after thawing, by high-pressure liquid chromatography (HP 1090) with ODS hypersil and Pinnacle IBD columns. The eluent was a 20:80% mixture of methanol and water, and the wavelengths of the detector were set at 235 nm and 320 nm.

Nitrogen dioxide produced photochemically and released into the gas-phase was swept out of the irradiated zone by a steady helium flow (~10 cm^3 min^{-1}), and condensed downstream into a trap maintained at 77 K, in which 1 cm^3 of a 0.1 M NaOH solution had been previously frozen. The helium carrier was pre-purified by passage through molecular sieve at 77 K. Experiments were terminated by turning the lamps off, and then thawing the ice deposits by raising the temperature of the cold finger under carrier flow. The volume of the melt in the QS was measured and used to determine the average thickness of the ice layer (h). The condensing trap was then evacuated, sealed, thermalized at 298 K, and kept in the dark for about 12 hours to allow any NO_2 present to dissolve into the NaOH solution. The contents of this trap, as well as the melted ice left in the quartz sheath QS, were then analyzed for nitrite using the Saltzmann reagent (Saltzmann, 1954). The collecting yield of NO_2 by the condensing trap was determined to be (42 ± 5) % by flushing a known amount of calibrated NO_2 (g) through the cold trap with the same carrier gas as used in the actual experiments at similar flow rate (see appendix 4.2). The NO_2 values presented in this chapter have been corrected for this yield.

(a)

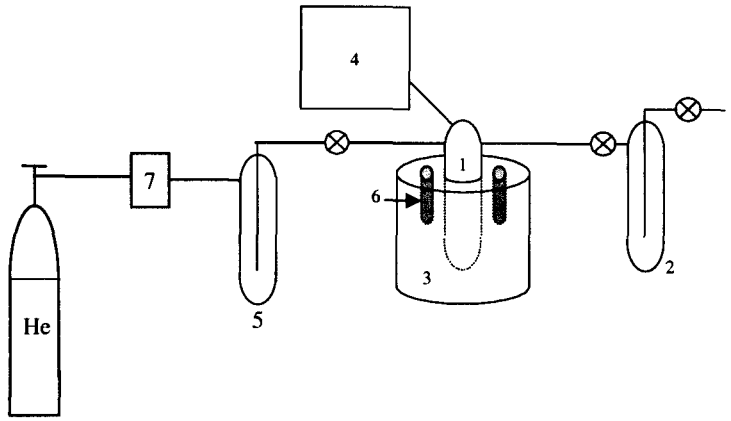

(b)

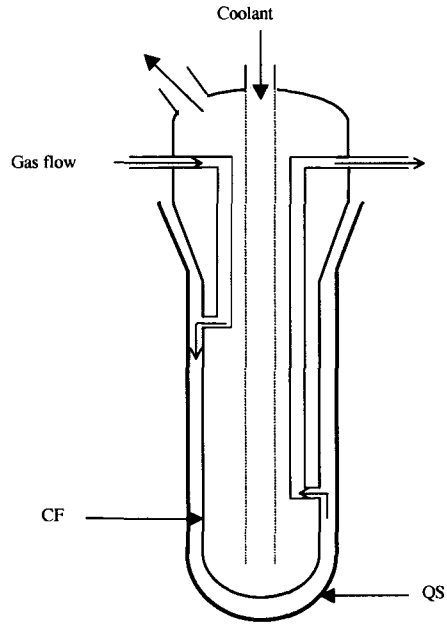

Figure 4.1a. Scheme of the experimental setup. 1: Reaction cell (see Fig. 4.1b); 2: NO_2 condensing trap; 3: Reflective reaction chamber; 4: Circulating cryostat; 5: Molecular sieve at 77 K; 6: Pen-Ray® UV lamps nominally emitting at 302 nm; 7: Flow meter.

Figure 4. 1b. The reaction cell. CF: Gold coated cold finger. QS: Quartz sheath.

4.4 Results and Discussion

The $\lambda > 300$ nm photolysis of nitrate in aerated aqueous solutions at pH < 6 proceeds via two pathways:

$$NO_3^- + H^+ + h\nu \rightarrow NO_2 + OH \quad (1)$$

$$NO_3^- + h\nu \rightarrow NO_2^- + O(^3P) \quad (2)$$

Peroxynitrous acid, ONOOH, the product (not shown) of yet another possible channel at shorter wavelengths, is apparently absent at $\lambda > 300$ nm (Mack and Bolton, 1999). The O-atoms generated in reaction 2 may react with O_2 ($[O_2]_{water} \sim 0.3$ mM) via reaction 3 or , preferably, with nitrate via reaction 4 at $[NO_3^-] \geq 5$ mM. Nitrite ($\varepsilon_{max} = 22.5$ M^{-1} cm^{-1} at 360 nm) will undergo secondary photolysis, reaction 5, and oxidation by OH radicals, reaction 6:

$$O_2 + O(^3P) \rightarrow O_3 \qquad k_3 = 4 \times 10^9 \ M^{-1} \ s^{-1} \quad (3)$$

$$NO_3^- + O(^3P) \rightarrow NO_2^- + O_2 \qquad k_4 = 2 \times 10^8 \ M^{-1} \ s^{-1} \quad (4)$$

$$NO_2^- + H^+ + h\nu \rightarrow NO + OH \quad (5)$$

$$NO_2^- + OH \rightarrow NO_2 + OH^- \qquad k_6 = 2 \times 10^{10} \ M^{-1} \ s^{-1} \quad (6)$$

The excitation of the NO_3^- $n \rightarrow \pi^*$ band in aqueous media, whose maximum decadic absorption coefficient is $\varepsilon_{NO_3^-} = 7.5$ M^{-1} cm^{-1} at 305 nm, leads to the formation of OH and $O(^3P)$ in relatively low quantum yields: $\phi_1 \sim 9 \times 10^{-3}$, $\phi_1 / \phi_2 \sim 9$. ϕ_1 increases at

shorter and longer wavelengths within the $n \rightarrow \pi^*$ band, and increases by a factor of 2.2 between 273 K and 308 K (Jankowski, 1999).

Most solutes molecules are too large to be incorporated within the ice lattice. Depending on the rate of freezing, crystallization may follow the equilibrium phase diagram of the water-solute system, or undergo sudden solidification. In the former case, the solid phase will consist of pure ice, down to the eutectic temperature, below which solute will also separate from the solution to become interspersed within the crystal grains of ice as a distinct phase. (Gross et al., 1977, 1987; Dash et al., 1995). Spray-freezing involves the rapid cooling of solution micro-droplets upon contact with a borosilicate surface at 248 K. Each frozen droplet, covered by the rejected solute, provides the substrate on which new droplets freeze in turn. However, as a result of the rapid freezing (i.e., lack of equilibrium) it is likely that not all of the solute will be excluded from the ice matrix. Thus, the solute is microscopically, rather than molecularly, dispersed in the ice, at the grain boundaries and in interstitial pores.

Grain boundaries and ice-air interface, such as the surface lining the interstitial pores, are known to be covered by a quasi-liquid layer whose thickness d varies, for example, between ca. 40 nm at 268 K and ca.15 nm at 248 K in ice produced by freezing 10 mM KCl solutions (Doppenschmidt and Butt, 2000). If a complete rejection of solutes into this quasi-liquid layer is assumed, then, upon spray-freezing mM KNO_3 solutions into ice particles larger than a few μm, the KNO_3 accumulated in the liquid film will exceed its eutectic concentration, [KNO_3] ~ 1 M ($T_{eutectic}$ = 270.2 K; Seidel, 1940), and will start precipitating. These considerations suggest that, under the present experimental

conditions, NO_3^- in the spray-frozen ice will be mainly embedded and partially dissolved within the liquid-like environment and. By analogy with liquid-phase experiments, NO_3^- photolysis will generate NO_2 and NO_2^- as primary photochemical products with local quantum yields of the order of 1%. Actual quantum yields will be ultimately determined by the extent of light penetration into the medium, and by the probability of NO_2 escape from the ice network.

We probed light transmission through the ice layers by means of the in situ photoisomerization of 2-nitrobenzaldehyde into 2-nitrosobenzoic acid, an intramolecular process whose quantum yield is phase-independent (Pitt et al., 1965; George and Scaiano, 1980; Filby and Gunther, 1981). We found that photoisomerization rates in spray-frozen 33 μM 2-NBA solutions, as determined from the yields of 2-nitrosobenzoic acid in the melt, are independent of ice thickness (h), confirming uniform rates of light absorption across the deposits depth. Limited light penetration would have led to smaller isomerization quantum yields in the thicker layers. The same observation applies to the stationary nitrite concentrations reached during the photolysis of 10 mM KNO_3 spray-frozen solutions at 263 K (Fig. 4.2).

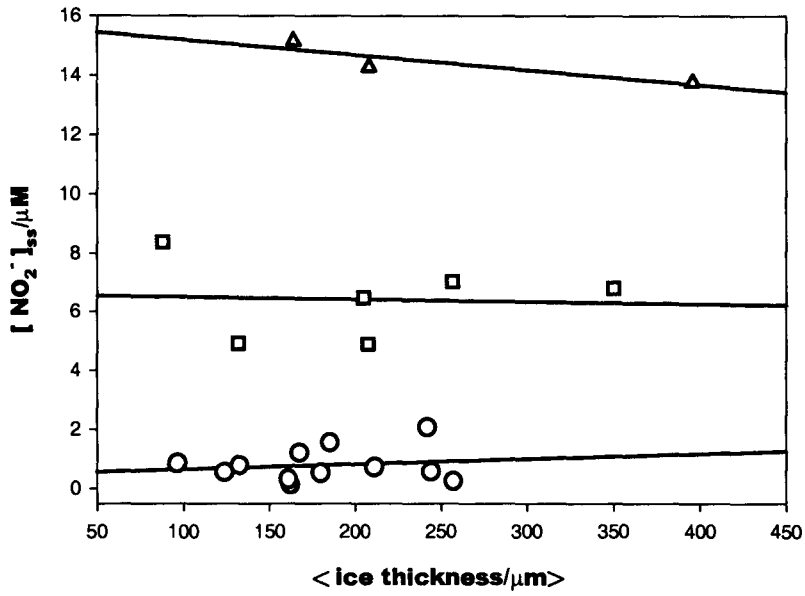

Figure 4.2 Photostationary nitrite concentrations $[NO_2^-]_{ss}$ as a function of average ice layer thickness, *h*, at different nitrate concentrations $[NO_3^-]$/mM: 0 (Open circles), 10 (open squares) and 50 (open triangles). T = 263K. Solid lines are linear fits. $[NO_2^-]_{ss}$ is considered to be independent of *h* within the experimental error.

The evolution of $[NO_2^-]$ during the photolysis of NO_3^- is given by

$$\frac{d[NO2-]}{dt} = \phi_2 I_{a,NO_3^-} - \phi_5 I_{a,NO_2^-} - k_6 [OH]_{ss} [NO_2^-] \ , \qquad (7a)$$

where the I_a's are the absorbed photon rates (in photons cm^{-3} s^{-1}), and the ϕ's the corresponding quantum yields; $[OH^-]_{ss}$ is the rapidly attained steady-state OH radical concentration during the photolysis. Since $I_{a,NO_2^-} \propto [NO_2^-]$, Eq. 7a can be rewritten as

$$\frac{d[NO2-]}{dt} = \phi_2 I_{a,NO_3^-} - k_{decay} [NO_2^-] \ . \qquad (7b)$$

Integration of Eq. 7 leads to

$$[NO_2^-] = \frac{a}{b}[1 - \exp(-bt)] \quad , \tag{8}$$

where $a/b = \phi_2 \, I_{a,NO_3^-} / k_{decay}$ and $b = k_{decay}$. A fit to the $[NO_2^-]_{ss}$ vs. time data in the photolysis of $[NO_3^-]$ = 10 mM at 263 K (Fig. 4.3) yields $a = 3.9 \times 10^{-10}$ M s^{-1}, $b = 5.3 \times 10^{-5}$ s^{-1}. Therefore, an estimate of I_{a,NO_3^-} will provide a ϕ_2 value.

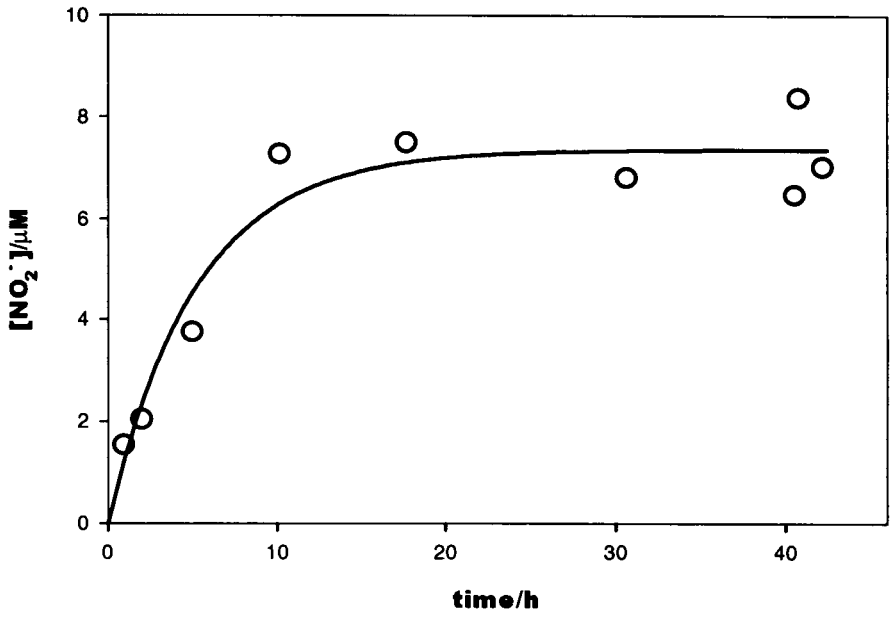

Figure 4.3 Nitrite concentration as a function of irradiation time. $[NO_3^-]$ = 10 mM, 263 K. Open circles are data points. The solid line correspond to $[NO_2^-]$ = 7.36 μM × [1 - exp(-0.19 × t)]. Photostationary nitrite concentrations are approached after about 10 hours.

As mentioned before, I_{a,NO_3^-} can be calculated from 2-NBA in situ photoisomerization rates. The increase of 2-nitrosobenzoic acid concentration with irradiation time indicated that a frozen 33 μM 2-NBA solution absorbs (7 ± 1) × 10^{16}

photons L^{-1} s^{-1}. In order to calculate I_{a,NO_3^-} from this result, it is necessary to evaluate the average extinction coefficients $\langle \varepsilon_i \rangle$ of the various species over the lamps output spectrum (see Appendix 4-3):

$$\langle \varepsilon_i \rangle = \frac{\int_{295nm}^{335nm} \varepsilon_{i,\lambda} I_{lamp}(\lambda) d\lambda}{\int_{295nm}^{335nm} I_{lamp}(\lambda) d\lambda} \tag{9}$$

where $I_{lamp}(\lambda)$ is the lamp emission intensity at λ, and $\varepsilon_{i,\lambda}$ is the absorption coefficient of species i at λ. We find that $\langle \varepsilon_{NO_3^-} \rangle$ = 2.2 M^{-1} cm^{-1} and $\langle \varepsilon_{2\text{-NBA}} \rangle$ = 976 M^{-1} cm^{-1}. Hence, from

$$\frac{I_{a,NO_3^-}}{I_{a,2-NBA}} = \frac{\langle \varepsilon_{NO_3^-} \rangle}{\langle \varepsilon_{2-NBA} \rangle} \cdot \frac{[NO_3^-]}{[2-NBA]} \tag{10}$$

we obtain I_{a,NO_3^-} = (4.9 ± 1.2) $\times 10^{16}$ photons L^{-1} s^{-1} for $[NO_3^-]$ = 10 mM. Therefore, $\phi_2 = \phi_{NO_2^-} = a / I_{a,NO_3^-}$ = (4.8 ± 1.5) $\times$ 10^{-3}. This value is within a factor of two of the previously reported quantum yields of nitrite formation in the λ > 300 nm photolysis of aqueous nitrate solutions in the presence of radical scavengers at room temperature: $\phi_{NO_2^-} \sim 6 \times 10^{-3}$ (Warneck and Wurzinger, 1988; Alif and Boula, 1991; Jankowski et al., 1999). In

Fig. 4.4 we show $[NO_2^-]_{ss}$ as function of $[NO_3^-]$ in photolyses at 268 and 263 K, as well as in a dark experiment, in the presence of 10 mM CH_3OH as radical scavenger at 263 K, and in the liquid phase T ~ 285 K. It is apparent that $[NO_2^-]_{ss}$ in the liquid phase at $[NO_3^-]$ = 10mM is about a factor of two larger than in ice at 268 K. The lack of NO_2^- production during the dark experiment and the dependence of $[NO_2^-]_{ss}$ on $[NO_3^-]_0$, indicate that NO_2^- is a product of NO_3^- photolysis. $[NO_2^-]_{ss}$ is slightly higher in the presence of 10mM CH_3OH, however, this increase is still within the error range.

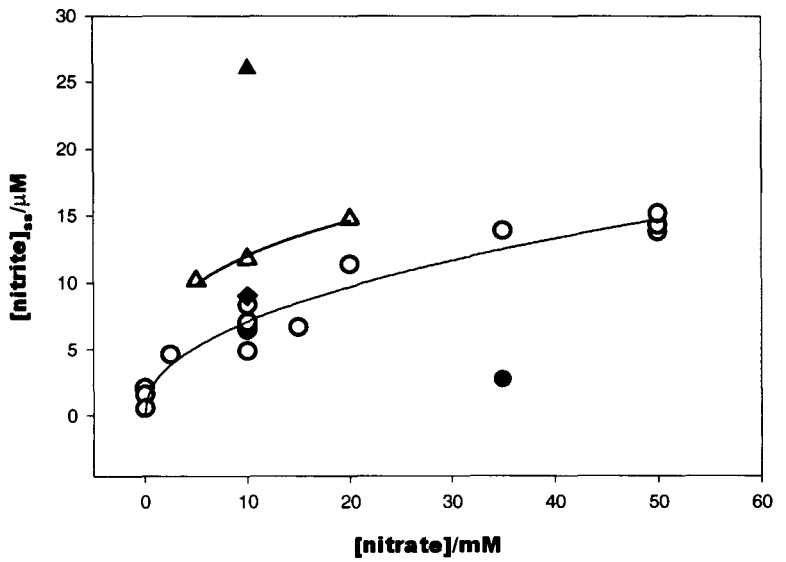

Figure 4.4 $[NO_2^-]_{ss}$ as function of $[NO_3^-]$ in nitrate photolyses: in ice at 268 K (Open triangles), 263 K (open circles), in the presence of 10 mM CH_3OH as radical scavenger at 263 K (full diamond), and in the liquid phase at T ~ 285 K (full triangle). The full circle is a dark experiment at 263 K.

In contrast with the inference from Fig. 4.2, that the light is uniformly absorbed within the ice layer (at least up to h = 400 μm), the NO_2 fluxes into the gas-phase in the same experiments are nearly independent of h (Fig. 4.5). In other words, NO_2 emission rates remain constant despite of the fact that more NO_3^- is photolyzed in the thicker ice layers. The inevitable conclusion is that only the NO_2 produced in outer region of the ice deposits is able to escape into the gas-phase. Actually, with $\langle \varepsilon_{NO_2} \rangle$ = 210 M^{-1} cm^{-1}, calculated by means of Eq. 9 from literature NO_2 absorption cross-sections in the gas-phase (DeMore et al., 1997), secondary photolysis appears to be the main fate of trapped NO_2:

$$NO_2 + h\nu \rightarrow NO + O(^3P) \qquad (11)$$

Nitric oxide, the product of reaction 11, is undetectable by our analytical procedures.

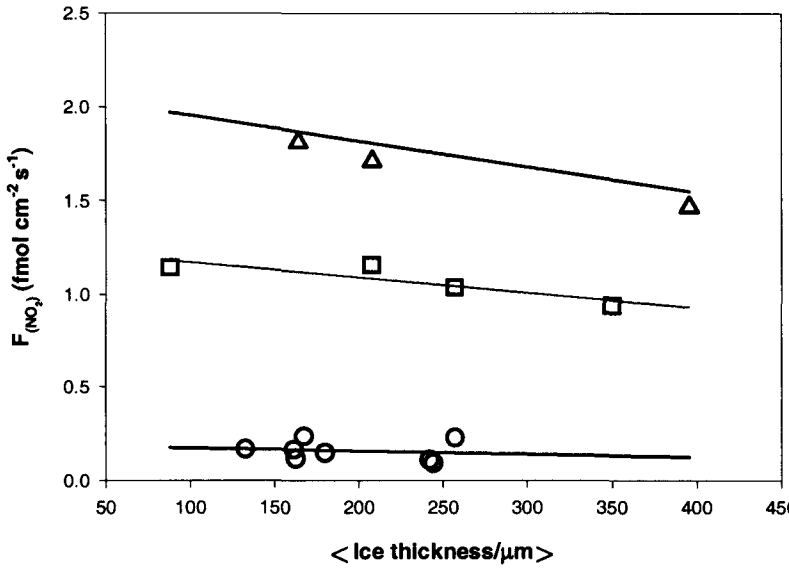

Figure 4.5 NO_2 flux, F_{NO_2}, as a function of average ice thickness at different $[NO_3^-]$/mM: 0 (Open circles), 10 (open squares) and 50 (open triangles). T = 263 K. Solid lines are linear fits.

In Fig. 4.6, we present F_{NO_2} as function of $[NO_3^-]$ at three ice temperatures, as well as F_{NO_2} data for dark experiments, in the presence of 10 mM CH_3OH, and in the liquid phase. F_{NO_2} from liquid phase photolysis at 283 K are more than a factor of three larger than in ice at 268 K, a result that reflects the competition between the higher NO_2 solubility and faster diffusion in the fluid medium. As was observed for $[NO_2^-]_{ss}$, F_{NO_2} is detectable only when the NO_3^- doped ice is illuminated and it increases with $[NO_3^-]_0$, indicating that NO_2 (g) is also a product of NO_3^- photolysis. No *increase in* F_{NO_2} *is*

observed in the presence of 10mM CH_3OH, which might be a result of insufficient CH_3OH concentration ($[CH_3OH]_0/[NO_3^-]_0 = 1$).

Since about 40% of NO_2 is photolyzed during its residence time (τ = 17.7 min) in the illuminated zone at typical carrier flow rates, we consider that that actual F_{NO_2} values at the ice surface are a factor of 1.67 larger than determined experimentally. Therefore, we estimate an apparent quantum yield for NO_2 release: $\phi_1' = \phi'_{NO_2} = 1.67\ (F_{NO_2} / h)/ I_{a,NO_3^-} = (1.2 \pm 0.8) \times 10^{-3}$ at $[NO_3^-]$ = 10 mM, h ~ 220 μm, 263 K. However, the primary quantum yield ϕ_1 is expected to be somewhat larger, because F_{NO_2} remains nearly constant down to h ~ 100 μm, implying that $\phi_1 > 2.6 \times 10^{-3}$ at $[NO_3^-]$ = 10 mM, 263 K.

The latter is in reasonable accord with ϕ_{OH} previously measured in aqueous solutions and extrapolated to 263 K (using Ea = 16.3 kjoule $mole^{-1}$; Zellner and Herrman, 1990; Jankowski et al., 1999): $\phi_{OH} \sim 5 \times 10^{-3}$ (Zepp's et al., 1987), $\phi_{OH} \sim 3 \times 10^{-3}$ (Jankowski et al., 1999), and $\phi_{OH} \sim 3 \times 10^{-3}$ (extrapolated from Warneck and Wurzinger data in the presence of 1 mM scavenger; Warneck and Wurzinger, 1988).

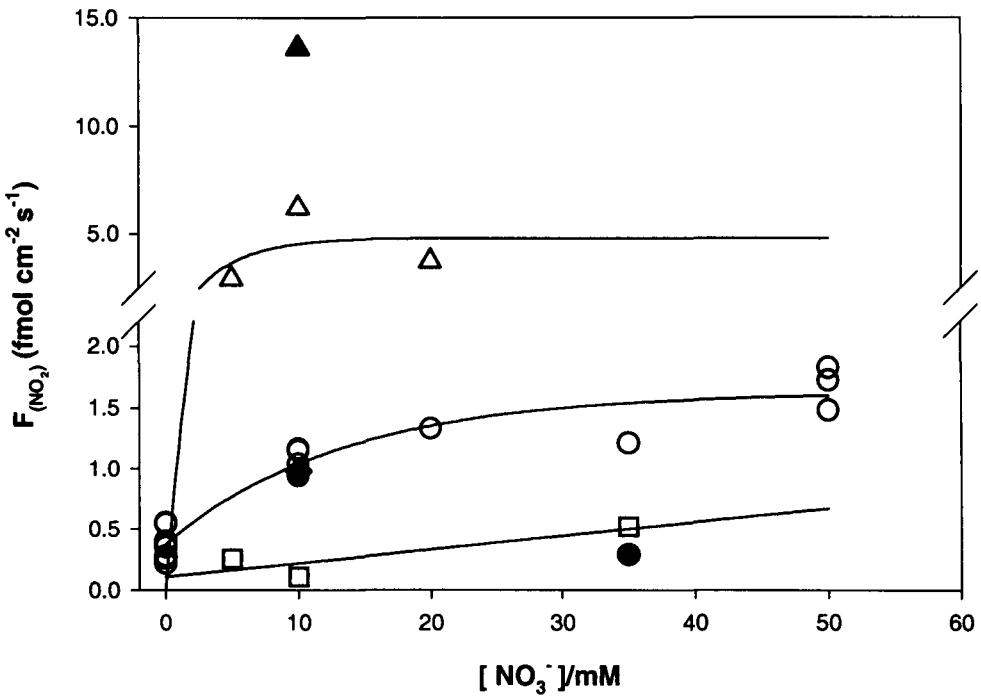

Figure 4.6 NO_2 flux, F_{NO_2}, as function of [NO_3^-] in photolyses in ice at 268 K (Open triangles), 263 K (open circles), 248 K (open squares), in the presence of 10 mM CH_3OH as radical scavenger at 263 K (full diamond), and in the liquid phase at T ~ 285 K (full triangle). The full circle is a dark experiment at 263 K.

As shown in Fig. 4.5, F_{NO_2} is independent of h down to about 100 μm. In order estimate the maximal diffusion rate of NO_2 through the ice layer, it may be assumed that about 50% of the NO_2 produced within 100 μm thick ice can diffuse into and be detected in gas-phase. Then it is possible to estimate the effective diffusion coefficient of NO_2 in spray-frozen ice from: $D'_{NO_2} = h_{min}^2 / (2\,\tau) \sim (10^{-2}\ \text{cm})^2 / (2 \times 1275\ \text{s}) = 4 \times 10^{-8}\ \text{cm}^2\ \text{s}^{-1}$ (τ is the time required to photolize 50% of the formed NO_2, see appendix 4-4). The latter

is intermediate between $D_{NO_3H} \sim 2 \times 10^{-11}$ cm^2 s^{-1} in bulk ice at 258 K and $D_{NO_3H} \sim 3 \times 10^{-7}$ cm^2 s^{-1} on ice surfaces below 253 K (Laird et al., 1999; Sommerfeld et al., 1998; Domine and Thibert 1998). The estimated value of the effective diffusion coefficient D'_{NO_2} suggests that only the NO_2 produced within a few tens of microns from the ice/air interface is actually released into the gas-phase.

The temperature dependence of ϕ_1' for $[NO_3^-]$ = 10 mM, $h \approx 200$ μm, (Fig. 4.7) is given by

$$\log \phi_1' = 5.42 - \frac{2187}{T} \quad , \tag{12}$$

which indicate an activation energy for the release of NO_2 of the order of 10 kcal mol^{-1}.

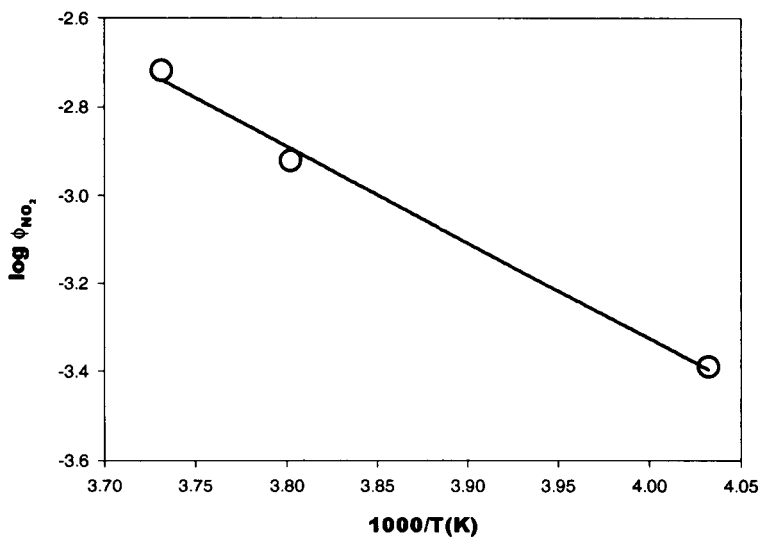

Figure 4.7 Apparent quantum yield of NO_2 production from irradiation of 10 mM nitrate doped ice as a function of temperature. Average ice thickness varies between 125μm at 268 K, 224 μm at 263 K and 176 μm at 248 K.

The stronger temperature dependence of F_{NO_2} relative to nitrite photochemical production (Fig. 4.4) under the same conditions could be ascribed to the enhanced probability of NO_2 escape from the solid and/or the thicker liquid films prevalent at higher temperatures.

4.4.1 Atmospheric implications

4.4.1.1 Polar boundary layer

Snowpacks are highly reflective dispersed materials (effective albedo $\beta \sim 0.90$ - 0.95; Perovich and Govoni, 1991); about 40% of the total snow volume consists of ice microparticles. The actinic solar flux penetrating into the snowpack is partially absorbed by pure ice and by impurities (e.g., organic matter), leading to overall exponential snow absorptivities of the order of $\alpha \sim 15$ m^{-1} (Mellor, 1977; Warren, 1982; Perovich and Govoni, 1991). Nitrate itself, present in submicromolar concentrations, is a minor chromophore in snowpacks. Therefore, if $\langle J_\lambda \rangle$ is the average solar flux at the surface of the snowpack, the photon flux absorbed by nitrate in a snow column of depth l is given by

$$< J_{NO_3^-} >=< J_\lambda > \cdot (1 - e^{-\alpha \ell}) \cdot \frac{< \varepsilon_{NO_3^-} > \cdot [NO_3^-]}{\alpha} \qquad (13)$$

from which the maximum possible NO_2 flux released from the snowpack can be calculated as

$$F_{NO_2} = \phi_1 \langle J_{NO_3^-} \rangle \qquad (14)$$

Jones et al. (2000) report $F_{NO_2} = 4.2 \times 10^7$ molecules cm^{-2} s^{-1} from l = 20 cm cubic blocks of natural snow containing $[NO_3^-]$ = 50 ng/g = 0.8 μM, at 266 K, under a solar irradiance of $\langle J_\lambda \rangle$ = 30 W m^{-2} = 5×10^{15} photons (λ = 337 nm) cm^{-2} s^{-1}, at the Neumeyer Antarctic station (70° S, 8° W). Assuming $\alpha = 0.15$ cm^{-1} (water equivalent, for δ = 0.4 g cm^{-3} snow density), with $\langle \varepsilon_{NO_3^-} \rangle$ = 0.54 M^{-1} cm^{-1} between 290 and 385 nm (i.e., the spectral interval over which $\langle J_\lambda \rangle$ is measured), we obtain $\langle J_{NO_3^-} \rangle = 1.0 \times 10^{10}$ photons cm^{-2} s^{-1}, and $\phi_1' = 4 \times 10^{-3}$, i.e., within a factor of four of the ϕ_1' value we find for $[NO_3^-]$ = 10 mM in ice. The accord is certainly within the uncertainties associated with the assumed properties of snow, and the assumed independence of ϕ_1' on $[NO_3^-]$ below 10 mM.

4.4.1.2 Cirrus clouds

It was suggested recently that the overprediction of the $[HNO_3]/[NO_x]$ ratio in the upper troposphere by current models could be due to the photochemical conversion of HNO_3 into NO_x on ice particles in cirrus clouds (Hoffmann, 1996; Honrath et al., 1999). In order to evaluate this suggestion, we used the quantum yield measured in the present study to estimate the production rate of NO_2 via this pathway. We calculate a maximum production rate of 48 NO_2 molecules cm^{-3} s^{-1} under optimal conditions, i.e, at constant cirrus cover with a surface area of 2×10^{-4} cm^2 cm^{-3} (Toon, 1996), complete adsorption (Abbatt, 1997; Leu, 1988) of the extant 400 pptv HNO_3 concentration at 10 km altitude, 35°N (Singhet al., 1996), an actinic flux of $\langle J_\lambda \rangle = 1.6 \times 10^{16}$ photon cm^{-2} s^{-1} over the range 290-380 nm (DeMore et al., 1997), and $\langle \sigma_{NO_3^-} \rangle = 9 \times 10^{-22}$ cm^2 $molecule^{-1}$. Considering that $[NO_2]$ ~ 40 pptv ($[NO_2] = [NO_x] - [NO]$ as measured at 10 km; Singh et

al., 1996), this flux corresponds to NO_2 lifetime of 68 days, which is much longer then the actual lifetimes (5-7 days) in the upper troposphere (Abbatt, 1997; Leu, 1988). Thus, the NO_3H/NO_2 recycling via absorption and photolysis on ice particles does not seem to resolve the discrepancy between the predicted and measured $[HNO_3]/[NO_x]$ ratio.

4.4.1.3. Ice core records

As mentioned before, nitrate levels within ice cores may provide valuable information on the past photochemical and oxidative states of the troposphere (Wolff, 1995). However, there is mounting evidence for postdepositional losses of nitrate from surface snowpack (e.g., Wolff, 1995). One candidate process is photochemical degradation of nitrate. The loss of nitrate with depth was found to be anticorrelated with snow deposition rate (Mayewski and Legrand, 1990). This might be, in part, a result of longer exposure to sunlight at sites with lower accumulation rates.

The photochemical degradation of nitrate as a function of depth (Z) can be expressed as follows (eq. 15):

$$\frac{d[NO_3^-]}{dz} = \frac{d[NO_3^-]}{dt} \cdot \frac{dt}{dz} = -\frac{1}{A} \cdot I_0 \cdot e^{-\alpha z} \cdot \phi \cdot <\sigma_{nitrate}> \cdot [NO_3^-] \qquad (15)$$

$$C = \frac{1}{A} \cdot I_0 \cdot \phi \cdot <\varepsilon_{nitrate}>$$

$$[NO_3^-]_z = [NO_3^-]_0 \cdot e^{\frac{C}{\alpha}(e^{-\alpha z}-1)}$$

Considering an annual average actinic flux (I_0), 300 nm – 340 nm, of 5.48×10^{-3} einstein cm^{-2} y^{-1} at 70°N (Leifer, 1988), $<\sigma_{nitrate}>$ = 1760 cm^2 $mole^{-1}$ (calculated based on nitrate absorption spectrum in aqueous solution and surface solar spectrum from DeMore et al., 1997), snow accumulation rate (A) of 7.5 cm y^{-1}(equivalent to 3 ng cm^{-2} y^{-1} with snow

density of 0.4 g cm^{-3}), $[NO_3^-]_0$ = 0.8 μM and a total quantum yield for nitrate photolysis of 6×10^{-3} ($= \phi_1 + \phi_2$), the following profile is calculated (Fig. 4.8):

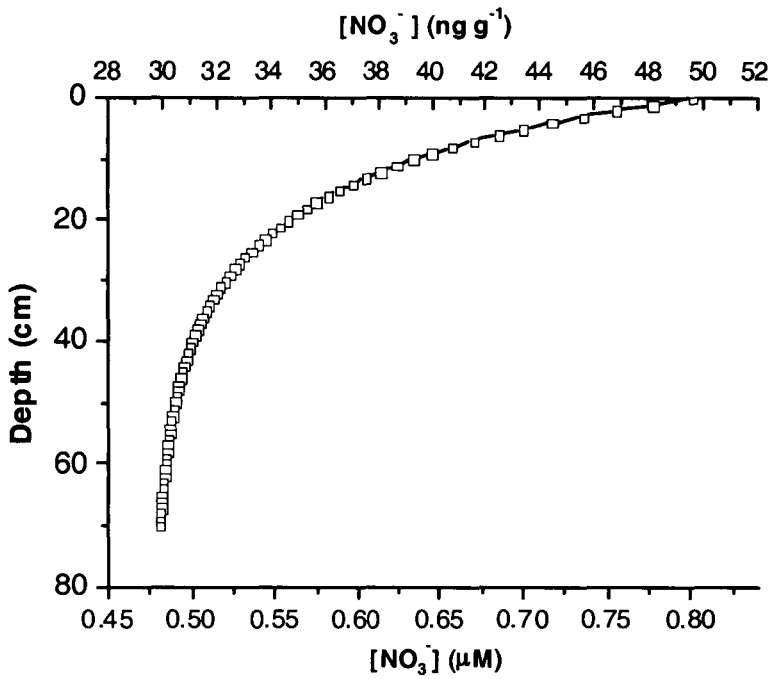

Figure 4.8 Nitrate concentration vs. depth as calculated from equation 15. Under the conditions used in the calculations (A = 7.5 cm/y; $I_0 = 5.48 \times 10^{-3}$ Einstein cm^{-2} y^{-1}, $\langle \varepsilon_{nitrate} \rangle$ = 1760 cm^2 $mole^{-1}$ and, $\phi = 6 \times 10^{-3}$), nitrate concentration decreases by ~40% within the upper 20 cm of the snowpack.

As can be seen from Figure 4.8, photochemical degradation of nitrate can be a significant factor that should be considered when trying to correlate nitrate levels measured in ice cores to paleoatmospheric levels. This is especially true if one considers the possibility of changes in snow accumulation rates over time. Furthermore, since nitrate photolysis produces OH and $O(^3P)$ radicals, the effect of this photolytic process on

concentrations of other chemical compounds that are present in the snow at lower concentrations and may react with these radicals (e.g., H_2O_2, HCHO and CO_2) could be even more significant.

When comparing our results (Fig. 4.8) with observed nitrate profiles (Fig. 4.9), it is clear that photochemistry may account for significant portion of the observed nitrate loss at sites with low accumulation rates, and that further studies are required to understand the fate of nitrate within snow/ice deposits.

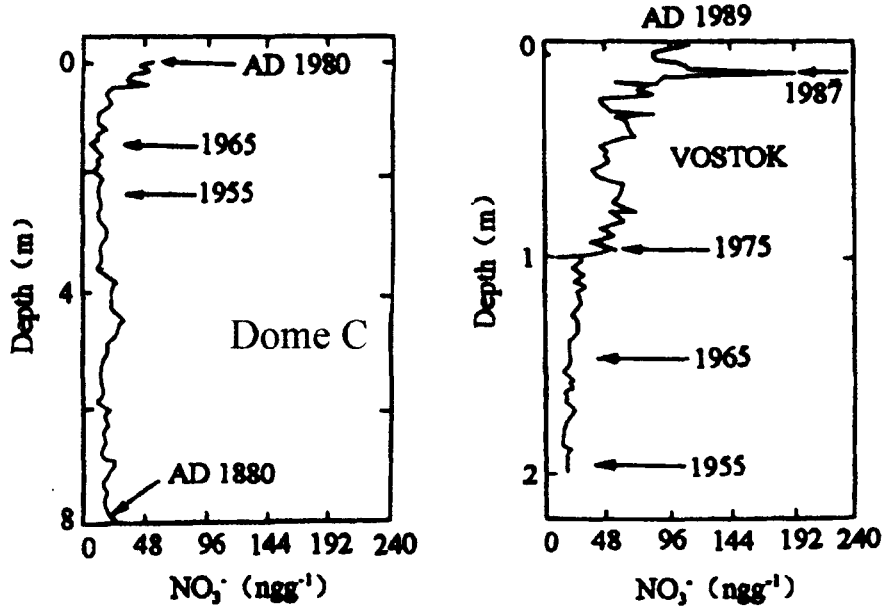

Figure 4.9 Nitrate concentrations along ice cores sampled at Dome C (accumulation rate of ~2 g cm^{-2} y^{-1}) and at Vostok station (accumulation rate of 2.3 g cm^{-2} y^{-1}) (Mayewski and Legrand, 1990). Nitrate levels tend to decrease with depth in the upper meter or so of the cores. This trend is known to be more pronounced at locations with lower snow accumulation rates.

References

1. Abbatt, J.P.D., Interaction of HNO_3 with Water-Ice Surfaces at Temperatures of the Free Troposphere, *Geoph. Res. Lett. 24* , 1479-1482, 1997.
2. Alif, A., and P. Boule, Photochemistry and Environment Part XIV. Phototransformation of Nitrophenols Induced by exitation of Nitrite and Nitrate Ions, *J. Photochem. Photobio. A: Chem., 59*, 357-367, 1991.
3. Calvert, J., and J.N. Pitts, *Photochemistry*, 783 pp., Wiley, New York, 1966.
4. Dash, J.G., H.Y. Fu, and J.S. Wettlaufer, The Premelting of Ice and Its Environmental Consequences, *Rep. Prog. Phys., 58*, 115-167, 1995.
5. Demore, W.B., S.P. Sander, D.M. Golden, R.F. Hampson, M.J. Kurylo, C.J. Howard, A.R. Ravishankara, C.E. Kolb, and M.J. Molina, *Chemical Kinetics and Photochemical Data for Use in Stratospheric Modeling*, Jet Propulsion Laboratory, 1997.
6. Domine, F., and E. Thibert, Comment on <Diffusion of HNO_3 in ice>, *Geoph. Res. Lett. 25*, 4389-4390, 1998.
7. Doppenschmidt, A., and H.-J. Butt, Measuring the Thickness of the Liquid-like Layer on Ice Surfaces with Atomic Force Microscopy, *Langmuir, 16*, 6709-6714, 2000.
8. Filby, G.W., and K. Gunther, ESR Studies of the o-Nitrobenzaldehyde Rearrangement: Estimation of the Quantum Yields of Radical Formation, *Zeitschrift fur Physikalische Chemie Neue Folge, 125*, 21-26, 1981.
9. George, M.V., and J.C. Scalano, Photochemistry of o-Nitrobenzaldehyde and Related Studies, *J. Phys. Chem., 84*, 492-495, 1980.

10. Gross, G.W., A. Gutjahr, and K. Caylor, Recent Experimental Work on Solute Redistribution at the Ice/Water Interface. Implications for Electrical Properties and Interface Processes, *Journal De Physique*, C1, 527-533, 1987.

11. Gross, G.W.; Wong, P.M.; Humes, K.; *J. Chem. Phys.* 1977, *67*, 5264.

12. Hoffmann, M.R., Possible Chemical Transformations in Snow and Ice Induced by Solar (UV Photons) and Cosmic Irradiation (Muons), in *Chemical Exchange Between the Atmosphere and Polar Snow*, edited by W. Wolff, and R.C. Bales, pp. 353-377, Springer, Berlin, 1996.

13. Honrath, R.E., S. Guo, M.C. Peterson, M.P. Dziobak, J.E. Dibb, and M.A. Arsenault, Photochemical Production of Gas-Phase NO_x from Ice-Crystal NO_3^-, *j. Geophys. Res. –Atmos.*, *105*, 24183-24190, 2000.

14. Honrath, R.E., M.C. Peterson, M.P. Dziobak, S. Green, J.E. Dihbb, and M.A. Arsenault, Release of NO_x from Sunlight-Irradiated Midlatitude Snow, *Geophys. Res. Lett. 27*, 2237-2240, 2000.

15. Honrath, R.E., M.C. Peterson, S. Guo, J.E. Dibb, P.B. Shepson, and B. Campbell, Evidence of NOx Production Within or Upon Ice Particles in the Greenland Snowpack, *Geophys. Res. Lett. 26*, 695-698, 1999.

16. Jankowski, J.J., D.J. Kieber, and K. Mopper, Nitrate and Nitrite Ultraviolet Actinometers, *Photochem. and Photobio. 70*, 319-328, 1999.

17. Jones, A.E., R. Weller, E.W. Wolff, and H.-W. Jacobi, Speciation and Rate of Photochemical NO and O_2 Production in Antarctic Snow. *Geophys. Res. Lett. 27*, 345-348, 2000.

18. Laird, S.K., D.A. Buttry, and R.A. Sommerfeld, Nitric Acid Adsorption on Ice: Surface Diffusion, *Geophys. Res. Lett. 26*, 699-701, 1999.

19. Leu, M.T., Laboratory Studies of Sticking Coefficients and Heterogeneous Reactions Important in the Antarctic Stratosphere, *Geophys. Res. Lett. 15*, 17-20, 1988.

20. Logan, J.A., Nitrogen Oxides in the Troposphere: Global and Regional Budgets, *J. Geophys. Res. 88*, 10785-10807, 1983.

21. Mack, J., and J.R. Bolton, Photochemistry of Nitrite and Nitrate in Aqueous Solutions: A Review, *J. Photochem. and Photobio. 128*, 1-13, 1999.

22. Mark, G., H.G. Korth, H.P. Schuchmann, and C. von Sonntag, The Photochemistry of Aqueous Nitrate Ion Revisited, *J. Photochem. and Photobio A: chemistry, 101*, 89-103, 1996.

23. Mayewski, P.A., W.B. Lyons, M.J. Spencer, M.S. Twickler, C.F. Buck, and S. Whitlow, An Ice-Core Record of Atmospheric Response to Anthropogenic Sulphate and Nitrate, *Nature, 346*, 554-556, 1990.

24. Mellor, M., *J. Glaciology*. 1977, *19*, 15.

25. Mulvaney, R., D. Wagenbach, and E.W. Wolff, Postdepositional Change in Snowpack Nitrate from Observation of Year-Round Near-Surface Snow in Coastal Antarctica, *J. Geophys. Res. 103*,11021-11031, 1998.

26. Neubauer, J., and K.G. Heumann, Determination of Nitrate At the Ng/G Level in Antarctic Snow Samples With Ion Chromatography and Isotope-Dilution Mass-Spectrometry, *Fresenius Zeitschrift Fur Analytische Chemie, 331*,170-173, 1988.

27. Neubauer, J., and K.G. Heumann, Nitrate Trace Determinations in Snow and Firn Core Samples of Ice Shelves At the Weddell Sea, Antarctica, *Atmos. Environ. 22*, 537-545, 1988.

28. Perovich, D.K., Observations of Ultraviolet-Light Reflection and Transmission By First-Year Sea-Ice, *Geophys. Res. Lett. 22*,1349-1352, 1995.

29. Pitt, J.N., L.D. Hess, E.J. Baum, A. Schuck, and J.K.S. Wan, The Transfer and Conversion of Elecronic Energy in Some "Model' Photochemical Systems, *J. Photochem. and Photobio*, *4*, 305-321, 1965.

30. Platt, U., The Origin of Nitrous and Nitric Acid in the Atmosphere, in *Chemistry of Multiphase Atmospheric Systems*, edited by W. Jaeschke, Springer-Verlag, New York, 1986.

31. Pomeroy, J.W., and H.G. Jones, Wind-Blown Snow: Sublimation, Transport and Changes to Polar Snow, in *Chemical Exchange Between the Atmosphere and Polar Snow, NATO ASI Ser., Ser. I*, edited by E.W. Wolff, and R.C. Bales, pp. 453-489, Springer-Verlag, New York, 1996.

32. Saltzman, B.E., Colorimetric Microdetermination of Nitrogen Dioxide in the Atmosphere, *Anal. Chem. 26*, 1949-1955, 1954.

33. Seidel, A., *Solubilities,* Van Nostrand, New York, 1940, vol. 1, pg. 833.

34. Silvente, E., and A. Legrand, A preliminary Study of the Air-Snow Relationship for Nitric Acid in Greenland, in *Ice Cores Studies of Global Biogeochemical cycles, NATO ASI ser. Ser I*, edited by R.J. Delmas, pp. 225-240, Springer-Verlag, New York, 1995.

35. Singh, H.B., D. Herlth, R. Kolyer, L. Salas, J.D. Bradshaw, S.T. Sandholm, D.D. Davis, J. Crawford, Y. Kondo, M. Koike, R. Talbot, G.L. Gregory, G.W. Sachse, E. Browell, D.R. Blake, F.S. Rowland, R. Newell, J. Merrill, B. Heikes, S.C. Liu, P.J. Crutzen, and M. Kanakidou, Reactive Nitrogen and Ozone over the Western Pacific: Distribution, Partitioning, and Sources, *J. . Geophys. Res. - Atmospheres*, *101*,1793-1808, 1996.

36. Sommerfeld, R.A., C.A. Knight, and S.K. Laird, Diffusion of HNO_3 in ice, *Geophys. Res. Lett. 25*, 935-938, 1998.

37. Toon O. B.; Paper presented at international workshop on modeling heterogeneous chemistry of the lower stratosphere/upper troposphere, Le Bischenberg, Bischoffsheim, France, 1996.

38. Warneck, P., and C. Wurzinger, Product Quantum Yield for the 305-nm Photodcomposition of NO_3^- in Aqueous Solution, *J. Phys. Chem.*, *92*, 6278-6283, 1988.

39. Wolff, E.W., Nitrate in polar ice, in *Ice Cores Studies of Global Biogeochemical cycles, NATO ASI ser. Ser I*, edited by R.J. Delmas, pp. 195-224, Springer-Verlag, New York, 1995.

40. Zepp, R.G., J. Hoigne, and H. Bader, Nitrate-Induced Photooxidation of Trace Organic Chemicals in Water, *Environ. Sci. Tech. 21*, 443-450, 1987.

Appendix 4-1: Colorimetric determination of NO_2(g) with Saltzman's reagent

The determination of the amount of NO_2 condensed in the trap included several steps: After thawing the trap, the NO_2 was dissolved in an NaOH solution to yield, via disproportionation, nitrate (nitric acid) and nitrite (nitrous acid) (rxn. 1). Saltzman's reagent (0.5% sulfanilic acid, 0.002% N-(1-naphthyl)-ethylenediamine dihydrochloride and 14% glacial acetic acid) was then added to the solution (at a molar ratio of 2:1). Under acidic conditions, the nitrous acid reacts with sulfanilic acid to yield diazotized sulfanilic acid (rxn 2). This intermediate then reacted with N-(1-naphthyl)-ethyl-enediamine dihydrochloride to form a red-violet complex (rxn 3). The azo-dye product was then measured colorimetrically (at λ = 548 nm) to quantify the nitrite (HONO) concentration.

$$2NO_2 \rightleftharpoons N_2O_4 \qquad (1)$$

$$H_2O + N_2O_4 \longrightarrow HNO_2 + HNO_3 \quad \text{or} \quad H_2O + NO_2 \longrightarrow HNO_2 + HNO_3$$

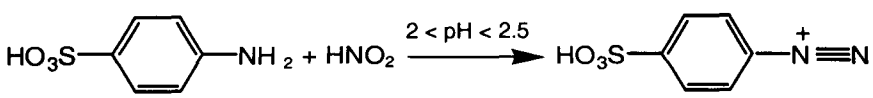

(2)

(Sulfanilic acid) (diazotized sulfanilic acid)

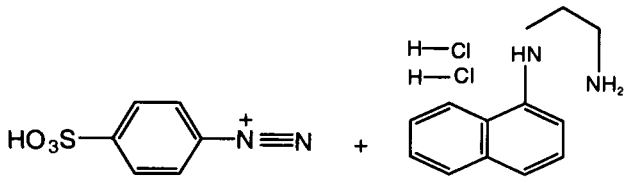

(3)

(N-(1-naphtyl)-ethylenediamine dihydrochloride)

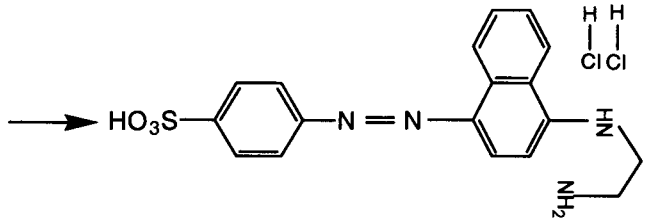

(reddish-purple color)

Appendix 4-2: NO_2 collection efficiency

In order to calculate the NO_2 trapping yield, a known amount of calibrated NO_2 (g) was flushed through the cold trap with the same carrier gas as used in the actual experiments at similar flow rate (Fig. 4.10)

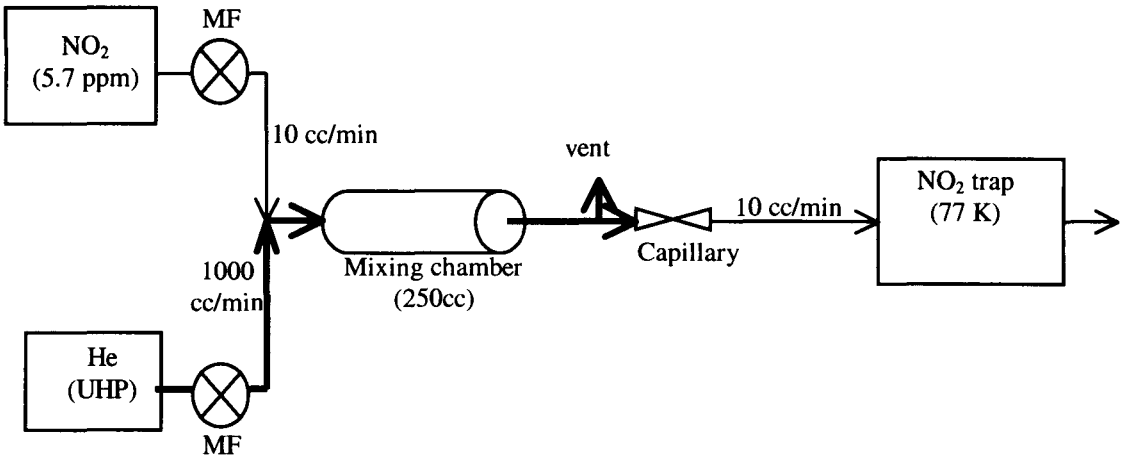

Figure 4.10 A schematic diagram of the setup for calibrating the trapping efficiency of the NO_2 condensation trap (MF stands for mass flow controllers). The NO_2 mixing ratio in the certified cylinder was determined with a NO_x analyzer (Thermoenvironmental model 42) calibrated with a certified NO cylinder.

The collecting efficiency ($X_{collect}$) was calculated as follows:

(1) $$n(NO_2)_{expected} = \frac{t \cdot f_{mix} \cdot [NO_2]_{mix} \cdot 10^{-9} \cdot P}{T \cdot R}$$

Where: t = duration of collection

f_{mix} = flow of the gas mixure (0.01 L/min)

$[NO_2]_{mix}$ = NO_2 concentration in the mixure (670 ppb)

P = presure (atm.)

T = temperature (K)

R = gas constant ($0.083\ L \cdot atm \cdot mole^{-1} \cdot K^{-1}$)

(2) $$X_{collect} = \frac{n\,(NO_2)_{measured}}{n\,(NO_2)_{expected}} = 0.42 \pm 0.05$$

Results presented in this chapter have been corrected for a 42% collecting efficiency.

Appendix 4-3: Lamp output Spectrum and the extinction coefficient of 2-NBZA and nitrate

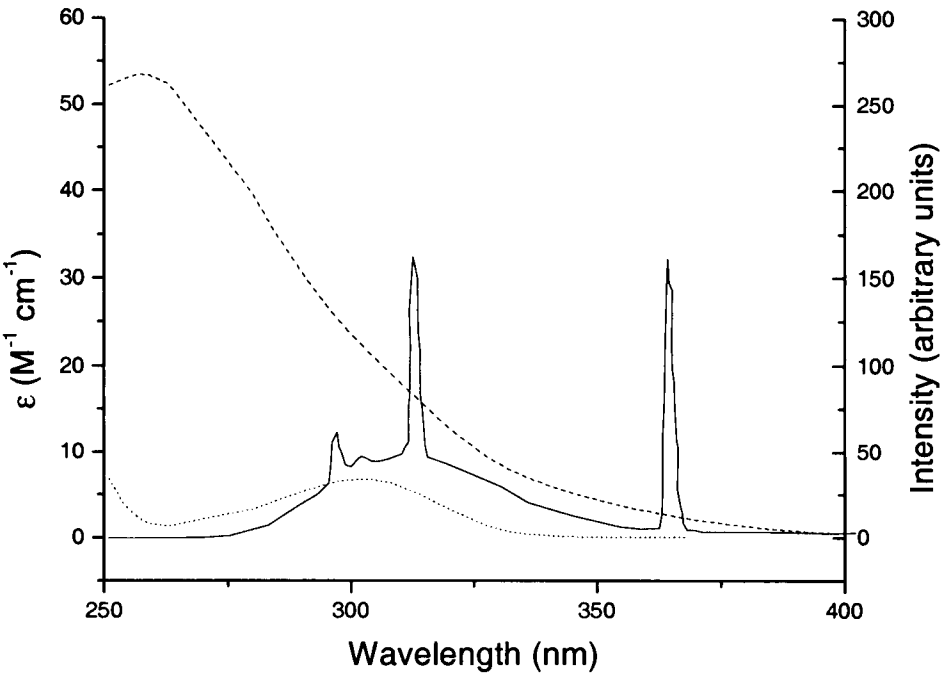

Figure 4.11 A spectrum of Hg Pen-Ray® UV lamps (UVP, modal 90-0001-04) (solid line) and the measured extinction coefficient of 2-nitrobenzaldehyde (divided by a factor of a 100; dashed line) and nitrate (dotted line). The output spectra of our lamps were measured, in relative units, by UVP.

Appendix 4–4: Error analysis

The measured NO_2 flux (F_m) was corrected for the collection efficiency ($X_{collect}$; see appendix #2) and for its secondary photolysis before its removal from the irradiated zone. The fraction of the released NO_2 that had been photolyzed ($X_{photolysis}$) was determined as follows (eq. 10)

$$X_{photolysis} = N/n = I_0 \cdot \tau \cdot \sigma = 0.40 , \qquad (10)$$

where

N is the number of photons absorbed by NO_2 during the residence time, τ (since $\phi_{(NO_2 \text{ to } NO)} \cong 1$, N = the number of the NO_2 molecules being photolyzed),

n is the total number of molecules of NO_2,

I_0 is the incident photon flux on quartz sheath: $(9.75 \pm 1.51) \times 10^{14}$ photon $\cdot$ $cm^{-2} \cdot s^{-1}$

τ is the residence time of the gas in the quartz sheath: 17.7 ± 0.4 min,

σ_{NO_2} is the averaged cross section for NO_2 over the lamp spectra between 295 to 335 nm: 3.85×10^{-19} cm^2·molecule^{-1} ; (σ values from DeMore et al., 1997).

The propagating error analysis was computed as follow:

1. $\sigma(X_{collect})$ was determined as one standard deviation between five tests of collection efficiency (= 0.05)

2. $\sigma(X_{photolysis}) = \frac{N}{n} \times \sqrt{\frac{\sigma^2 I_0}{I_0^2} + \frac{\sigma^2 \tau}{\tau^2}} = 0.06$ (Assuming $\frac{\sigma^2 < \sigma_{NO_2} >}{< \sigma_{NO_2} >^2}$ is negligable)

where $\sigma(I_0)$ was determined as one standard deviation between 12 actinometry measurements, and $\sigma(\tau)$ was defined as one standard deviation between measured flow rates.

3. $$F_{corrected} = \frac{F_m}{X_{collect} \cdot (1 - X_{photolysis})}$$

$$\Rightarrow \frac{\sigma(F_{corrected})}{F_{corrected}} = \sqrt{\frac{\sigma^2(F_m)}{F_m^{\,2}} + \frac{\sigma^2(X_{collect})}{X_{collect}^{\,2}} + \frac{\sigma^2(X_{photolysis})}{X_{photolysis}^{\,2}}}$$

$\frac{\sigma^2(F_m)}{F_m^{\,2}}$ was assumed to be negligable .

4. $$\Delta F_{corrected} = F_{corrected} - F_{blank}$$

$$\Rightarrow \sigma(\Delta F_{corrected}) = \sqrt{\sigma^2 F_{corrected} + \sigma^2 F_{blank}}$$

5. $$\phi = \frac{\Delta F_{corrected}}{I_{Abs}}$$

$$\Rightarrow \frac{\sigma(\phi)}{\phi} = \sqrt{\frac{\sigma^2 \Delta F_{corrected}}{\Delta F_{corrected}^{\,2}} + \frac{\sigma^2(I_{Abs})}{I_{Abs}^{\,2}}}$$

$\sigma(I_{Abs})$ was defined as 1σ of the calculated I_{abs} (2 - NBZA) (n = 6).

Thus for the average quantum yield the error should be

$$\sigma(\phi_{avg}) = \frac{1}{n} \cdot \sqrt{\sum_{i=1-n} \sigma^2 \phi_i}$$

However, since the error calculated in this way was smaller than 1σ of the calculated quantum yield during the various experiments (e.g., 2.4×10^{-4} vs. 7.6×10^{-4} at 10 mM NO_3^-, 263 K), we chose to use the later as the error for the calculated quantum yields.

Chapter 5

Nitrite formation during 302 nm band UV photolysis of nitrate in ice pellets from 233 K to 268 K.

5.1 Introduction

There is a growing interest in the photolysis of NO_3^- within and upon ice due to its potential role in the production of OH radicals and NO_x within snowpacks. This dynamic photochemistry may affect the overall chemistry of the snowpack and the atmospheric boundary layer above it (e.g. Honrath et al., 1999, 2000; Jones et al., 2000, Sumner and Shepson, 1999).

The ionic strength of snow is estimated to vary from $\leq 10^{-5}$ M in pristine areas to 10^{-3} M in areas impacted by anthropogenic deposition (Conklin and Bales, 1993). At these ionic strengths and at the temperatures present during spring and summer at mid and high latitudes, the existence of a significant quasi-liquid layer QLL on the crystals is expected (Honrath et al., 2000; Conklin and Bales, 1993).

The nature of the QLL has been the subject of many theoretical investigations (e.g. Fletcher, 1968; Wettlaufer, 1999; Bolton and Pettersson, 2000) and experimental studies (e.g. Conklin and Bales, 1993; Döppenschmidt et al., 1998; Döppenschmidt and Butt, 2000; Wei et al., 2001). While most of these studies seem to have confirmed the existence of quasiliquid layer on ice surface, the temperature range over which this layer exists, its thickness and physical properties are still debated. Wei and coworkers (Wei et al., 2001) showed that the disordering of the surface of hexagonal ice (using sub-frequency vibrational spectroscopy to measure orientational order of dangling OH bonds) becomes detectable at 200 K and increases dramatically with temperature. Furthermore, they have shown that, even at temperatures close to the bulk melting point, the quasiliquid layer on ice is structurally different from normal liquid water. On the other hand, experiments on interfacial melting against graphite and polystyrene (Maruyama et al., 1992; Gay et al., 1992; Fu, 1993) showed that the

diffusion coefficient of the quasiliquid layer is approximately equal to that of supercooled water.

Both experimental work (e.g., Conklin and Bales, 1993; D□ppenschmidt and Butt, 2000) and theoretcal studies (e.g., Wettlaufer, 1999) have shown that the thickness of the QLL increases with temperature and ionic strength, and under most conditions is higher than predicted by bulk freezing-point depression (~1.86 K mole-solute^{-1}).

Following our measurements of the quantum yields for NO_2 and NO_2^- from nitrate photolysis in ice with $[NO_3^-]_0$ in the mM range (see Chapter 4), we now investigate the formation rate of nitrite from nitrate photolysis as a function of temperature and $[NO_3^-]_0$, in order to better understand the apparent temperature dependence of ϕ observed in our previous study. Furthermore, knowledge of the activation energy for nitrite formation in ice may also provide additional information on the environment in which the primary photochemistry is occuring.

5.2 Experimental Methods

Solutions of 10 and 1 mM $NaNO_3$ (with and without 10 mM $NaHCO_2$) in milli-Q water were frozen by spraying into an alumina mortar filled with liquid nitrogen. The resulting solid was then pulverized while at 77 K. 13 mm × 4 mm polycrystalline ice pellets (ρ ~ 1 g/cm^3) were made from the pulverized ice powder under an applied pressure of 3.8×10^6 Pa using a French press. After annealing at the desired experimental temperature under ambient pressure (10^5 Pa), the ice pellets were irradiated with light at a wavelength of 313 ± 10 nm. A high pressure 1000 W Hg-Xe arc lamp was used as a light source in combination with a 320 nm band filter (Melles

Griot, UG 11) and a solution of 1mM potassium chromate in 2.3% potassium carbonate (in 1 cm quartz sleeve). The incident light intensity was determined to be $2.4 \pm 0.2 \times 10^{16}$ photons$\cdot s^{-1} \cdot cm^{-2}$ using potassium ferrioxalate as a chemical actinometer (Hatchard and Parker, 1956). During the experiments, the ice pellets were placed (consecutively) in an isolated slot in a copper block. The temperature of the copper block was controlled by a cooling bath (Neslab ULT-80) and was monitored using a chromium-aluminum thermocouple (Omega Engineering) attached to its upper surface by a small frozen water droplet. After irradiation, the pellets were thawed and analyzed for nitrite using the Saltzmann reagent (Saltzmann, 1954; See also Appendix 4-1). Light absorbancy of the nitrate in the pellets was determined (before irradiation) using a UV-VIS spectrophotometer (Shimadzu UV-2101 PC) with an attached integrating sphere (Shimadzu ISR-260). The average intensity of scattered light was measured by a photomultiplier located at the bottom of the integrating sphere, which quantifies the light transmission through the pellet, with air used as a reference. The reflections from the pellets were measured off of the ice pellets contained in a slit at the wall of the integrating sphere (with a depth equal to the pellet thickness), with pressed $BaSO_4$ powder used as a reference.

5.3 **Results**

The method used to measure the light absorption spectrum of nitrate in 4 mm ice pellets has been described previously (See Chapter 3 - Results). In general, the percentage of light transmittance through the ice and the reflectance off the ice pellets was measured using an integrating sphere technique. The percent of incident light absorbed by 10 mM nitrate distributed in ice pellets (Fig. 5.1) was determined to be

(5.4 ± 1.3) % (i.e. absorption = 0.024), based on a light flux balance (equation 1, chapter 3), where pure H_2O ice pellets were used as a reference blank.

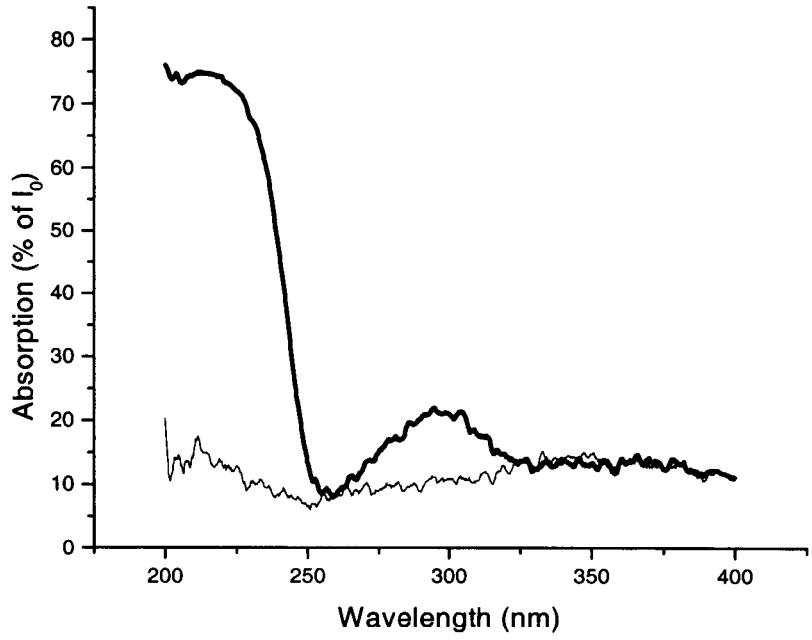

Figure 5.1 Absorption spectra of 10 mM nitrate in pellets (thick line; n = 9) and pure ice pellets (thin line; n = 4). Both sets of pellets were 4 mm thick.

Analogous to the aqueous solution case, the UV absorption spectrum of nitrate in ice pellets shows the two main absorption bands at 200 and 300 nm (Fig. 5.2). The higher absorption in the ice pellets than in aqueous solution at 302 nm is probably due to a pathlength longer than 4 mm due to multiple scattering inside the pellet. The large decrease in the absorption in the 200 nm band in ice pellets vs. aqueous solution may be in part a result of higher noise in the measurements of the integrating sphere at these short wavelengths.

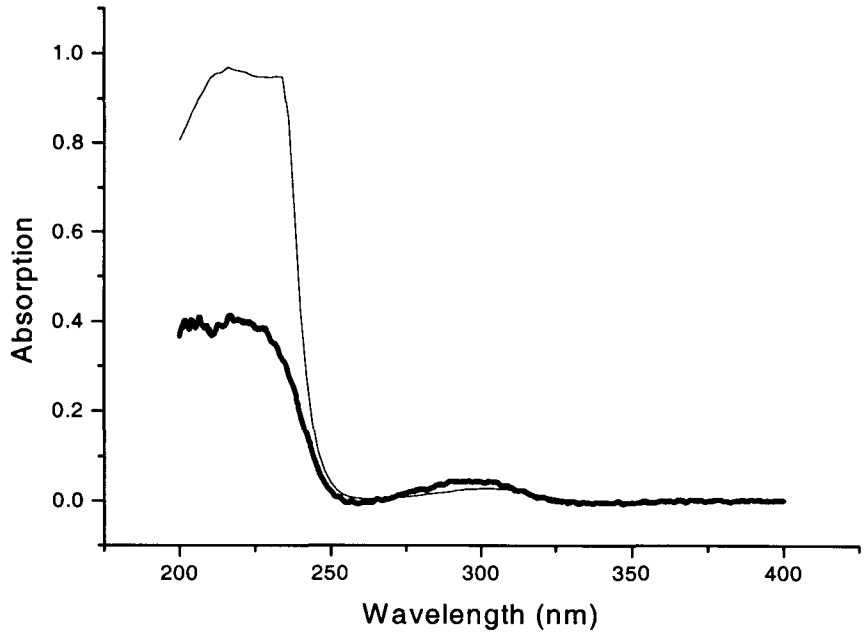

Figure 5.2 Absorption spectra of 10 mM nitrate in pellets (thick line) and in aqueous solution (thin line). For comparison, the absorption results of the latter (measured in a 1 cm deep cuvet) were translated to a pathlength of 4 mm.

As was previously observed in aqueous solutions (Bayliss and Bucat, 1975), the rate of nitrite formation in nitrate doped ice pellets decreases as a function of irradiation time (Fig. 5.3). At lower temperatures the steady state concentration of NO_2^- was lower (Fig. 5.3). In the presence of HCO_2^-, which acts as an OH scavenger (Eq. 1), the formation rate of nitrite remained linear at least on time scales of up to two hours (Fig. 5.4).

$HCOO^- + OH \longrightarrow H2O + CO_2^-$ $\quad k = 4.3 \times 10^9\ M^{-1}\ s^{-1}$ (1a)

$CO_2^- + O_2 \longrightarrow O_2^- + CO_2$ $\quad k = 2.4 \times 10^9\ M^{-1}\ s^{-1}$ (1a)

$O_2^- + H+ \longrightarrow HO_2$ $\quad pK = 4.8$ (1c)

$2HO_2 \longrightarrow H_2O_2$ $\quad k = 8.3 \times 10^5\ M^{-1}\ s^{-1}$ (1d)

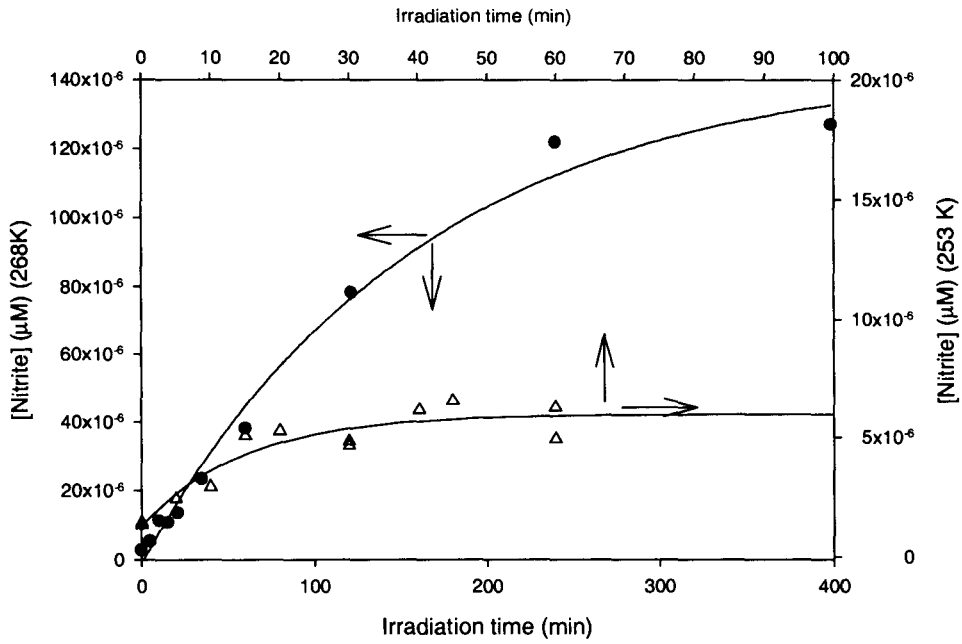

Figure 5.3 NO_2^- concentration as a function of the irradiation time of ice pellets containing 10 mM $NaNO_3$ at two temperatures: 268 K (solid circles; referring to the bottom X axis and left Y axis) and 253 K (open triangles; referring to the top X axis and right Y axis).

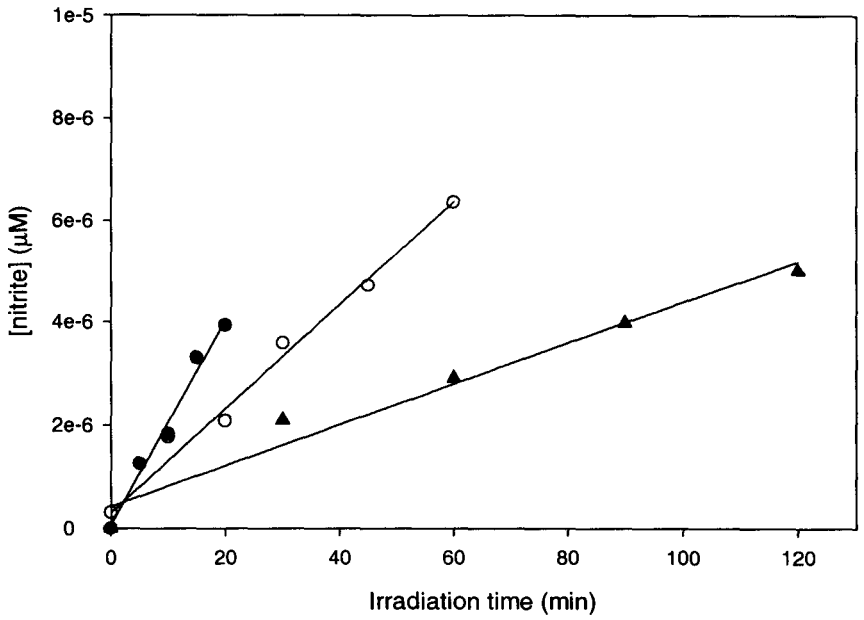

Figure 5.4 NO_2^- concentration as a function of irradiation time of ice pellets containing 1 mM $NaNO_3$ and 10 mM $NaHCO_2$ at two temperatures: 268 K (solid circles) and 253 K (open circles), and 236 K (solid triangles).

The initial rate constants observed for nitrite formation during the photolysis of nitrate in ice pellets are summarized in Table 1. Based on these rate constants and the light absorption measurements (see above), we can estimate the activation energy and quantum yield for these reactions.

The activation energy (E_a) for the rate of nitrite formation can be derived from the linear regression of a plot of ln k versus 1/T (Fig. 5.5), following the Arrhenius equation

$$k = A \cdot \exp(-E_a / RT) \quad , \qquad (2)$$

where both A, the frequency factor (with corresponding rate constant units), and E_a are assumed to be temperature independent over the 233 – 273 K range.

NO_3^- (mM)	HCO_2 (mM)	T (K)	k (s^{-1})	Time interval (minute)
1	10	268	3.23E-06	25
1	10	263	3.21E-06	25
1	10	243	1.15E-06	25
1	10	233	6.66E-07	120
1	10	243	1.62E-06	30
1	10	263	3.10E-6	40
1	10	253	1.69E-06	60
1	0	256	3.56E-07	20
1	0	268	1.14E-06	60
1	0	268	1.15E-06	60
1	0	263	6.88E-07	60
1	0	248	2.62E-07	185
1	0	263	1.89E-06	80
1	0	268	2.27E-06	60
1	0	248	6.88E-07	120
10	0	268	1.14E-06	40
10	0	263	8.42E-07	60
10	0	263	7.26E-07	60
10	0	263	9.09E-07	60
10	0	258	5.27E-07	60
10	0	258	5.19E-07	60
10	0	258	4.91E-07	45
10	0	253	3.43E-07	20
10	0	268	7.76E-07	30
10	0	268	1.03E-06	120
10	0	248	6.42E-07	10
10	0	253	3.74E-07	20
10	0	238	2.37E-07	13
10	0	238	1.92E-07	15

Table 5.1 Initial rate constants for nitrite formation during irradiation (λ = 313 nm) of nitrate doped ice pellets determined from data for the time intervals shown.

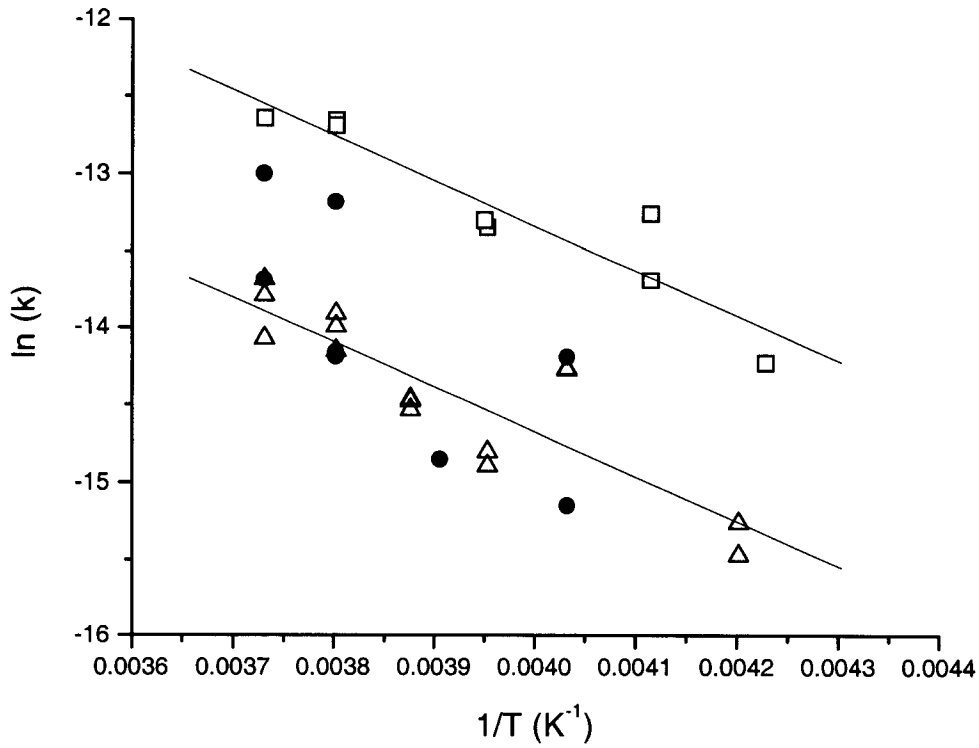

Figure 5.5 Natural logarithm of the 313 nm rate constants for NO_2^- production during the irradiation of ice pellet doped with: 10 mM $NaNO_3$ (open triangles), 1 mM $NaNO_3$ (solid circles), 1 mM $NaNO_3$ and 10 mM $NaHCO_2$ (open squares). The slopes calculated based on linear fit through the data are: 2902 ± 471 (10 mM $NaNO_3$), 2923 ± 459 (1 mM $NaNO_3$ and 10 mM $NaHCO_2$), and 4320 ± 1483 (1 mM $NaNO_3$).

As can be seen in Table 5.2, calculated activation energies (5.8 ± 0.9 kcal $mole^{-1}$) are the same for nitrite formation in irradiated ice pellet doped with 10 mM nitrate and in pellets doped with 1 mM nitrate and 10 mM HCO_2^-. The linear regression through the data of the 1 mM $NaNO_3$ pellets in the absence of OH scavenger suggests a higher activation energy (~9 kcal mol^{-1}). However, because of the large scatter in this data, the calculated value can not be considered.

composition	E_a (kcal $mole^{-1}$)	σ
10mM $NaNO_3$	5.8	0.9
1mM $NaNO_3$ + 10mM $NaHCO_2$	5.8	0.9
1mM $NaNO_3$	8.6	2.9

Table 5.2 Activation energies calculated based on linear regression fits through observed rate constant as shown in Figure 5.5.

The quantum yields for the formation of NO_2^- were calculated as follows:

$$\phi = \left[\frac{d[NO_2^-]}{dt}\right]_0 \times \frac{V}{I_{abs}} \qquad (3)$$

Where $(d[NO_2^-]/dt)_0$ is the initial formation rate of nitrite (M s^{-1}), V is the volume of the irradiated ice pellet (L), and I_{abs} represents the photon flux absorbed by nitrate within the pellets (Einstein s^{-1}). The latter was calculated based on the measured incident photon flux, the pellet surface area, and the absorbance of nitrate as it was measured in the integrating sphere. Since the absorbance of nitrate at 313 nm is low (see above), we were unable to measure it directly for $[NO_3^-]$ = 1 mM. Thus, in order to calculate the quantum yield for the experiments with 1 mM nitrate, we assumed that the absorbance followed the *Beer-Lambert* law (i.e. $A_{1\ mM\ NO_3^-} = 0.1 \times A_{10\ mM\ NO_3^-}$). The derived quantum yields vary from 5×10^{-4} to 1×10^{-2} as a function of temperature and the presence of an OH scavenger (Figure 5.6). Both in the presence and absence of formate, the quantum yield decreases with decreasing temperature. The addition of formate induces an increase in the observed quantum yield by a factor of ~ 5.

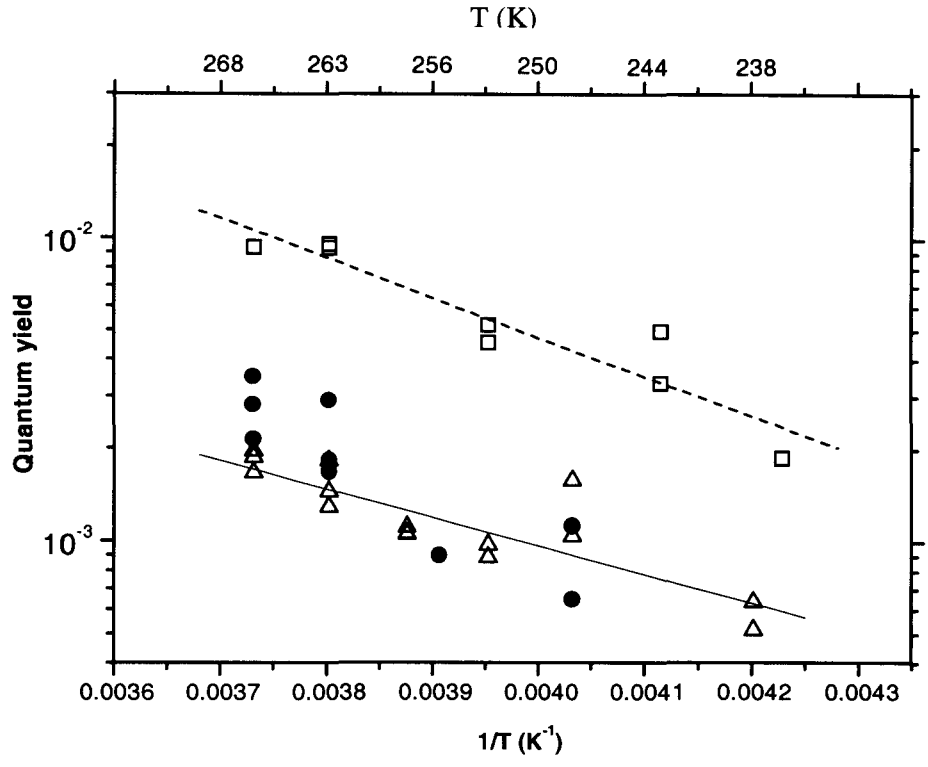

Figure 5.6 Quantum yields for NO_2^- production during the irradiation (λ = 313 nm) of ice pellet doped with: 10 mM $NaNO_3$ (open triangles), 1 mM $NaNO_3$ (solid circles), 1 mM $NaNO_3$ and 10 mM $NaHCO_2$ (open squares). No guiding line is shown for the 1mM $NaNO_3$ data due to the large noise in this data set.

5.4 Discussion

The concentration of the primary product nitrite is expected to reach a steady state due to reaction with OH radicals and due to secondary photolysis (ε = 9.9 M^{-1} cm^{-1} at 313 nm; Fischer and Warneck, 1996) (eq. 4):

$$\frac{d[NO_2^-]}{dt} = J_{nitrate}[NO_3^-] - J_{nitrite}[NO_2^-] - k_{OH}[^{\cdot}OH][NO_2^-] \quad (4)$$

$$[NO_2^-]_{ss} = \frac{J_{nitrate}[NO_3^-]}{J_{nitrite} + k_{OH}[OH]}$$

where J is the reaction frequency and is equal to the rate of photon absorption by the chromophore (I_a) multiplied by its quantum yield.

The fact that the steady state concentration is positively correlated with temperature (Fig. 5.3 and Fig 4.4 in Chapter 4) suggests that as temperature decreases the reaction rate with OH radicals increases and/or that the ratio between $J_{nitrate}/J_{nitrite}$ decreases. As light absorption by nitrate and nitrite are not expected to change significantly with temperature (Fig. 5.2), a decrease in $J_{nitrate}/J_{nitrite}$ will reflect a higher activation energy for NO_3^- than for NO_2^-. Since the strength of the solvent cage was found to be the dominant factor in the temperature dependence of the $J_{nitrate}$ (see discussion below), it is hard to believe that $J_{nitrite}$ will have a very different E_a (as was observed in aqueous solutions; Zellner et al., 1990). There is also no obvious reason for k_{OH} to increase at lower temperatures, therefore, an enhanced rate of NO_2^- oxidation by OH radicals at lower temperatures may indicate higher [OH] at the local environment. Hence, the observed decrease in $[NO_2^-]_{ss}$ with decreasing temperature may be the result of a thinner and more viscous QLL, which would increase the recombination probability for these two primary products. It maybe possible then to use the rate of formation and the $[NO_2^-]_{ss}$ to estimate the thickness of the QLL.

The activation energy we observed for the formation of NO_2^- from the photolysis of nitrate in ice pellets (5.8 kcal $mole^{-1}$) is higher than the activation energy previously reported for the formation of OH radicals in aqueous solutions (ca. 4 kcal $mole^{-1}$; Zellner et al., 1990; Jankowski et al., 1999). We were unable to find in the

literature the E_a of nitrite formation in aqueous solution at the 300 nm band photolysis of nitrate. However, since the probability of escaping the solvent cage during nitrate photolysis is the limiting factor in the formation of both NO_2^- and OH in aqueous solution, the activation energies for both products are expected to be the same. The question arises whether the observed increase in E_a is only a result of increasing water viscosity (i.e., stronger cage effect) as the temperature drops, or whether there is an additional effect due to changes in the nature of the QLL over the studied temperature range. Considering the viscosity of water between 263 - 298 K (CRC, 1975), we estimate that the free activation energy for flow in liquid water is 4.5 kcal mol^{-1} at $T > 273$ K and 5.4 kcal mol^{-1} at $T < 273$ K (Figure 5.7). These values are similar to the observed activation energies for the formation of NO_2^- and OH at the relevant temperature range (see above), suggesting that E_a observed in aqueous solution and in ice (under our experimental conditions) are dominated by the increasing viscosity of *liquid* water with decreasing temperature.

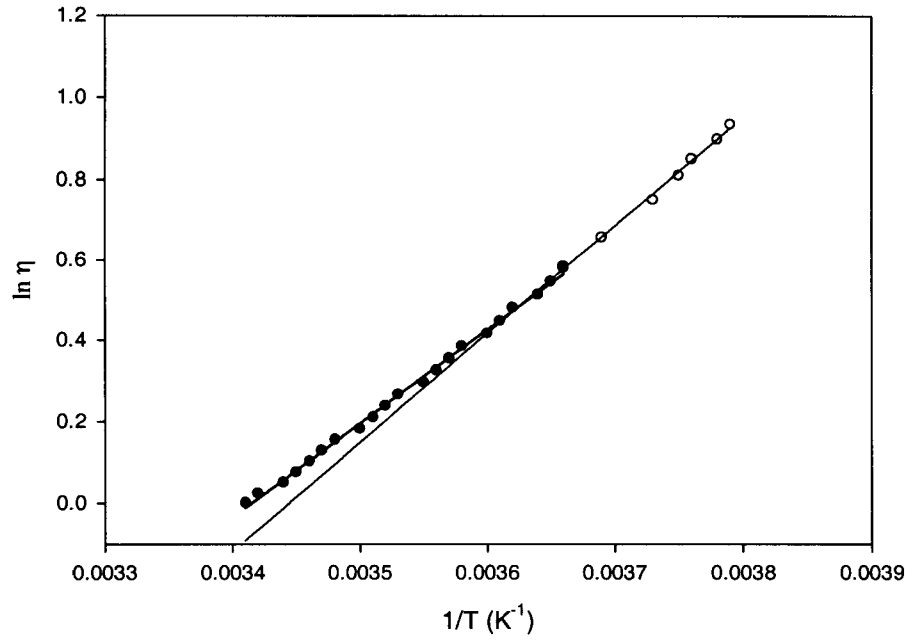

Figure 5.7 Natural logarithm of the viscosity of liquid water as a function of temperature. linear regression through the data indicate free activation energies for flow of 4.5 and 5.4 kcal mol^{-1} at temperatures above and below 273 K respectively. Based on data obtained from the *CRC Handbook of Chemistry and Physics* (1976).

As was observed in aqueous solution (Mark et al., 1996), the quantum yield for nitrite formation ($\phi_{+NO_2^-}$) increases significantly in the presence of an OH scavenger (Figure 5.6). This indicates that in the ice pellets nitrate and formate are present at the same locations, allowing formate to act as an efficient OH scavenger. $\phi_{(+NO_2^-)}$ in ice pellets containing formate was about 0.01 at 268 K. This value is very similar to the $\phi_{(+NO_2^-)}$ observed at λ = 305 nm photolysis of aqueous $NaNO_3$ solutions in the presence of formate at room temperature: $\phi_{(+NO_2^-)} \sim 9 \times 10^{-3}$ (Warneck and Wurzinger, 1988).

The quantum yield, $\phi_{NO_2^-}$, for nitrite formation obtained from ice pellets doped with10 mM $NaNO_3$ at 263 K, $(1.5 \pm 0.3) \times 10^{-3}$ is of the same order as $\phi_{(+NO_2^-)}$ observed during the photolysis of sub-millimeter ice film doped with 10 mM KNO_3, $(4.8 \pm 1.5) \times 10^{-3}$. The moderate difference between these quantum yields may be the result of the substantially different methods used in the two sets of experiments. In each case the ice generation techniques, the nitrate salts employed ($NaNO_3$ vs. KNO_3), the light sources, and the methods used to determine light absorption by nitrate were different.

Irradiation of 10 mM $NaNO_3$ aqueous solutions under identical conditions (in a small beaker, V = 4 ml, placed in the Cu block slot) at temperatures between 278 K and 288 K, do not indicate any significant change in $\phi_{(+NO_2^-)}$ between the two phases (considering the temperature dependence) (Fig. 5.8).

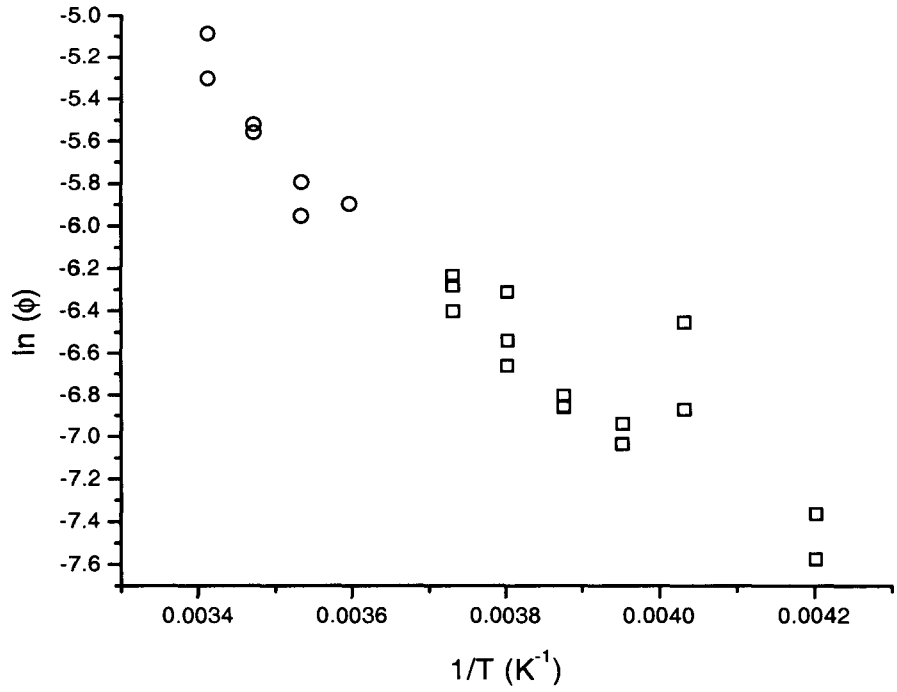

Figure 5.8 Natural logarithm of the quantum yield for nitrite formation during the photolysis (λ = 313 nm) of 10 mM nitrate in ice pellets (open squares) and in aqueous solution.

Nitrate, like most other solutes, is expected to be excluded from the ice matrix during freezing, and to accumulate in the QLL at the surface of ice crystals and in between adjacent crystals. However under the fast freezing conditions in the present study, only partial exclusion from the ice matrix is expected. The similarity between the quantum yields for nitrite formation in aqueous solution (extrapolated to low temperature) and in ice pellets as well as the similarity between the observed activation energy and the energy of the cage of supercooled water, suggest that under the conditions of our experiments (T = 268 – 237K, $I_0 = 10^{-2}$ M) NO_3^- photolysis occurs mainly in the QLL that behaves as a super-cooled solution. This conclusion is in accord with interfacial melting experiments of ice against graphite and polystyrene

showing that diffusion coefficient of the quasi-liquid layer is approximately equal to that of supercooled water (Maruyama et al., 1992; Gay et al., 1992; Fu, 1993).

Reference

1. Bayliss N. S. and Bucat R. B. (1975) The Photolysis of Aqueous Nitrate Solutions. *Aust. J. Chem.* 28, 1865-1878.
2. Bolton K. and Pettersson J. B. C. (2000) A molecular dynamics study of the long-time ice Ih surface dynamics. *J. Phys. Chem. B* 104, 1590-1595.
3. Conklin M. and Bales R. C. (1993) SO2 Uptake on Ice Spheres: Liquid Nature of the Ice-Air Interface. *J. Geophys. Res.* 98,16851-16855.
4. *CRC Handbook of Chemistry and Physics*, (1975) R. C. Weast (Ed), CRC press, 56th addition, Cleveland, Ohio.
5. Doppenschmidt A. and Butt H.-J. (2000) Measuring the Thickness of the Liquid-like Layer on Ice Surfaces with Atomic Force Microscopy. *Langmuir* 16, 6709-6714.
6. Doppenschmidt A., Kappl M., and Butt H. J. (1998) Surface properties of ice studied by atomic force microscopy. *J. Phys. Chem. B* 102, 7813-7819.
7. Fischer M. and Warneck P. (1996) Photodecomposition of Nitrite and Undissociated Nitrous Acid in Aqueous Solution. *J. Phys. Chem.* 100, 18749-18756.
8. Fletcher N. H. (1968) Surface Structure of Water and Ice, 2, A Revised Model. *Philos. Mag.* 18, 1287-1300.
9. Fu H. Y. and Dash J. G. (1993) Characterization of Frost Susceptibility of Soils by Mercury Porosimetry. *J. Colloid. Interf. Sci.* 159, 343-348.
10. Gay J. M., Suzanne J., Dash J. G., and Fu H. Y. (1992) Premelting of Ice in Exfoliated Graphite - a Neutron- Diffraction Study. *J. Crystal Growth* 125, 33-41.
11. Hatchard C. G. and Parker C. A. (1956) *Proc. Roy. Soc. Ser. A.* 235, 518.

12. Honrath, R.E., Guo, S., Peterson, M.C., Dziobak, M.P., Dibb, J.E., and Arsenault, M.A. (2000) Photochemical Production of Gas-Phase NO_x from Ice-Crystal NO_3^-, *J. Geophys. Res. –Atmos.*, 105, 24183-24190.

13. Honrath, R.E., Peterson, M.C., Dziobak, M.P., Green, S., Dihbb, J.E., and Arsenault, M.A. (2000) Release of NO_x from Sunlight-Irradiated Midlatitude Snow, *Geophys. Res. Lett.* 27, 2237-2240.

14. Honrath R. E., Peterson M. C., Guo S., Dibb J. E., Shepson P. B., and Campbell B. (1999) Evidence of NOx Production Within or Upon Ice Particles in the Greenland Snowpack. *Geophys. Res. Lett.* 26, 695-698.

15. Jankowski J. J., Kieber D. J., and Mopper K. (1999) Nitrate and Nitrite Ultraviolet Actinometers. *J. Photochem. and Photobio.* 70, 319-328.

16. Jones A. E., Weller R., Wolff E. W., and Jacobi H.-W. (2000) Speciation and Rate of Photochemical NO and NO_2 Production in Antarctic Snow. *Geophys. Res. Lett.* 27, 345-348.

17. Mark G., Korth H. G., Schuchmann H. P., and von Sonntag C. (1996) The Photochemistry of Aqueous Nitrate Ion Revisited. *J. Photochem. and Photobio A: chemistry* 101, 89-103.

18. Maruyama M., Bienfait M., Dash J. G., and Coddens G. (1992) Interfacial Melting of Ice in Graphite and Talc Powders. *J. Crystal Growth* 118, 33-40.

19. Saltzman B. E. (1954) Colorimetric Microdetermination of Nitrogen Dioxide in the Atmosphere. *Anal. Chem.* 26, 1949-1955.

20. Sumner A. L. and Shepson P. B. (1999) Snowpack Production of Formaldehyde and its Effect on the Arctic Troposphere. *Nature* 398, 230-233.

21. Warneck P. and Wurzinger C. (1988) Product Quantum Yield for the 305-nm Photodecomposition of NO_3^- in Aqueous Solution. *J. Phys. Chem.* 92, 6278-6283.

22. Wei X., Miranda P. B., and Shen Y. R. (2001) Surface Vibrational spectroscopic study of surface melting of ice. *Phys. Rev. Lett.* 86, 1554-1557.

23. Wettlaufer J. S. (1999) Impurity effects in the premelting of ice. *Phys. Rev. Lett.* 82, 2516-2519.

24. Zellner R., Exner M., and Herrmann H. (1990) Absolute OH Quantum Yields in the Laser Photolysis of Nitrate, Nitrite and Dissolved H_2O_2 At 308 and 351 nm in the Temperature-Range 278-353 K. *J. Atmos. Chem.* 10, 411-425.

Chapter 6

Conclusions

In the present study, the photochemical transformations of 4-nitrophenol and nitrate in ice were quantitatively studied under temperatures and pressures that resemble those at mid- and high-latitudes. To the best of our knowledge, this research effort represents the first attempt to determine quantum yields for photochemical reactions in ice quantitatively.

Two techniques were used in order to determine light absorption by the chromophores embedded in packed ice. In the first technique, doped ice pellets were used and the absorption spectrum was measured using an integrating sphere. When larger volumes of ice were needed, *in situ* photoisomerization of 2-nitrobenzaldehyde (which is known to have phase independent quantum yield) was used as an actinometer.

A quantum yield of $\phi_{ice} = (2.3 \pm 0.4) \times 10^{-4}$ was obtained for the photochemical degradation of 4-nitrophenol over wavelengths ranging from 300 to 370 nm in ice pellets (pH 5.6). The measured value of ϕ_{ice} is of the same magnitude as the aqueous-phase quantum yield which we measured under similar irradiation conditions ($\phi_{aq} \approx 7.7 \times 10^{-5}$). Five reaction products were positively identified: hydroquinone, benzoquinone, 4-nitrosophenol, nitrate, and nitrite. Indirect evidence indicated the formation of organic polymers. The similarities of these results to those found for 4-nitrophenol photolysis in aqueous solutions suggest that comparable mechanisms are operative in both phases.

Upon irradiation ($\lambda = 313 \pm 15$ nm) of NO_3^--doped submillimeter ice layers produced by freezing aqueous KNO_3 sprays on cold surfaces, the formation of $NO_2(g)$ and NO_2^- was observed. The measured fluxes of NO_2 released into the gas phase, F_{NO_2}, increased lightly with $[NO_3^-]$ between 5 and 50 mM, and increased markedly with

temperature over the range of 268 to 248 K. The photostationary *concentration* of NO_2^-, and the *quantum yield* of 2-nitrobenzaldehyde during *in situ* photoisomerization were found to be nearly independent of the ice layer thickness, *d,* between 80 – 400 μm. We infer that radiation was uniformly absorbed over the depth of the ice layers, where NO_3^- was photodecomposed into NO_2 (+ OH) and NO_2^- (+ O), but that only the NO_2 produced on the outermost layer was able to escape into the gas-phase. The remaining NO_2 trapped in the ice was further photolyzed to NO. At 263 K, we obtained $\phi_{NO_2^-} \sim 4.8 \times 10^{-3}$ (i.e., comparable to the quantum yield of nitrite formation in neutral NO_3^- aqueous solutions) and an apparent quantum yield for NO_2 release $\phi'_{NO_2} \sim 1.3 \times 10^{-3}$ (about a factor of 5 smaller than solution ϕ_{OH} data extrapolated to 263 K). Present ϕ'_{NO_2} data, in conjunction with snow absorptivity data, lead to F_{NO_2} values in reasonable agreement with recent measurements in Antarctic snow under solar illumination. These quantum yields also suggest that NO_3^- photolysis within the surface snow may also act as a significant source of OH radicals. These radicals may further react with impurities present in the polar snow (e.g., organic matter) causing chemical alterations of important species such as H_2O_2 and H_2CO and CO_2.

The formation rate of NO_2^- during the photolysis of NO_3^- as a function of temperature and initial NO_3^- concentration was further investigated using ice pellets. The quantum yields varied from $\sim 6 \times 10^{-4}$ at 235 K to $\sim 1.8 \times 10^{-3}$ at 268 K for ice pellets doped with 10 mM $NaNO_3$. Similar values were observed during the irradiation of pellets containing 1 mM $NaNO_3$. As in aqueous solutions, the addition of an OH scavenger (HCO_2^-) yielded a significant increase in the measured quantum yields, indicating that both solutes are present in the same region of the ice sample. The measured quantum yields for nitrite formation during irradiation, at 263 K, in ice

pellets doped with 10 mM $NaNO_3$ (Chapter 5) and in submillimeter ice films doped with 10 mM KNO_3 (Chapter 4) are in reasonable agreement.

The activation energy obtained for nitrite formation, 5.8 kcal $mole^{-1}$, is equal to the energy required to overcome the cage effect of supercooled water. These results suggest that under our experimental conditions (235 K < T < 268 K, I > 0.01 M) the QLL, where the photolysis is believed to take place, behaves as a supercooled solution. Thus, the higher activation energy for NO_2 release observed in submillimeter ice films (Chapter 4), is probably the result of changing ice morphology, i.e., higher probability to escape the ice at higher temperatures.

The photochemical decomposition of 4-nitrophenol and nitrate under conditions resembling those of mid- and high-latitudes (i.e., temperature, pressure, and UV wavelength range), supports the view that significant photochemical processing may occur in polar snowpacks and sea ice during spring and summer. These alterations may affect the chemistry within the snowpack and also the chemistry of the overlaying atmospheric boundary layer as was observed recently at high latitudes (summarized in Chapter 2). Although the chemistry of snowpacks has attracted much attention over the last few years, we are still far away from understanding these systems. In order to determine the chemical stability of important species present in polar snow and ice, more studies are needed on fundamental parameters in ice (e.g., extinction coefficients, quantum yields, reaction products). The goal of the present work was to contribute to a better understanding of this field by providing new techniques for estimating light absorption by chromophores embedded in packed ice and by providing more quantitative information of the photolysis of nitrate and 4-nitrophenol in ice.

Since about 50% of the northern hemisphere surface area is covered with snow during the winter, the photochemical processes outlined in this thesis may be relevant not only to the Polar Regions but also to a much broader array of snow and ice regimes.